CHARGE TRANSFER MECHANISMS IN ELECTROSPINNING

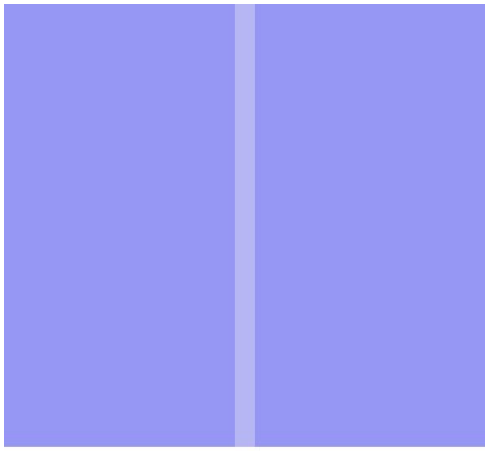

A thesis submitted in partial fulfilment of

the requirements for the Degree

of Master of Science in Physics

at the University of Canterbury

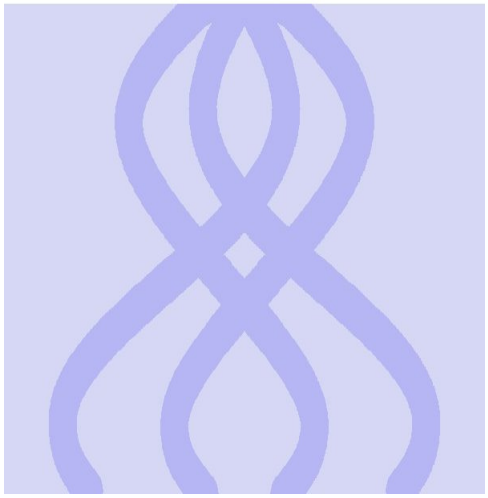

by J. J. Stanger

University of Canterbury

2008

Contents

ACKNOWLEDGEMENTS

I would like to thank Dr. Nick Tucker, Dr. Mark Staiger and Dr. Roger Reeves for their supervision, support and encouragement during this project. Without them this project would have never existed and I am so glad you chose me and allowed me to explore this fascinating area of science.

For funding and hosting of my research I would like to thank the Foundation for Research, Science and Technology (FoRST), Dr. Nigel Larsen and Crop and Food Research Ltd. Without the funding from the Foundation I would have likely starved. And without the continual support of Dr. Nigel Larsen this project may have been cut short before its prime. I hope that this project can soon start giving something back to Crop and Food Research as thanks for the gracious hosting of this work.

I would like to thank Warwick University in Coventry for hosting a short period of my research. I would like to specifically thank Dr. Kerry Kirwan, Stuart Coles and Daniel Jacobs for their valuable experience and assistance during my stay at Warwick University. I gained far more than just experimental data while there.

I would like to make special mention of the talents of Neil Buunk, who took my prototype design and produced the amazing ES1 and ES4 electrospinning apparatus.

For their contributions I would like to thank Andrew Wallace for his assistance and advice to help navigate the sticky world of statistics, Astrid Erasumason for most of the beautiful figures and Robert Lamberts for the photography. I would also like to specifically thank Jason Kerr, Lasse Hansen and Alexander Ferguson for their assistance with gathering experimental data, your help was much appreciated and helped to expand the strength of this thesis. I would like to acknowledge the assistance with editing provided by Simon Fullick helped by bringing the perspective of the intelligent layman. Thanks also to Heather Thompson for the last minute formatting and collation work.

This thesis would have never been possible without the never ending support from my parents, Paul and Jill Stanger, my siblings, Peter, Michael and Katie Stanger and my many friends over the years leading up to this work. I would also like to make special mention of the lecturers at the Physics Department as the University of Canterbury and Andrea Graves for the inspiration to and the belief that I really can achieve my dreams. If it wasn't for the people believing in me I might never have found the strength to see this through to the end.

And finally I would like to thank the members of the bands Jakob, This will destroy you and *shells for the amazing music they have produced to date. Without this music to relax my mind I would have definitely gone mad trying to achieve so much.

ABSTRACT

Electrospinning is a method of producing nano structured material from a polymer solution or melt using high strength electric fields. It is a process that has yet to find extensive industrial application yet shows promise if obstacles such as low rate of production overcome perhaps by more complete theoretical modelling. This work examines the effects of adding an ionic salt to a solution of poly(vinyl alcohol) in water. The direct effect was an increase the charge density and electric current. It was found that an increase in charge density decreases the mass deposition rate and forms a thinner initial jet. When the sign of the charge on the polymer solution was changed from positive to negative the charge density increased and the initial jet diameter and mass deposition rate also decreased. It was proposed that a smaller radius of curvature is formed by the Taylor cone at higher charge densities resulting in a smaller "virtual orifice". The extent of the bending instability was explored and it was found that adding ionic salt results in a decrease in the bending instability resulting in thicker fibres. Changing the sign of the charge on the polymer solution from positive to negative resulted in an increase in the bending instability and resulted in thinner fibres. The charge transfer mechanisms used in different electrospinning models are explored and some assumptions not explicitly stated are discussed. From this discussion a generalized equation describing the charge transport mechanisms is proposed.

CHAPTER 1

INTRODUCTION

INTRODUCTION

The interaction between electric fields and fluids has been known since early times (Gilbert 1628). During the twentieth century two important areas of application have been developed, electrospraying and electrospinning (Doshi and Reneker 1995). Electrospraying has been applied in a number of areas from analytical instruments such as mass spectrometry to domestic applications in inkjet printers. However this study will examine aspects of the latter process of electrospinning.

Electrospinning is a method of using high strength electric fields (>1kV/m) to draw a jet of polymer to diameters ranging from microns to a few nanometers. Academic interest in electrospinning has been growing since 1995 (Huang 2003), demonstrated by an increasing number of journal papers containing the term “electrospinning” with 1,200 papers published as of September 2007. The interest in electrospinning has been due to the potential for a method of continuous production of nano-scale material and because of the wide range of processing materials. As of September 2007 the only significant commercialization of electrospinning into the industrial sector has been from Donaldson Company Inc., Bloomington, MN, USA and Elmarco, Liberec, Czech Republic. A major obstacle to industry uptake of electrospinning is the interdisciplinary nature of the process, incorporating aspects of electrostatics, fluid dynamics and physical chemistry.

Due to the lack of a complete model of the electrospinning process it can be difficult to predict the behaviour of a new polymer in the electrospinning process. The most complete model to date (Thompson 2007) was composed by Yarin et al. 2001 yet does not incorporate the initial Taylor cone generation and uses the charge carried by the jet as an initial parameter taken from experimental observations rather than predicting an initial charge to be carried. The lack of models that address the nature and generation of charge carriers is of great concern when all the existing models include either charge density or surface charge as a factor in the model (Reneker et al. 2000, Hohman et al 2001, Yarin et al. 2001, Feng et al. 2002 and Reznik et al. 2004).

To further understand the physical phenomenon of charge generation and transport between the electrospinning electrodes the influence of an ionic salt on the behaviour of the electrospinning process was undertaken. Experimental observations from a previous report submitted for the postgraduate course PHYS480 at the University of Canterbury, Christchurch, New Zealand are revisited and discussed in relation to the change in behaviour observed when an ionic salt is introduced into the polymer solution. In this study the implicit assumptions present in the current models of the electrospinning process will also be examined and discussed.

The motivation behind the addition of an ionic salt into a solution to be electrospun comes from the low number of papers dealing with the effect of ionic salts and the contradictions between these papers. The addition of an ionic salt to a solution results in increasing the conductivity. As some authors (Reznik et al. 2004 and Yarin et al. 2001) have been able to derive plausible electric current flows from the treatment of electrospinning solutions as conductors, a change in conductivity should show a response in the measured electric current flowing in the jet. In addition to the electric current the mass deposition rate, initial jet diameter and final fibre diameter are also measured. As an increase in the electric current by definition corresponds to an increase in the quantity of charge being transported between the two electrospinning electrodes the effect of this increase in transported charge could then be examined through analysis of the additional measured quantities.

There are two main processes that occur during electrospinning, the generation of the Taylor cone with the associated fluid jet ejected from the tip of the cone and the bending instability that occurs during flight that is responsible for the small final diameter of the deposited fibre. By exploring the trends in the mass deposition rate, initial jet diameter and final fibre diameter resulting from the addition of an ionic salt some further understanding of how charge behaves in the electrospinning process can be reached. This is important as it is difficult to directly measure the charge generated in the polymer solution without affecting the measured result. Hence by exploring the observed trends and having a good approximation of how the localized behaviour at certain points in the electrospinning process are linked to the quantity and location of charge details about the generation and behaviour of the charge can be inferred.

An exploration of the flow of charge is also undertaken from a theoretical point of view to assist in the analysis of the experimental observations. Reviewing the existing treatment of the flow of charge in literature reveals a number of assumptions that may not be correct and have no experimental evidence to support them. As such each assumption is carefully explored and an attempt to generalize the equations where the assumptions appear has been made. Where possible other established theoretical models and observations have been drawn on to justify the correction of the assumption.

CHAPTER 2

LITERATURE SURVEY AND BACKGROUND INFORMATION

LITERATURE SURVEY AND BACKGROUND INFORMATION

1. HISTORY

In the late 1500's William Gilbert set out to describe the behaviour of the known magnetic and electrostatic phenomenon. His work (Gilbert 1628) is an early example of what would become the modern scientific method and he was knighted for his work. He distinguished between the force arising from a loadstone and the force from rubbed amber (Saslow 2002) and invented the term electricity to describe the force from amber. One of his more obscure observations was that when a suitably charged piece of amber was brought near a droplet of water it would form a cone shape and small droplets would be ejected from the tip of the cone. This is the first recorded observation of electrospraying.

In 1902 the next major movement towards modern electrospinning occurred when a dentist by the name of William James Morton filed a United States patent entitled "Method of Dispersing Fluids". In his US patent (number 705691) he describes a method of using high voltage power supplies to generate a cobweb-like deposition of fibres. Even at this early stage it was recognized that the fluid must be sufficiently viscous with a solvent volatile enough to evaporate and allow hardening and that the electric stresses must be controlled properly to give fibres.

In 1914 the next significant development was achieved by John Zeleny, who published work on the behaviour of fluid droplets at the end of metal capillaries. His effort began the attempt to mathematically model the behaviour of fluids under electrostatic forces, continued in the works of Sir Geoffrey Ingram Taylor between 1964 and 1969. Taylor's work was done during his retirement after a broad career including developing a model for turbulent mixing of air at the arctic, significant contributions to the fields of fluid mechanics and solid mechanics, working on the Manhattan project, working on the development of supersonic aircraft and inventing the CQR anchor. Taylor's work contributed to electrospinning by mathematically modelling the shape of the cone formed by the a fluid droplet under the effect of an electric field and working with J. R. Melcher in developing the "leaky dielectric model" for conducting fluids (Melcher and Taylor 1969). This cone has since been known as the Taylor cone.

In between the work of Zeleny and Taylor came a sequence of patents by Anton Formhals filed between 1932 and 1940 (Formhals 1934, 1943 and 1944). A new kind of apparatus was proposed by Formhals compared to Morton's apparatus in order to produce continuous fine fibres for use on standard textile machinery. The process was discovered to be a potential source of nano-structured material by Doshi and Reneker in 1995 who whilst investigating electrospraying found that fibres formed with suitable solutions that had diameters on the nanometre scale. Huang et al. (2004) noted that between 1995 and 2000 less than 10 papers were published each year, however from 2000 onwards the number of papers has been increasing reaching over 50 papers by 2002 showing the growing interest in electrospinning.

During this period, there are further theoretical developments of the driving mechanisms of the electrospinning process. Reznik et al. (2004) describes extensive work on the shape of the Taylor cone and the subsequent ejection of a fluid jet. Once in flight the work by Hohman et al. (2001) investigates the relative growth rates of the numerous proposed instabilities in an electrically forced jet. Finally work by Yarin et al. (2001) endeavoured to describe the most important instability to the electrospinning process, the bending (whipping) instability.

2. BACKGROUND THEORY

2.1 Polymers

Polymers have existed almost as long as life itself as nature has used them in the form of proteins and polysaccharides (i.e. starches and cellulose). Throughout the history of man many applications have been found such as the production of clothing from cotton or silk and the production of paper from cellulose. In the 18th century a resin from rubber trees was turned into numerous useful products and later around 1870 celluloid was produced marking man's first steps into synthetic polymers. Further detail can be found in "Fundamentals of Polymer Engineering" by Arie Ram (1997). A polymer is a molecule that consists of many repeating smaller units known as monomers. These monomers are joined in such a way to form long chains that can be linear or branched. The monomer units upon which it is based determine the physical properties of a polymer.

2.2 Polymer Solutions

2.2.1 Intermolecular and Solute/Solvent Interactions in Polymers

A polymer molecule can be thought of as a coiled ball of string. This conformation (the 3D structure of a molecule) is due to the tetrahedral nature of the carbon atoms that form the backbone of most polymers. A collection of these balls where the coils are entangled represents the amorphous (random molecular orientation) state of a polymer as opposed to the crystalline state where the molecules are more ordered. In a solvent a polymer will open up its coil or separate from the crystal surface to allow solvent molecules to surround the chain. The extent to which this occurs depends on the solvent-polymer interaction. If there is poor interaction the polymer will not dissolve and is simply dispersed. If the interaction is strong then the coil will be very open due to a significant number of solvent molecules surrounding the chain. If the solvent-polymer interaction is equal to that of the intramolecular interaction (interaction between different parts of the same molecule) then the resulting solution is known as an ideal solution. A polymer melt can also be thought of as an ideal solution since the "solvent" is simply other polymer molecules of the same type.

2.2.2 Viscoelasticity

In order to talk about a bulk material property such as viscoelasticity one first needs to define the quantities of stress, normal stress, shear stress and strain. Stress in one dimension is the force exerted (F) divided by the area (A) (see Equation 1). Normal stress (often shortened to simply stress) is force perpendicular to the face of the material whereas shear stress is force parallel to the face of the material. Strain is the change in length per unit length (see Equation 2 where $\delta\ell$ is the change in length and ℓ is the total length). Viscoelasticity describes the behaviour of a material that is both viscous and elastic under stress, so it has properties of both the solid and the liquid phase. A viscous material will undergo viscous flow to relieve the application of shear stress as described by Newton's law (see Equation 3). This behaviour can be modelled with a dashpot which is a loosely fitting piston in a cylinder containing a fluid of viscosity η (see Figure 1). A perfectly elastic material obeys Hooke's law (see Equation 4 where E is the elastic modulus) and hence behaves like a perfect spring. As such this behaviour could be modelled by a perfect spring which acts as an energy storage element, gaining energy with extension and releasing it when the material returns to its original shape.

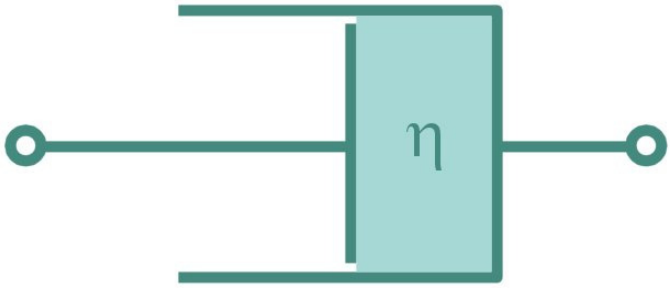

Figure 1: Diagram of a dashpot with a fluid of viscosity η.

The combination of a viscous and elastic behaviour shown by polymers and polymer solutions becomes more complicated. The stress strain behaviour shows elements that obey Hooke's law however unlike an elastic response the viscous response acts to dissipate energy as heat resulting in hysteresis and creep. Hysteresis is due to the viscous response causing the loss of energy meaning that the material cannot return to its original shape. Creep is the tendency of a material to slowly deform under continuous stress below the yield strength in order to relieve the applied stress.

One of the first models of viscoelastic behaviour is the Maxwell model (Cowie 1991). The Maxwell model assumes that the contribution to the strain from the elastic and viscous behaviour is additive (i.e. $\varepsilon = \varepsilon_{elast} + \varepsilon_{visco}$). As such, mathematically it represents a spring element in series with a dashpot element. Another early model was the Voigt-Kelvin model (Cowie 1991). This model proposes that the applied stress is now shared between the elastic and viscous response, mathematically represented by a spring element in parallel with a dashpot element (see Equation 5, where $\tau = \eta\varepsilon_S / \sigma_S$). Typically in modern modelling situations the Standard Linear Model is used that consists of a spring element in series with the Voigt-Kelvin model and a further dashpot in series. This better represents the important features in the typical behaviour of a polymer. For a full treatment of viscoelasticity see Cowie (1991).

$$\sigma = \frac{F}{A} \qquad \text{Equation 1}$$

$$\varepsilon = \frac{\delta \ell}{\ell} \qquad \text{Equation 2}$$

$$\sigma_S = \eta \frac{d\varepsilon_S}{dt} \qquad \text{Equation 3}$$

$$\sigma = E\varepsilon \qquad \text{Equation 4}$$

$$\varepsilon(t) = \sigma_0 J\left(1 - e^{t/\tau}\right) \qquad \text{Equation 5}$$

2.2.3 Surface Tension

A molecule in a solution is surrounded on all sides by other molecules that will normally interact with it. When the solution exists in an equilibrium state the pull from each of the surrounding molecules is matched by the pull from another molecule on the opposite side. However, consider the molecule is on the surface of a boundary between two fluids. On this surface there will be an imbalance in the forces as the force between the molecules of the two fluids will be different from the force when the molecule surrounded by its fluid. This results in a force that pulls the liquid in such a way as to minimize the surface area to volume ratio. In the case of the air-liquid interface, air has little interaction with the liquid so the force is near its maximum. When considering the physical meaning of surface tension it can be constructive to look at the approximate definition, Equation 8[*].

The typical shapes adopted by a fluid under the forces of surface tension are spherical, as this is the minimum surface area for a given volume. Figure 2 shows diagrammatically the forces experienced by fluid molecules. As there is a force acting on the outer surface it is possible to calculate the amount of work required to change the shape of the fluid. Equation 6 gives the energy (work) that must be either expended or will be generated when the surface changes its area (where γ is the surface tension, E is the work energy and δA is the change in area). It is also possible to calculate the pressure due to the force from surface tension from Equation 7 (where P is the internal droplet pressure and r is the radius of the droplet). In a free droplet

[*] Approximate definition is taken from Wolfram Research's website "World of Physics" accessed on 16 March 2008 at http://scienceworld.wolfram.com/physics/SurfaceTension.html

this pressure is the same from all sides but for a hemispherical droplet at the end of a fluid filled capillary this pressure would need to be matched by the fluid pressure within the capillary. It can be said that for any fluid that has reached its equilibrium state there will need to be some other force acting in order for the fluid to adopt any shape other than that of the least surface area.

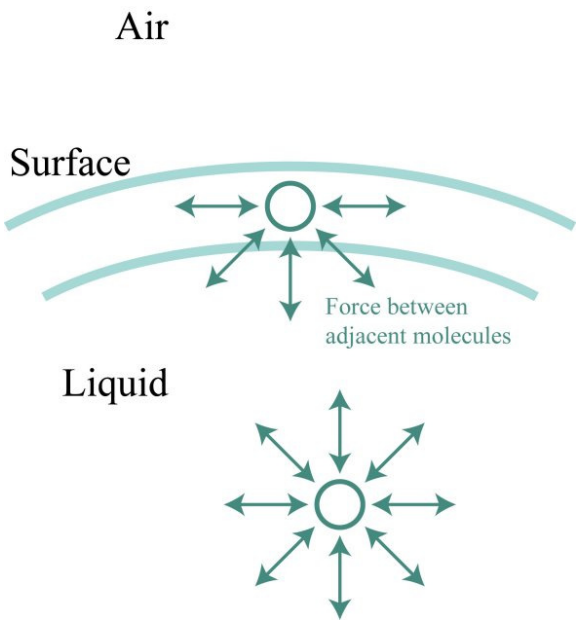

Figure 2: Diagram of the forces experienced by molecules in a liquid.

$$E = \gamma \delta A \qquad \text{Equation 6}$$

$$P = \frac{2\gamma}{r} \qquad \text{Equation 7}$$

$$\gamma \approx \frac{\left(\frac{[molecules]}{[area]}\right)\left(\frac{[binding\_energy]}{[molecule]}\right)}{[fraction\_of\_unbound\_bonds]} \qquad \text{Equation 8}$$

2.2.4 Conductivity

The conductivity of a solution is determined by the potential for bulk motion of ions in the solution. When a potential difference is applied across a volume of solution a current will flow that is proportional to the type of ions in solution and their respective concentrations. Conductivity due to a particular ion type in aqueous solutions can be seen in tables of molar conductivity (Λ). For very dilute solutions the contribution to the conductivity of a solution can be calculated from the Debye-Huckel-Onsager equation (CRC-Press, 2004) (Equation 9 where Λ is the molar conductivity, Λ_0 is the molar conductivity at infinite dilution, c is the ion

concentration and A and B are typically taken to be 60.20 and 0.229 respectively). At higher concentrations a strong electrolyte typically has a constant molar conductivity whereas a weak electrolyte will often vary over all concentrations. The conductivity of a given cell is related to the molar conductivity by Equation 10, where κ is conductivity with units of mS/cm, c is ion concentration with units of mol/L and hence the molar conductivity, Λ has units of Scm^2/mol.

$$\Lambda = \Lambda_0 - (A + B\Lambda_0)c^{1/2} \qquad \text{Equation 9}$$

$$\Lambda = \frac{\kappa}{c} \qquad \text{Equation 10}$$

2.3 External Forces

2.3.1 Electrodynamic Force

A single electron (having a negative charge) travelling in a vacuum in the presence of an electric field will experience a force given by Equation 11 (where F is the force exerted, q is the charge and E is the electric field). As it is a force, this is a vector equation and hence the electron will travel in the direction of the electric field. A proton (having a positive charge) would experience a similar force but in the opposite direction of the electron. All charge produces its own electric field. Like lines of magnetic flux (lines perpendicular to the equipotential surfaces), lines of electric flux cannot cross. A negative charge acts as a sink for field lines and a positive charge as a source. All field lines must either travel from a source to a sink or to the edge of infinity which can be either a source or sink. For further discussion of electric forces see Halliday et al. (2001).

$$F = qE \qquad \text{Equation 11}$$

2.3.2 Surface Charge

If two charges of the same sign are next to each other there will be a force repelling them from one another. As like charges will both act as either a source or a sink for lines of electric flux (example Figure 3), this force is the result of the field warping to a higher energy state as the lines of electric flux cannot cross. The force of this repulsion is given by Coulomb's law (Equation 12 where F is the force, q_1 and q_2 are charge, d is the distance between the charges and ε_0 is the permittivity of free space). Therefore if you were to imagine a number of equally spaced charges of the same sign

on the surface of a balloon then it should be evident that the surface would be stretched until the elastic force of the rubber was balanced with the repulsion force from the charge.

The case of the droplet present at the moment the electric field is applied to initiate electrospinning is similar to the balloon example above. In this situation surface tension is acting like the elastic force of the rubber, trying to contract the total volume to the minimum possible. As shown in Section 2.2.5 of this Chapter the force from surface tension can be seen as a pressure pointing inwards whereas the force from the self repulsion of the charge built up on the surface will be a pressure pointing outwards. This pressure is given by a similar relationship (Equation 13 where V is the applied voltage and r is the droplet radius) to Equation 7 from Section 2.2.5 (Headley et al. 1970). Both equations can be combined to give Equation 14, a relationship for the total pressure inside the droplet. It should be noted that this does not include the attraction due to the electric field present, only the force due to surface charge repulsion and becomes invalid once the droplet changes shape as it is based on a spherical capacitor approximation.

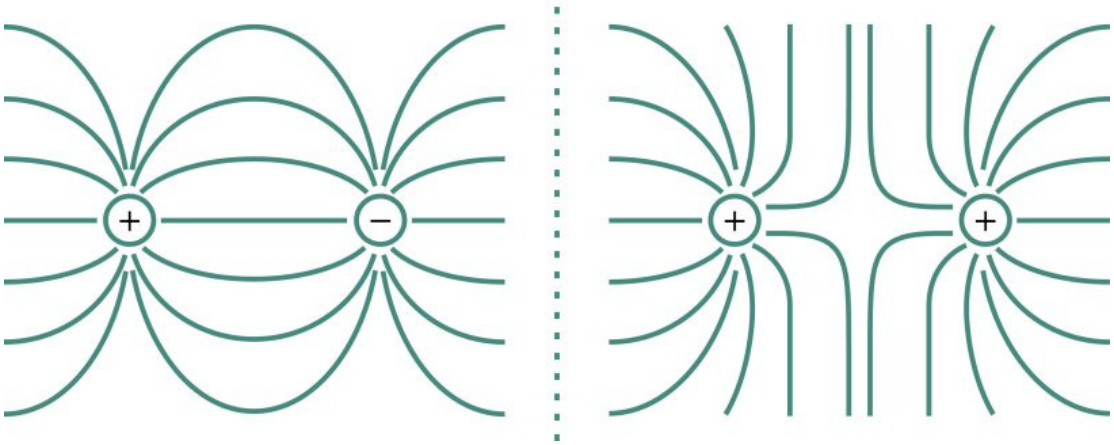

Figure 3: Electric flux lines from a source and a sink.

$$F = \frac{1}{4\pi\varepsilon_0}\frac{|q_1||q_2|}{d^2} \qquad \text{Equation 12}$$

$$P = \frac{\varepsilon_0 V^2}{r^2} \qquad \text{Equation 13}$$

$$P_T = \frac{2}{r}\left(\gamma - \frac{\varepsilon_0 V^2}{2r}\right) \qquad \text{Equation 14}$$

2.3.3 Fluid Pressure

Pressure can be generated in a fluid in a number of ways. Hydrostatic pressure resulting from the weight of fluid above a chosen point is given by Equation 15. This is also known as the head pressure. Pressure can also be supplied by pressurizing the supply tank for the fluid typically with an inert gas. In this case as a liquid is typically incompressible the pressure from the gas will be directly translated to the other boundaries of the fluid. Another common procedure in electrospinning is the use of a syringe pump. Here, as long as the fluid pressure does not exceed the power of the syringe pump the pressure will be related to the other forces and geometry in the system.

$$p = \rho g h \qquad \text{Equation 15}$$

3. ELECTROSPINNING PROCESS AND APPARATUS

3.1 Simple Process Description

3.1.1 Axis Conventions

In order to discuss the electrospinning process in a concise and transparent method it is important to make a quick note regarding the common axis conventions in models. Typically a cylindrical co-ordinate system is used (Calculus by Anton 1999). This is a system where to describe a point in 3 dimensional space you are given a distance along a Z axis followed by an angle to rotate around the Z axis then a distance to travel perpendicular to the direction of the Z axis. This is outlined diagrammatically in Figure 4. The direction of the Z axis is chosen to be such that the maximum level of symmetry is obtained around said axis. If the axis is chosen such that it passes through the centre of the first electrode, then through the centre of the polymer droplet and lastly through the centre of the second electrode it often obtains the maximum symmetry possible. This axis can then be referred to as the primary axis.

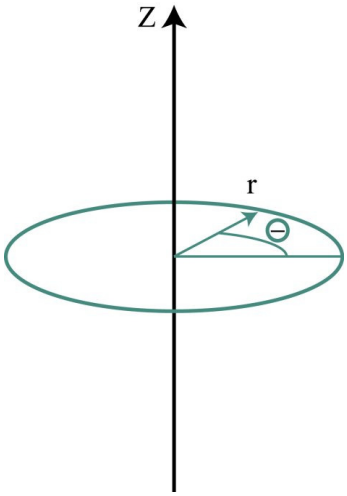

Figure 4: Cylindrical axis convention.

3.1.2 Basic Physics of Electrospinning

Electrospinning can be viewed as a special case of electrospraying*. The latter process is a method of atomizing fluids and has found extensive use in the field of chemistry as part of mass spectrometry and in industrial applications for painting of cars and in inkjet printers.

As with electrospraying, the feedstock for electrospinning is connected to a power supply to raise the fluids electrostatic potential to a high voltage. Polymer solutions or melts that possess a high degree of molecular cohesion due to intermolecular interactions are usually used as the feedstock. Increasing the electrostatic potential increases the surface charge of the liquid. Normally the shape of a volume of fluid is dictated by its surface tension. However, when the fluid is charged the surface charge acts in the opposite manner to surface tension resulting in the fluid changing shape, for axisymmetric considerations typically forming a conical structure called a Taylor cone (Taylor 1964).

If the surface of a conductor forms a sharp point the electric stresses will concentrate on that point. In the case of a Taylor cone, there is a sharp point at the tip of the cone hence, the concentration of electric stresses leads to the ejection of a fluid jet due to the increased electrical attraction at the tip. As this fluid jet carries a charge it will be drawn in the direction of the local electrostatic field. After a certain amount of flight time this jet will become vulnerable to a number of instabilities. Careful control of these instabilities ensures successful fibre formation. For instance, the axisymmetric

* **Electrospraying**: Using a high strength electric field to cause a fluid to atomize (break up into small droplets) rather than *via* aerodynamic or mechanical forces.

Plateau-Rayleigh* instability which is responsible for atomization in the electrospraying process needs to be avoided to ensure fibre formation. Included in the electrospinning process is the off axis bending instability that is largely responsible for the narrow fibre diameter obtained during electrospinning (Reneker et al. 2001).

The off axis bending instability occurs due to small perturbations in the straight line trajectory of the fibre which will generate a force perpendicular to the primary axis due to the self repulsion of the charged jet when perfect symmetry is lost (see Figure 5). This force is very small and is initially countered by the viscoelastic nature of the polymer solution. The viscous component will resist the motion generated by this force and the elastic component will work to restore the perturbed fibre to its original position. However, at some point the perturbation force will exceed the damping in the jet and the bending instability becomes significant. From this point the instability increases throughout the rest of the jet's flight causing a significant portion of the stretching experienced by the jet (Reneker et al. 2001).

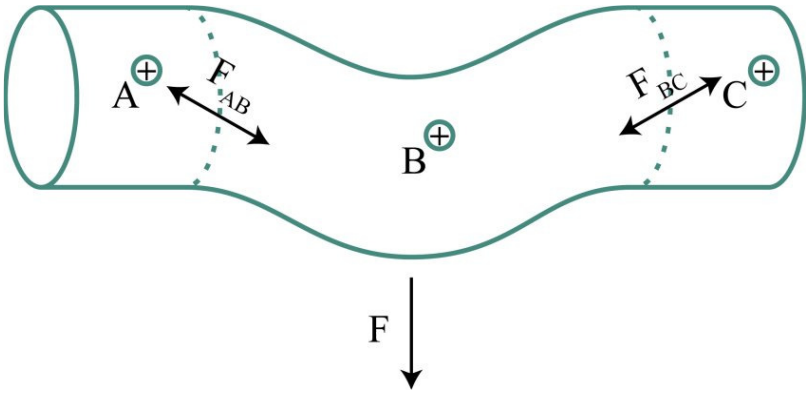

Figure 5: Physical diagram of perturbations causing the bending instability (modified from Ramakrishna et al. 2006).

The high surface area of these narrow fluid jets allows rapid solvent loss leading to the conversion of the fluid jet into a solid fibre within the short flight time. It has been observed that polymer molecules within these fibres have a high degree of crystallinity (Wang et al. 2006). This has been explained both by the alignment of polymer molecules due to the electrostatic field and due to the high draw ratio experienced by the fibre while in flight.

* **Plateau-Reyleigh instability** is the result of surface tension reinforcing small perturbations in a fluid column's surface eventually leading to the breaking up of the fluid column and the formation of droplets. For a full mathematical treatment see Lecture 7.5 of the MIT course 1.63J/2.21J Advanced Fluid Dynamics of the Environment accessed on the 12 March 2008 from http://web.mit.edu/1.63/www/lecnote.html

3.2 Current Models

The current model of the process is still incomplete. However in the last 13 years significant advancements have been made since the work of Zeleny (1914) and Taylor (1964). Many of the proposed models have had some validation against experimental data and have been used to help explain experimental observations. This suggests that a good understanding in the models, though unable to fully predict results, can significantly reduce research and development time for new fibre applications. Thompson et al. (2007) claims in reference to Yarin et al. (2001) that the proposed model is "the only existing model of electrospinning, accounting for the large nonlinear perturbations, viscoelasticity, evaporation and solidification". This would make it the most complete model proposed at this time. The following sections expand the discussion outlined in Section 3.1.2.

3.2.1 Jet Initiation

Jet initiation is one of the direct consequences of exposing a fluid drop in contact with a conductor to a strong electric field. As a result much of the work on jet initiation has been done in tandem with theoretical treatments of electrospraying. Many authors (Zeleny 1914, Taylor 1964, and Hendricks et al. 1964) have focused on the concept of a critical voltage; being the voltage where discharge of mass begins (either of a smooth fluid jet or aerosol jet).

Taylor (1963, 1964 and 1969) undertook the first theoretical examination of jets being initiated from a polymeric fluid on the end of metal capillaries. In this work Taylor described cone formation (now named after him) for any conducting fluid which had a semi-vertical angle of 49.3^{o} (see Figure 6). The validity of this cone geometry has been questioned more recently by Yarin et al. 2001 and Reznik et al. 2004 who find it to be $\leq 33^{o}$. Taylor found a relationship between his initial conditions and the formation of his cone (Equation 16). Here H is the distance between electrodes, L is the length of the capillary tube (syringe needle), R is the radius of the tube and γ is the fluid's surface tension (all expressed in CGS units as per the original paper). As it was shown that Taylors model of electrospinning was not entirely correct (Reznik et al. 2004) it therefore may only hold true for specific cases. However, since his simple equation negates the need for extensive modelling method it can be used to assist in

prediction of the critical voltage required to begin jet initiation, saving some time on experimental work.

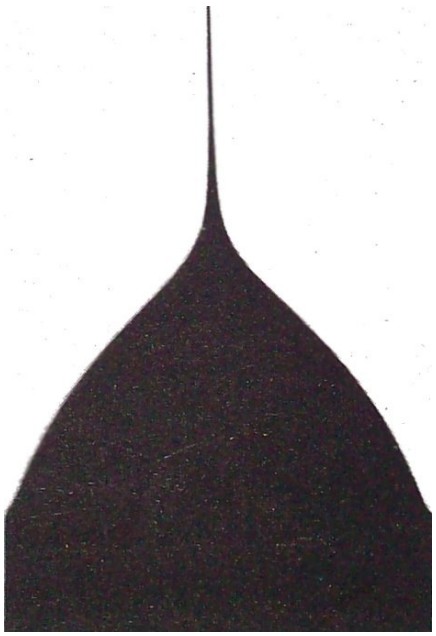

Figure 6: Taylor cone formed by a 98% glycerine and 2% of a 10% NaCl solution with an exposure time of 1 ms (Taylor 1969).

Later work by Reznik et al. (2004) on the evolution of droplets on an infinite plane over time showed that the static contact angle formed by the fluid droplets was critical in describing jet initiation. Reznik et al. (2004) introduces the concept of the electric Bond number (as defined in Equation 17 where E_∞ is the applied field, γ is the surface tension and a_0 is the equivalent-volume drop radius or characteristic length) allowing the description of the relative importance of electric and capillary stresses. For a range of contact angles the critical value for the electric Bond number were calculated (Figure 7) and hence, the critical voltage needed to form the Taylor cone can be calculated for a given a polymer solution.

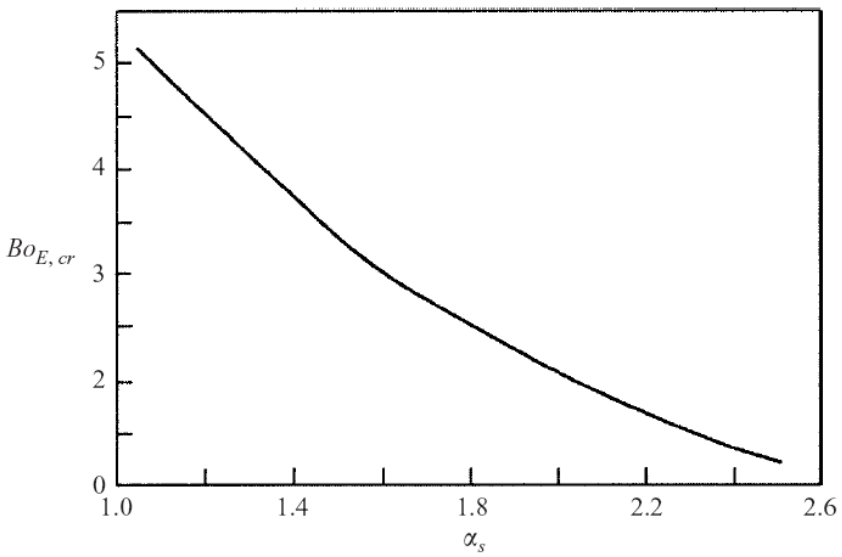

Figure 7: Critical electric Bond number (found via mathematical model) versus static contact angle where contact angle is given independent of surface tension in the model (Reznik et al. 2004).

Evolution of a droplet shape can be divided into subcritical or supercritical evolution. If the electric Bond number is low then a subcritical evolution occurs. Here the droplet adopts a partial cone shape, however the hydrodynamic forces still dominate and hence the droplet will not evolve into a jet. If the electric Bond number is above the critical level then a supercritical evolution towards the typical Taylor cone will occur such that mechanical stresses from the electric field dominate the droplet evolution. Concentration of electric stress at the tip of the cone (Yarin et al. 2001) will cause the continued formation of a typical electrospinning jet.

$$V_C^2 = 4\frac{H^2}{L^2}\left(\ln\frac{2L}{R} - \frac{3}{2}\right)(0.117\pi\gamma R) \qquad \text{Equation 16}$$

$$Bo_E = \frac{a_0 E_\infty^2}{\gamma} \qquad \text{Equation 17}$$

3.2.2 Jet Thinning

Once the jet has left the Taylor cone it will begin to thin due to the forces acting on it and the requirements of conservation of mass, until it impacts with the collector electrode. The thinning of the jet can be divided into two different stages. The initial stage is a period of thinning as a straight jet and the later stage is a period of thinning due to the bending instability that will be addressed later (see Section 3.2.4).

The initial thinning behaviour of the jet can be described simply with the Bernoulli principle* (Batchelor 2000). For the case of electrospinning viscid flow must be incorporated into Bernoulli's formula and electrodynamic forces replace gravity as the driving force. This treatment, such as that by Spivak et al. (2000), results in one dimensional axisymmetric differential equation (Equation 18, where $\tilde{R}$ and $\tilde{z}$ are dimensionless lengths, N_W is the relevant Webber number, N_E is the relevant Euler number and N_R is the relevant Reynolds number) that typically can be solved directly.

As the jet continues to thin its surface area increases and hence the potential for solvent loss increases. Typically at some point all the solvent is lost and the jet is no longer fluid, resulting in a change to the mode of thinning. Solidification results in a much higher portion of the stretching force being taken up by an elastic mode of stretching, hence a significant reduction in the rate of thinning (Huang et al. 2004).

$$\frac{d}{d\tilde{z}}\left\{\tilde{R}^{-4}+\left(N_W\tilde{R}\right)^{-1}-N_E^{-1}\tilde{R}^2-N_R^{-1}\left(\frac{d\tilde{R}^{-2}}{d\tilde{z}}\right)^m\right\}=1 \qquad \text{Equation 18}$$

3.2.3 Fluid Instabilities

Fluid instabilities are generally considered to be detrimental to the electrospinning process as they are the cause jet break up resulting in no fibre being produced (*i.e.* electrospraying occurs). However, the bending instability according to Reneker et al. (2001) is vital to the electrospinning process. Elimination of fluid instabilities leading to jet breakup is what differentiates electrospinning from electrospraying. Elimination can be accomplished by changing solution properties such as increasing the polymer component leading to an increase in inter-molecular interaction. Work by Hohman et al. (2001) has shown that there are typically three types of instability that may occur in the charged electrospun jet. The first is the classical Rayleigh-Plateau (Tabeling 2005) instability, the second is a similar axisymmetric instability caused by having a conductive jet and the third is the bending or "whipping" instability that will be addressed later.

The Rayleigh-Plateau instability is a phenomenon dependant on the fluid's surface tension, and is commonly observed when water from a tap breaks up from a stream

* **Bernoulli Principle**: that for an incompressible inviscid flow that the summation of all forms of mechanical energy along a streamline is constant

into droplets (see Figure 8). It occurs because the fluid attempts to minimise its surface area for a given volume. The surface area is significantly reduced if a column of water is broken up into a series of spheres. As such when a perturbation is introduced into the governing equations it is found that some of the wavelengths will grow rapidly and eventually result in the jet breaking up into droplets. Work by Shin et al. (2001) and Hohman et al. (2001) showed that this instability only occurs at low external electrostatic fields where the electric field stresses are small compared to the capillary stresses.

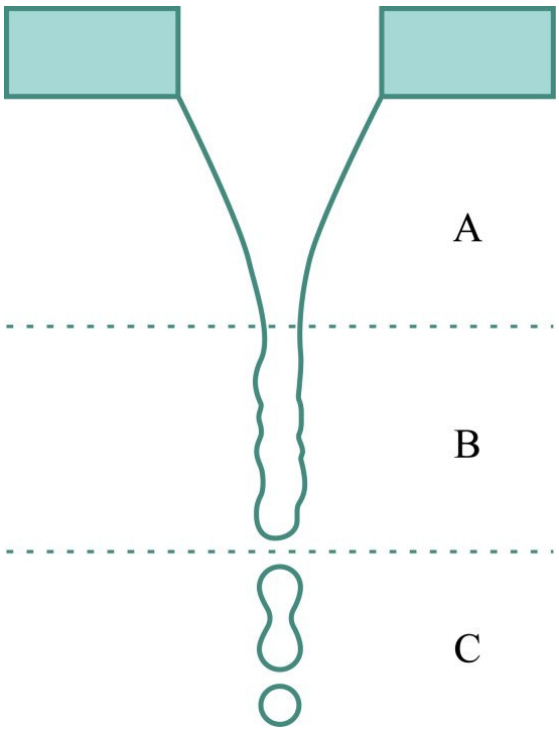

Figure 8: Rayleigh-Plateau instability where A is the stable region, B is where perturbations begin to become visible and C is when the perturbations have become larger than the radius causing droplets to form.

The second axisymmetric instability replaces the Rayleigh-Plateau instability at higher field strengths. This instability only occurs because the jet has a finite conductivity and carries an initial surface charge. In this case electrical stresses as a result of perturbation waves on the surface of the jet cause shifting of the surface charge in order to maintain a constant electric field flux in the jet column. The result of this is that the perturbation is reinforced and the jet will eventually break up into droplets. Hohman et al. (2001) found that this instability would preferentially develop rather than the desired bending instability in mathematical models unless "reasonable estimates for the surface charge density" are included in the model (example: $\sigma = 9.8 \times 10^{-8}$ C/m^2).

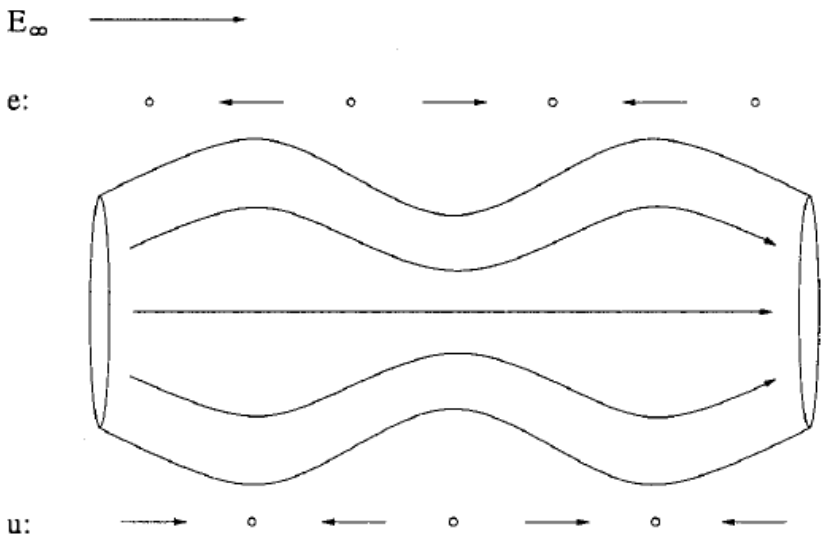

Figure 9: Axisymmetric instability for a perfectly conducting fluid column where e is the electrostatic contribution to the perturbation of the flow and u is the velocity contribution to the perturbation of the flow due to an introduced radial perturbation. Hohman et al. (2001).

Other instabilities can also occur such as another dripping mode proposed by Reznik et al. (2004). This only occurs if the surface-liquid interfacial energy for the solution and the tip is high enough to generate a contact angle of above ~0.8π radians; then excess mass is ejected from the tip of the Taylor cone to sustain a jet (Figure 10). Reznik et al. (2004) proposes this as an explanation for the large droplets sometimes ejected from the Taylor cone.

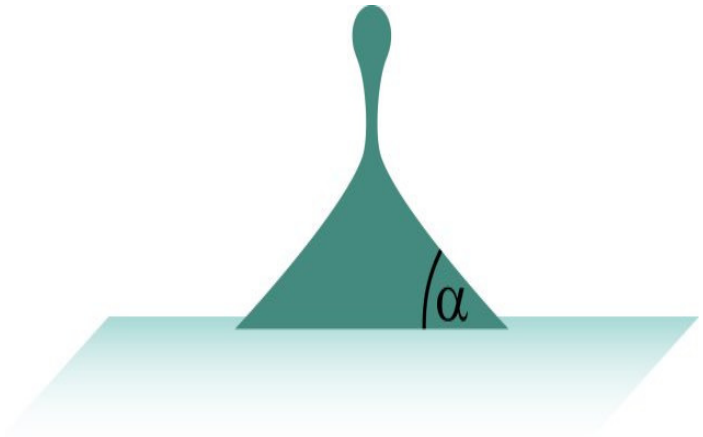

Figure 10: Formation of a droplet being ejected from the tip of a Taylor cone when the contact angle is above ~0.8π radians.

3.2.4 Bending Instability

Initially it was proposed (Doshi and Reneker 1995) that the primary mechanism for production of nanofibres was due to the surface charge reaching a critical value causing the single jet to split into multiple jets, called "splaying". However subsequent work with high speed photography using an exposure time of 18ns (Shin

et al. 2001) has shown that this "splaying" observation is simply an optical artefact caused by the speed of the fibre when the instability sets in. The true instability is a fast moving "whipping" jet that forms multiple expanding loops which eventually deposit on the collector electrode. Typically, the bending instability is idealized as a series of neatly expanding loops (see Figure 11).

This bending instability allows the jet to undergo far more stretching during its flight time than would be allowed by a simple linear jet. By taking a localized approximation of the electrostatic force between two points on a curved three dimensional fibre Yarin et al. (2001) showed it is possible to derive an equation for the force driving the bending instability (see Equation 19 where σ_S is the surface charge, L is the characteristic length, a is the jet radius, k is the jet curvature and ξ is the co-ordinate system along the central axis of the bent jet). The equation is sufficiently similar to the form of the equation for the force that drives the aerodynamic bending instability also described by Yarin et al. (1993) that substitution into previous work by Yarin et al. (1993) could be done. Yarin et al. (2001) also showed that the path of individual jet elements is such that the loops formed by the bending instability grow in radius by thinning and stretching. Experimental observations are matched by incorporation of jet solidification which limits the rapid expansion of the loops. As such, control and possibly enhancement of the bending instability currently appears to be a primary concern for the production of desired electrospun fibre properties.

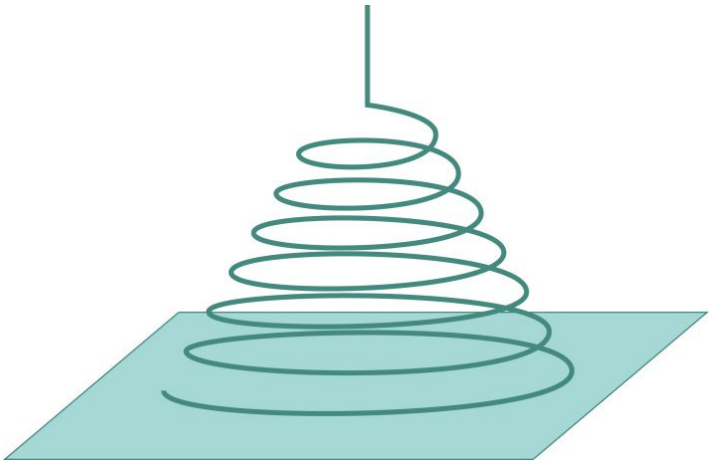

Figure 11: Typical representation of the bending instability.

$$F = -\sigma_S^2 \ln\left(\frac{L}{a}\right)|k|d\xi \qquad \text{Equation 19}$$

3.2.5 Polymer Chain Alignment

In the work by Wang et al. (2006) it was shown by calculating draw ratios that during the process of electrospinning the fibre undergoes large amounts of stress parallel to the fibre axis. Due to these draw ratios there was a consequent high degree of crystallinity. It was proposed that the high draw ratios in the electrospinning act like the drawing of a fibre in traditional fibre processing where the fibre is stretched to align the polymer chains and increase crystallinity so that the final fibres tensile strength is increased.

Zhao et al. (2004) demonstrated that if given sufficient flight time, electrospun fibre produced under a higher potential difference, hence a stronger electric field, would result in improved crystallinity. It is possible that the improved crystallinity is due to additional stretching of the jet under the action of the stronger electric field. However it could be possible that the electric field encourages the alignment of the polymer molecules and hence a stronger field would result in more molecules being aligned. This has not been widely investigated as yet.

3.3 Parameters Affecting the Process

In electrospinning, numerous parameters (Mit-Uppatham et al. 2004a) have been identified as affecting the final properties of the electrospun fibre, these factors will be explored further here. Generally speaking these parameters can be broken down into three broad categories as done by Mit-Uppatham et al. (2004a). Firstly, the properties of the solution used as the feedstock form the solution parameters category. Secondly, parameters associated with the design, geometry and operation of the electrospinning apparatus form the processing parameters category. Finally, many atmospheric and local processing environment parameters form the environmental conditions. Presented here in Table 1 is an expanded list of parameters from that previously compiled followed by a review of common parameters in literature.

Solution Parameters	Process Parameters	Environmental Conditions
Concentration	Electrostatic Potential	Temperature
Viscosity	Electric Field Strength	Humidity
Surface Tension	Electrostatic Field Shape	Local Atmosphere Flow
Conductivity	Working Distance	Atmospheric Composition
Dielectric Constant	Feed Rate	Pressure
Solvent Volatility	Orifice Diameter	

Table 1: Processing parameters that are known to affect the electrospinning process (extended from Mit-Uppatham et al. 2004a).

3.3.1 Solution Parameters

The solution volatility, dielectric constant, solution conductivity and surface tension are typically due to the choice of solvent when no additives are used. Jarusuwannapoom et al. (2004) provides an excellent study of the effects of using different solvents with a wide range of properties. When a solvent with a very low volatility is used wet fibres (i.e. appearance of a film with pores rather than a fibre mat) are collected. However if the solvent is too volatile the Taylor cone will solidify halting the production of fibre. The same study also found that the dipole moment of the solvent and the solution conductivity must both be of a sufficient level to enable electrospinning to occur.

A recent theoretical study (Thompson et al. 2007) has shown that surface tension has almost no effect on the final properties of the electrospun fibre. This finding is consistent with the work of Hohman et al. (2001) and Yarin et al. (2001) who both find that once the bending instability sets in the electric stresses are far larger than the capillary stresses. However examples such as Fong et al. (1999) show that modification of surface tension (by surfactant or solvent mixes) can assist in the formation of smooth fibres. Introduction of additives to the solution, often ionic salts, enable the modification of either the solution conductivity (Zhang et al. 2005) or surface tension (Zeng et al. 2003). For solutions with very low conductivity adding ionic salts to increase the solution conductivity has been shown to enable jet formation to occur but further addition beyond this is currently debated in the literature (see Section 5.2).

In addition to the work done by Jarusuwannapoom et al. (2004) work done by Eda et al. (2007) and Koski et al. (2004) shows the importance of polymer concentration in the solution. This is due to the requirement for a sufficient level of intermolecular interaction that will help to damp the fluid instabilities and prevent jet breakup. When the concentration is too low a deposition pattern similar to that expected for electrospraying occurs. As the concentration is raised a bead-on-a-string morphology (Fong and Reneker 1999) is observed with the beads slowly becoming more spindle-like and merging into the fibre as concentration increases. At a suitable concentration a smooth fibre is obtained. Directly linked to the polymer concentration is the solution viscosity which has been shown to be important (Megelski et al. 2002 and Deitzel et al. 2001) in both the jet initiation and the final fibre properties. As the solution viscosity increases it has been observed that the fibre diameter increases (Demir et al. 2002).

3.3.2 Processing Parameters

The operation of a typical electrospinning apparatus will involve the modification of the applied electrostatic potential, the working distance and the feed rate. Variation of the applied electrostatic potential and the working distance will also cause variation of the electric field strength. Typically researchers will look at either the electrostatic potential (Lee et al. 2004) or the electric field strength (Buchko et al. 1999). It has been found that increasing the electrostatic potential will result in thinner fibres (Megelski et al. 2002).

The working distance together with the electrostatic potential will determine the strength of the electric field. However to complicate things the working distance also changes the total flight time available to the fibre. As such in some cases increasing the working distance results in thinner fibres (Reneker et al. 2000) due to more time for the bending instability to develop and hence more time for the jet to be stretched. However in other cases increasing the working distance results in a reduction of the electric field so will result in thicker fibres (Zhong et al. 2002). However at too long or short of a distance jet initiation becomes difficult due to the electric field being too strong or weak.

Typically the electric field strength required to initiate electrospinning is a value between 0.5 and 1.5 kV/cm. If the localized electric field value exceeds the dielectric

strength for the atmosphere then a corona will be generated of which the effects are currently unknown. There are comparatively few experiments done examining the feed rate (Rutledge et al. 2001 and Zhong et al. 2002), likely due to feed rate being used as a control parameter for stabilization of the Taylor cone (see Appendix B). However in the study by Yuan et al. (2004) a low feed rate was shown to form very thin and dry fibres. Work by Rutledge et al. (2001) demonstrated with increased feed rates the fibres became much thicker and beads-on-a-string fibres were formed.

The electrode geometry and addition of secondary electrodes can be used to control deposition patterns or the extent of the bending instability. Work such as Teo et al. (2005) shows that the modification of the electric field allows control over the fibre flight and hence the modification of the final fibre alignment. In addition the design consideration of the orifice diameter for the spinning head has been examined by some authors (Mo et al. 2004 and Thompson et al. 2007). It was found that larger orifices resulted in thicker fibres (Mo et al. 2004). When the orifice size was very large it was difficult to obtain a stable Taylor cone and very small orifices become impractical as the Taylor cone will dry out or the polymer will be too viscous to flow through (Zhao et al. 2004).

3.3.3 Environmental Conditions

Environmental parameters can be divided into those that are due to the local spinning conditions or properties of the atmosphere in which the spinning takes place. The study by Kim et al. (2005) found that increasing the local temperature resulted in the solvent evaporating faster and provided a simple solution to solvents with a low rate of evaporation. For excessively volatile solvents the Taylor cone will dry out. It is possible to introduce a local flow of gas saturated with the solvent around the cone to prevent evaporation at the cone Larsen et al. (2004). Introduction of a dry gas has also been used to control the evaporation rate of the solvent in the jet (Buchko et al. 1999).

Electrospinning with an atmosphere composed of a high breakdown strength gas would enable much higher field strengths to be reached. Baumgarten (1971) found that using sulfur(VI) fluoride (SF_6), a gas with a high dielectric strength resulted in an increase in the fibre diameter. It was asserted by Ramakrishna et al. (2006) that "generally, reduction in the pressure surrounding the electrospinning jet does not

improve the electrospinning process". However due to the lower vapour pressure under a vacuum solvent loss would be faster and could solve the problem of low evaporation rate solvents. Humidity has been shown by Casper et al. (2004) and Megelski et al. (2002) to allow control over the formation of micro pores on the surface of the individual fibre.

3.4 Core Apparatus

In its simplest form an electrospinning apparatus need not be anything more than a high voltage power supply, a drop of polymer solution and an earthed electrode (Figure 12). The often quoted 1934 patent by Formhals shows an apparatus not far removed from the basic elements required (Figure 13). A typical electrospinning apparatus used in research, such as those produced by Electrospinz, Blenheim, New Zealand (Figure 14), consists of a polymer supply, a high voltage electrode, a spinning head* and a collector electrode.

The polymer is supplied to the capillary tip in order to form a hemispherical droplet by either a pressure system or a syringe pump. This depends on if the designer considers constant volume or constant pressure to be preferable. Constant pressure is typically provided by either a gravity fed constant head system (see Appendix B, Section 4) or an air pressure system. Constant volume flow rate is typically supplied by a syringe pump (Gupta and Wilkes 2003).

The high voltage electrode is used to conduct the charge to the polymer solution. It typically is constructed from a syringe needle (Buchko et al. 1999) and takes on the additional role of being the spinning head. Another common method of charging the solution is a bare wire and inserted into the polymer solution (Doshi and Reneker 1995).

Collector electrodes come in many shapes and sizes but are commonly some form of flat metallic sheet (Mit-Uppatham et al. 2004b). This electrode is typically connected to ground, hence carrying the opposite charge to the high voltage electrode. They are often mounted in such a way to allow their position relative to the spinning head to be changed.

* **Spinning Head**: Describes either a metal capillary or some other nozzle or orifice that the polymer solution or melt is supplied through

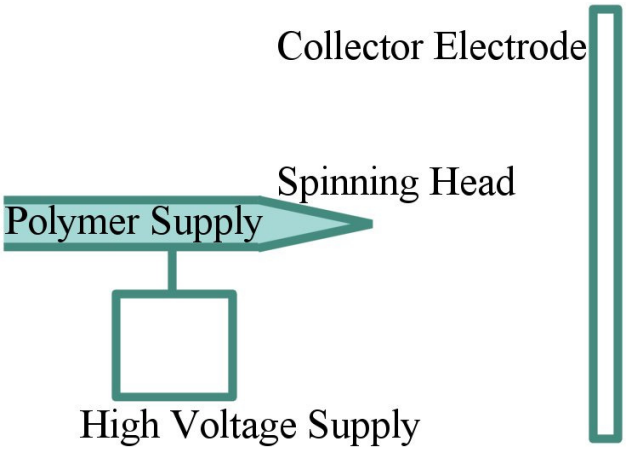

Figure 12: Simple elements required for electrospinning.

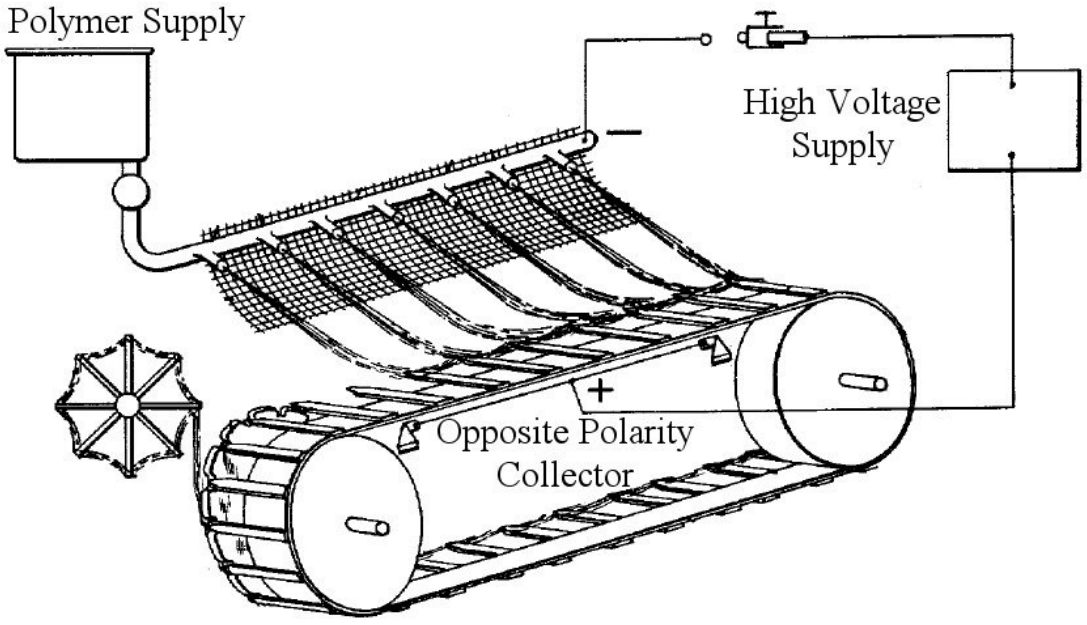

Figure 13: Diagram of the apparatus proposed by Formhals (Formhals 1938).

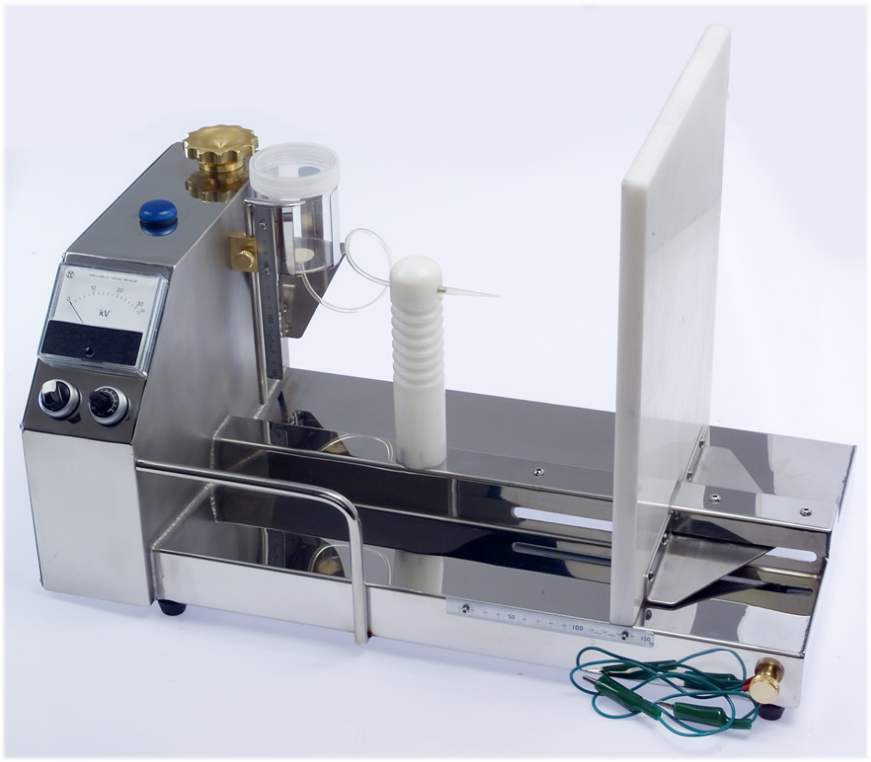

Figure 14: Electrospinz ES1 apparatus.

3.5 Modifications and Additions to Core Apparatus

3.5.1 Polymer Supply Modifications

Typical motivation for the modification of the polymer supply is to increase the quantity of electrospun fibre produced. One of the earliest modifications to the polymer supply mechanism is to have a supply to multiple spinning heads (Fang et al. 2003). Following a similar line of thinking an unusual method was developed by Yarin and Zussman (2004) whereby floating a layer of polymer solution on top of a layer of mineral oil containing magnetic particles the application of a magnetic field resulted in the formation of multiple spikes in the fluid that jets can be evolved from.

A recently commercialized method is to use a roller partially immersed in a bath of polymer solution. The roller acts as the polymer charging electrode and the polymer supply mechanism as a thin film is maintained on its surface. This patented process is capable of producing numerous jets from the top of the roller allowing continuous sheets of an electrospun mat to be produced (Jirsak et al. 2006).

Another useful modification is the addition of a gas flow around the capillary that the polymer is electrospun from. The gas can be an inert gas used to aerodynamically control the jet behaviour (Lin et al. 2008) or a gas that is saturated with solvent to

prevent a volatile polymer-solvent mixture from drying out at the end of the capillary before electrospinning can occur.

Hollow or composite nanofibres can be produced by using a nested capillary such as demonstrated by Li and Xia (2004). Here the centre capillary is supplied with mineral oil and the outer capillary is supplied with poly(vinyl pyrrolidone). After spinning the mineral oil is removed via pyrolysis leaving a hollow fibre.

3.5.2 Electrostatic Field Modifications

Three approaches are taken to modification of the electrostatic field. One is to modify the field at the capillary where the polymer is electrospun from. Another is to perform modifications to the collector that will be discussed further in Section 3.4.3. Beyond modifications to the existing electric field, the introduction of a new external electric field has also been proposed.

One approach to electric field modification at the capillary is to surround the capillary with a poly(vinyl chloride) (PVC) tube. Yang et al. (2008) proposes that this will create a more uniform and concentrated electric field leading to better control of the fibre deposition. Work by Kim (2006) demonstrated the use of an auxiliary electrode placed around the capillary that was charged from the same power supply as the polymer solution in the capillary. It was found that this auxiliary electrode stabilized the initial straight portion of the jet.

Use of an auxiliary electrode is normally the only way to introduce a new external electric field. The work by Dabirian et al. (2007) used a negatively charged bar to direct the electrospun jet towards a rotating collector. In the work by Gu et al. (2007) an auxiliary electrode was used to create twisted nano-fibre yarns. The introduction of two parallel bars in the path of the electrospun fibre allowed Chuangchote and Supaphol (2006) to collect a mat of both aligned fibres from the parallel bars and a random orientated mat deposited on the collector behind the bars.

3.5.3 Collector Modifications

A typical motivation for the modification of the collector from a flat metal sheet is to provoke some degree of alignment in the deposited fibres. This is demonstrated by the widely reported use of a rotating mandrel and parallel bars to form aligned mats. Some methods of polymer supply have geometries that can be taken advantage of in

the collector shape. In the patent by Jirsak et al. (2006) the polymer is supplied from the surface of a cylinder. Jirsak et al. (2006) describes a collector that has a shape formed from half a cylinder making it equidistance from the top half of the polymer supply. One interesting modification of the collector that has a different modification is that of Simonet et al. (2007). Here the refrigeration of the collector allows the formation of ice crystals as the electrospun fibre is deposited. These ice crystals can then be used as a removable void template to create a porous 3D polymer mesh.

A good example of the use of a rotating mandrel is shown in the work by Sundaray et al. (2004) where the use of a high speed rotating mandrel is shown to produce aligned fibres. Sundaray et al. (2004) also takes it a step further and uses an insulating mandrel with a sharp moving pin as the counter electrode to reduce the size of the deposition area concentrating the aligned fibres. Work by Teo and Ramakrishna (2005) used a similar concept by taking a rotating knife edged disk as their collector. They were able to collect a mat of aligned hollow fibres.

The first patent by Formhals (1934) described a toothed belt where each tooth acted as a collector electrode. It was proposed that this arrangement would result in the production of a continuous tow of aligned fibre that could later be processed by standard textile means. A good example of the use of parallel bars to allow the alignment of electrospun fibre is shown in the work by Li et al. (2004). Here the parallel bars that are used are gold electrodes mounted on a quartz substrate that under the action of fast switching of each electrode to ground the fibres will jump between two bars creating an aligned mat. This was then extended to multiple axes on the 2D substrate to create layers of aligned fibres in different directions. Another example of such a technique is shown in the work by Li et al. (2004) and Li et al. (2005).

4. APPLICATIONS

Interest in electrospinning for real world applications is due to three aspects of the electrospinning process. First the size of the fibre is in the nano scale leading to different modes of interaction with other materials compared to macro scale materials. Second is that due to the high draw ratio it is expected that the fibres produced will have exceptional strength. Third is that the fibres produced inherently have a high surface area to volume ratio. Combinations of these three aspects give rise to

applications in filtration, cellular matrices, catalyst substrates, ultra strong composites, bio reactors, functional textiles, drug encapsulation and wound dressing.

5. MODIFICATION OF CHARGE IN ELECTROSPINNING

5.1 Opening Remarks

In Section 3.2 of Chapter 2 the effects of charge on the electrospinning process are discussed. In the theoretical modelling work by Reznik et al. (2004), Hohman et al. (2001), Yarin et al. (2001), Reneker et al. (2000) and Feng et al. (2002) the charge, be it surface charge or charge density, plays a vital role in shaping how the electrospinning process behaves. It is however difficult to modify the quantity or nature of the charge in electrospinning without modifying the type of polymer and solvent, hence changing most of the solution properties (see Section 3.3.1). Two methods that have been asserted to modify the quantity and nature of charge in electrospinning; the addition of an ionic salt and changing the sign of the charge induced in the polymer solution at the spinning head will be explored further here. Additionally some authors have asserted that the size of ions will affect the electrospinning process. Possibly due to a potential limit on the number of ions that can co-exist on the surface hence a limit on the surface charge density that can be achieved.

5.2 Literature Relevant to the Effect of Ionic Salt Addition

There has been little work done on the general principle of adding ionic salts to modify the conductivity of the polymer solution. However, it has been shown that an increase in conductivity would result in an increase in the fibre diameter (Demir et al., 2002, Mit-uppatham et al., 2004, Qin et al., 2007). However in far more papers the effect of conductivity has been proposed to cause a decrease in the fibre diameter (Choi et al., 2004, Zeng et al., 2003, Li et al., 2006, Son et al., 2005, Son et al., 2004b, Son et al., 2004a, Zhang et al., 2005).

In the work by Choi et al. (2004) the addition of benzyl trimethyl ammonium chloride to poly(3-hydroxybutyrate) dissolved in chloroform resulted in an increase in conductivity. With only the addition of 0.1% wt. of salt the fibre diameter decreased from 2.6 μm to ~1.2 μm. Further addition of salt did not appear to decrease the fibre diameter significantly. The work by Zhang et al. (2005) involved the addition of

NaCl to PVOH dissolved in water resulting in an increase in conductivity. With the addition of 0.05% wt. of salt the fibre diameter decreased from 214 ± 19 nm to 190 ± 19 nm. Although this puts the decrease within the limits of error further addition resulted in the average fibre diameter continuing to decrease suggesting that the decrease may be valid.

The results of Son et al. (2005) showed that by changing the pH of a PVOH solution the conductivity increases significantly. This was true for acidic or basic conditions. Electrospinning was undertaken using a positive voltage. The pH was modified using HCl and NaOH. It was found that under acidic conditions electrospinning was not continuous and resulted in a "beads-on-a-string" structure as well as typically similar fibre diameter to that of neutral pH. However for basic conditions the increase in conductivity resulted in gradually thinning fibres from 290 nm to 240 nm. It was observed that the rate of thinning was not directly related to the fibre diameter as each increase in conductivity result in a smaller decrease in diameter. However, this may correspond to an inverse relationship with an asymptote just below 240 nm. Further to this in the work by Son et al. (2004b) involved a similar experiment outlined above for cellulose acetate from an acetone/water mixed solvent (15% wt. water). The pH was modified using formic acid and ammonia solution. Under acidic conditions there was a slight increase in fibre diameter whereas under basic conditions there was a significant decrease in fibre diameter. This is ambiguous as to the effects of conductivity as this was not measured but follows a similar trend to the work for PVOH.

In the further work of Son et al. (2004a) a polyelectrolyte was used to increase the conductivity of poly(ethylene oxide) dissolved in water. The polyelectrolytes used were poly(allylamine hydrochloride) (PAH) and poly(acrylic acid sodium salt) (PAA). The addition of these polyelectrolytes up to 4% wt. did not significantly change the solution viscosity or surface tension. A steady increase in conductivity was observed for both polyelectrolytes with similar values at each concentration. These solutions were electrospun using a positive voltage. For PAH the fibre diameter decreased from 0.4 μm to ~0.175 μm with only 0.1% wt. of PAH. This showed an approximately inverse relationship with an asymptote at ~0.125 μm. For PAA the fibre diameter decreased from 0.4 μm to ~0.2 μm with only 0.1% wt. of

PAA. This showed an approximately inverse relationship with an asymptote at ~0.14 μm.

Work by Zeng et al. (2003) involved the addition of three different surfactants triethyl benzyl ammonium chloride, sodium dodecyl sulphate and aliphatic PPO-PEO ether. The addition of the ionic surfactant is expected to increase the conductivity however this was not measured explicitly. The result was that with the addition of each surfactant the electrospun solution would result in significantly thinner fibres and a narrower distribution. The ionic surfactant outperformed the other surfactants by a 2:1 margin. Specifically the control solution had a distribution of 0.34 - 4.20 μm compared to the non-ionic surfactants having ~0.45 – 1.35 μm. The ionic surfactant however resulted in a distribution of 0.36 – 0.5 μm. This suggests that an increase in conductivity results in a thinner average fibre.

The work by Li et al. (2006) used a gelatin dissolved in 1,1,1,3,3,3-hexafluoro-2-propanol and blended in quantities of polyaniline, a conductive polymer. Unfortunately other changes in properties such as viscosity or surface tension were not measured but changes in conductivity were tabulated. The result was that as conductivity increased the fibre diameter decreased from ~800 nm to ~50nm.

The work of Demir et al. (2002) used polyurethane dissolved in dimethyl formamide (DMF) and added triethyl benzyl ammonium chloride as an ionic surfactant. It was measured that with the increase in ionic salt the total mass ejected from the tip increased. This suggests that there would be either thicker fibres, more fibre or both. As with the work by Zeng et al. (2003) it is unclear if the effect is due to the surfactant effect or due to the change in conductivity.

5.3 Literature Relevant to the Effect of Ion Size

There has been less work done on the effect of ion size. In the work by Mit-uppatham et al. (2004) three different metal chlorides were added to solutions of 85% formic acid in different concentrations and electrospun with a positive voltage. The order of final fibre diameter was LiCl > NaCl > $MgCl_2$ > no salt. This also matches the order of solution conductivity. However the order of ionic radii for a decahedral crystalline matrix is $Na^+ > Li^+ > Mg^{2+}$. It should be pointed out that the fibre diameters for NaCl

and $MgCl_2$ are almost indistinguishable. Based on this it implies that ionic radius is irrelevant as Mg^{2+} ions are significantly smaller than Na^+ ions.

In the work by Qin et al. (2007) four different salts are added at 1% wt. to solutions of DMF and electrospun with an unknown polarity voltage. The order of final fibre diameter was LiCl > $NaNO_3$ > $CaCl_2$ > NaCl > no salt. Again this was the same order as the conductivity measured. The order for ionic radii for a decahedral crystalline matrix is $Na^+ > Ca^{2+} > Li^+$. If the polarity of the supply voltage was negative then all the ionic size is obviously $NO_3^- > Cl^-$. Again the order of ionic radii has no similarity to the order of fibre diameter.

In the work by Zong et al. (2002) three different ionic salts were added at 1% wt. to solutions of DMF and electrospun with a positive voltage. The order of final fibre diameter was KH_2PO_4 > NaH_2PO_4 > NaCl > no salt. The order of conductivity in the case is unknown as it was not measured. The order of ionic radii for a decahedral crystalline matrix is $K^+ > Na^+$. Here the order of ionic radii does seem to have some bearing on the fibre diameter. It should be noted that KH_2PO_4 was observed to have a significantly higher fibre diameter than that of both of the Na salts. Of the papers reviewed there have been none that examine ion size in aqueous solutions, hence much of tabulated literature used to analyse the results cannot be assumed to be correct.

5.4 Literature Relevant to Changing the Sign of the Charge on the Polymer Solution

Little work has been published on the effects of the sign of the charge on the polymer charging electrode. In the work by Mit-Uppatham et al. (2004) and Supaphol et al. (2005) polyamide-6 (PA-6) dissolved in formic acid. In both cases it was found that a negative charge on the polymer solution resulted in a thicker fibre and a larger deposition area with a lower density of fibre. Sutasinpromprae et al. (2006) used poly(acrylonitrile) (PAN) dissolved in dimethylformamide (DMF). It was observed that no significant difference in the fibre morphology resulted from changing the sign of the charge on the polymer solution. These observations were explained by the authors as a result of the existence and mobility of polymer ions formed when the polymer solution is prepared. In the case of the PAN / DMF it is claimed that PAN

does not form any charged species when dissolved and hence no difference in the charged species available when spinning.

5.5 Aims and Objectives of this Dissertation

This dissertations primary aim is to investigate deeper into the nature and mechanism of charge in the electrospinning solution. Beyond the assumptions made by Reznik et al. (2004), Hohman et al. (2001), Yarin et al. (2001), Reneker et al. (2000) and Feng et al. (2002) in order to produce working theoretical models there has been little systematic work that investigates the mechanisms for the generation and subsequent transport of charge between the two electrospinning electrodes. It can be seen from Section 5.2 and Section 5.3 that the effects of adding an ionic salt it currently unclear. It will be later shown that the mechanism proposed for the behaviour when the opposite sign of charge is induced in the polymer solution during electrospinning fails to predict the observed behaviour for poly(vinyl alcohol) (PVOH).

In order to achieve the primary aim, the results from two experiments, the addition of ionic salt to a PVOH solution and changing the sign of the charge induced in the polymer solution will be examined. With the addition of an ionic salt there is little change in the solution properties other than the conductivity. By examining how changes in conductivity and the subsequent changes in the charge carrier availability affect the electrospinning process a deeper understanding of the charge transport mechanisms may be obtained. By changing the sign of the charge induced in the polymer solution and determining if there is any response will show if the generation of charge carriers has any dependence on their sign.

CHAPTER 3

EXPERIMENTAL METHOD

EXPERIMENTAL METHOD

1. GENERAL EXPERIMENTAL METHOD

1.1 Experimental Materials

Electrospinning was carried out using poly(vinyl alcohol) (PVOH) (Chemiplas NZ limited, Wellington, NZ) with an average molecular weight of 118,000 $gmol^{-1}$ and a degree of hydrolysis (DH) range of 85-90%. The polymer solution was prepared by dissolving PVOH in distilled water for approximately 2 hrs at 60°C with constant stirring at 500 rev/min using an overhead stirrer with an impeller blade. The polymer concentration of the stock solution was determined using a Buchi Rotavapor (model B-114) at 60^{o}C to find the percentage by weight of PVOH in solution. This was done as it is impossible to prevent some solvent escaping and impossible to quantify the amount of solvent lost to a high degree of accuracy. The stock solution was diluted to required concentrations with distilled water at room temperature and stirred to uniformity (approximately 90s).

Ionic salts used to modify the conductivity of the solutions were purchased from Sigma-Aldrich and used as received. The salts used were Lithium Chloride (LiCl), Lithium Bromide (LiBr), Lithium Fluoride (LiF), Sodium Chloride (NaCl) and Potassium Chloride (KCl). As all the ionic salts are alkali halides dissolved in water the general electrostatic environment should be approximately the same for all the ions. This then allows the order of ionic radii to be directly read from a periodic table with increasing size as one moves from left to right or from the top to the bottom. The order of ionic radii for the cations is then $K^+ > Na^+ > Li^+$. For the anions the order is then $Br^- > Cl^- > F^-$. This gives a range of different ionic radii for both anions and cations, solubility and molar conductivities (CRC-Press, 2004) (see Table 2).

Ionic Salt	Molar Conductivity [mS/cm.mol]	Solubility in water @ STP
LiF	94.1	0.16g/100mL
LiBr	116.8	160g/100mL
LiCl	115.0	83.5g/100mL
NaCl	123.4	35.9g/100mL
KCl	150.0	34.2g/100mL

Table 2: Selected properties of ionic salts used in these experiments.

1.2 Electrospinning Apparatus

All electrospinning was performed on a laboratory scale electrospinning apparatus (see Section 3.4, Chapter 2). The apparatus used was the ES1 (see Appendix B, Section 4) model purchased from Electrospinz, New Zealand as shown in Figure 15. The ES1 model is capable of varying the working distance (distance between the tip and the collector), the potential difference between tip and collector and the hydrostatic pressure at the spinning tip. The apparatus consists of a stainless steel chassis with a central insulating column made from Acetal* that houses an electrode to charge the polymer and a movable insulating back plane also made from Acetal. The Taylor cone is formed at the end of a disposable polypropylene micropipette tip secured to a conducting insert retained in the central insulating column facing the insulating backplane (see Figure 15).

The insulating back plane travels on a set of linear bearings giving a working distance of between 0mm to 150mm. The central insulating column has a stainless steel insert that conducts the positive high voltage from the integral power supply to the solution flowing through it. The power supply provides a potential difference range of 0 to 33,000 volts. Polymer solution is held in a movable header tank providing a constant delivery pressure over short periods of time. The height of the header tank relative to the spinning tip has a range between 0mm to 150mm. The hydrostatic pressure this represents is dependent on the orifice diameter of the plastic tip used.

The polypropylene pipette tip used was an Axygen T-200-Y 200 μL pipette tip with an orifice diameter of 0.8 mm. Measurements of the processing parameters was done to an accuracy of ± 1 mm for the working distance, ± 250 V for the potential difference and ± 0.5 mm for the head distance that gives the hydrostatic pressure.

* Also commonly known as Polyoxymethlene (POM) or under DuPont's brand name Delrin

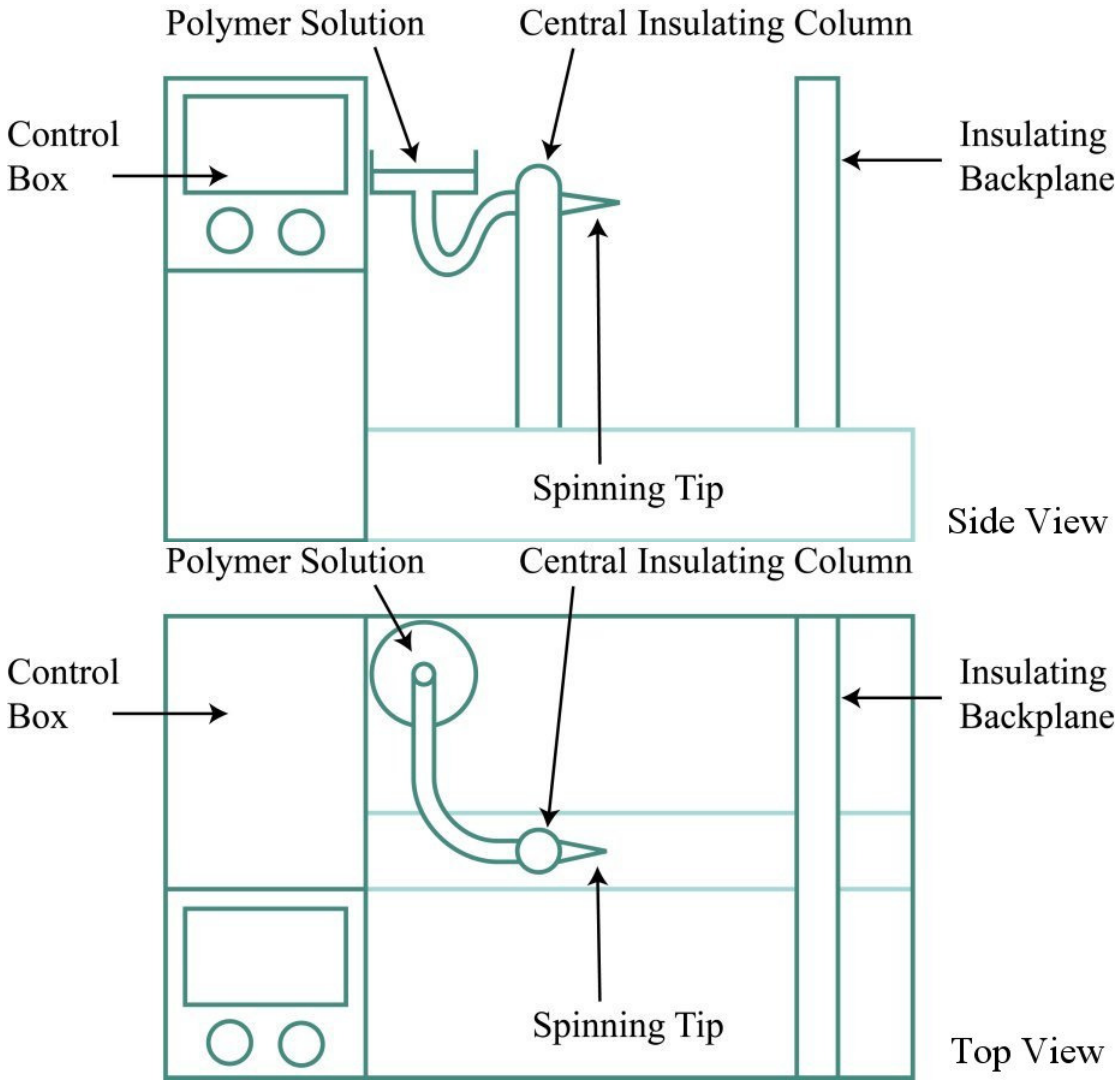

Figure 15: Schematic of the important features of the ES1 model electrospinning apparatus.

1.3 Samples

Each sample was produced on a separate collector electrode made from 15 cm x 15 cm sheets of aluminium. Each sample represents 15 minutes (900 s) of fibre deposition to ensure any jet variations over a long timescale were minimized and that enough mass to measure accumulates. Any samples where electrospraying occurs during the fibre deposition are rejected and a replacement sample was produced as the weight of the polymer from the electrosprayed droplets is comparable to the weight of the spun fibre mat and obscures the electrospinning mass deposition rate. Each sample was allowed to dry for at least 8 hours in an air conditioned lab (RH 40% temperature 25°C) before the final weight was measured.

1.4 Measurements

The mass deposition rate was taken to be the final weight of the collector electrode minus the initial weight of the collector electrode. Between each weighing the collector electrodes were handled with laboratory gloves and were dried while protected from potential airborne contaminants. A Mettler Toledo AG204 (accuracy to 0.0001g) four figure micro balance was used to weigh the collector electrodes. It was found that stability of the measurement increased if the electrode was placed on the balance pan, the balance was zeroed and the measured value was then read to be the difference in weight once the sample was removed. As such this method was used to improve accuracy using this balance. Each recorded weight was taken to be the average of 3 different measurements, each with a different orientation of the electrode on the balance pan.

The electrical current was measured with a Metrix MX0056C multimeter with a DC current resolution of 10nA. This multimeter was connected in series between the collector electrode and ground. The recorded current was taken to be the maximum current observed at approximately 450 s of each samples timed collection. This was done as some samples are particularly unstable in maintaining a jet and hence it was assumed that the peak current would correspond to the current flowing when the jet is in a typical stable mode.

Images of the electrospun fibre were collected using a Cambridge Instruments Stereoscan 90 scanning electron microscope at a 25 kV accelerating voltage. A 20mm electron microscope stub was first prepared with carbon tape and then pressed to the electrospun fibre mat and removed. This ensured that the top layers of the fibre mat would be attached to the stub and observed; as would have happened had the sample been directly mounted. This sample was then sputtered with gold using a Polaron sputtering apparatus. Once in the electron microscope the sample was divided into 4 quarters and 3 images were taken from quasi-random positions on each quarter. The selection method involved moving an unspecified distance in the x and y co-ordinate and then making fine corrections to ensure the image would contain a number of fibre sections that were smooth and continuous. Defects on fibres that were considered undesirable were the “bead on a string” morphology (Fong and Reneker 1999), junctions close together or multiple fibres merging into a single fibre.

These were avoided as they do not represent the true diameter of the fibre directly before impact with the collector. This ensures the fibre diameter measured is as close as possible to the final diameter of the jet after being stretched by the bending instability but just before it impacts the collector electrode.

1.5 Data Analysis

Fibre diameter was determined from the scanning electron microscopy (SEM) images using and an image analysis package (UTHSCSA ImageTool program (developed at the University of Texas Health Science Center at San Antonio, Texas[*]). The reported average fibre diameter was based on a minimum of 300 fibre diameters measured at a number of sites on the electrospun mat for each sample. Each fibre diameter was chosen in order to exclude any of the defects mentioned in the measurements section. All statistical analysis was performed with Minitab® Statistical Software version 15 (Minitab Inc., Pennsylvania, USA[†]) using the suggested program default settings.

2. EFFECT OF IONIC SALT ON AN 8% WT. PVOH SOLUTION

2.1 Statistical Analysis of the Electrospinning Process

Initially it is important to define a base line both for the expected behaviour of a known concentration of PVOH solution and for the expected variation between runs in the electrospinning process. To achieve this goal, six solutions of PVOH were prepared and samples were electrospun from each solution as described in Section 1.3. The solutions were prepared from the stock solution of PVOH described in Section 1.1 by diluting to 8% by weight. These dilutions have between 2 hours to 2 days of time between each preparation.

Directly after preparation of a solution three samples were electrospun with a potential difference of 7kV and working distance of 10cm. The mass deposition rate and electrical current were measured for each sample as described in Section 1.4. Of the three samples produced for each solution the sample with the median deposition rate was selected to obtain SEM images as described in Section 1.4. These images were then analysed as described in Section 1.5 to obtain the average fibre diameter for each solution prepared.

---

[*] available from the Internet by anonymous FTP from ftp://maxrad6.uthscsa.edu)
[†] web address www.minitab.com

2.2 Effect of Ionic Salt on the Electrospinning Process

A slightly different method is used to determine the effect of adding an ionic salt to a polymer solution being used in the electrospinning process. From the stock solution of PVOH described in Section 1.1 a dilution to 8% of PVOH by weight was prepared. Using the ionic salts described in Section 1.1 a series of solutions are prepared by the addition of one of these salts.

For each ionic salt two solutions are prepared at a concentration of 0.1% by weight of ionic salt relative to the total mass of the PVOH solution. After the salt was added the solution was stirred for a minimum of 30 minutes and visually inspected to ensure all the salt was dissolved. Two samples were then electrospun from each solution at a potential difference of 7kV and a working distance of 10cm as described in Section 1.3. The mass deposition rate and electric current were measured as described in Section 1.4.

Once the samples have been collected salt was added to each solution to increase the concentration to 0.25% by weight and the procedure of collecting samples was repeated. A further addition of salt to increase the concentration to 0.5% by weight was done to give a total set 12 samples per salt from 2 solutions per salt with concentrations of 0.1%, 0.25% and 0.5% by weight producing 2 samples per concentration and solution.

Deviation from the above standard experimental method occurred for KCl and LiF. These deviations are primarily motivated due to time restrictions. KCl was used for the initial feasibility study of this experimental technique. This early experiment used one solution and 3 samples were produced for each concentration of salt. The potential difference, working distance and salt and polymer concentrations were all kept the same as the above standard method.

LiF is almost insoluble in water so it is not compatible with the above standard experimental method. One solution was used and 3 samples were produced for each concentration. The concentrations are 0.01%, 0.025% and 0.1% by weight due to 0.1% by weight being close to the solubility limit. The potential difference and working distance are kept the same as the above standard method.

For each set of samples electrospun from a solution at different concentrations of salt a sample was selected for SEM as described in Section 1.4. For sets of two the sample closest to the mean deposition rate for that ionic salt was selected. For sets of three the sample with the median deposition rate was selected. The average fibre diameter was then determined as described in Section 1.5. For the standard experimental method described above the final average fibre diameter for each salt concentration was the average of the two samples selected for SEM.

3. FURTHER INVESTIGATION OF THE INITIAL JET DIAMETER

After examining the results of the experiment described in Section 2 a further experiment was preformed to test an aspect of the developed theory. It was thought that a lower mass deposition rate would correspond to a thinner initial jet diameter. Hence the initial jet diameter and the deposition rate were measured for a number of different conditions.

Two solutions were prepared from the stock solution of PVOH described in Section 1.1 by diluting to 8% by weight. One solution was prepared with a concentration of 0.25% by weight of NaCl relative to the total mass of the PVOH solution. After the salt was added this solution was stirred for a minimum of 30 minutes and visually inspected to ensure all the salt was dissolved. The other solution was used without further modifications. Four samples were then electrospun from each solution at a potential difference of 7kV and a working distance of 10cm as described in Section 1.3. An additional four samples were then electrospun using the same conditions but with a negative charge from the power supply.

Each sample was produced on the ES4 (see appendix B, Section 4) model of electrospinning apparatus from Electrospinz, Blenheim, New Zealand. The ES4 model contains the exact same layout at the ES1 model described in Section 1.2 (see Figure 15) however has an additional central column and spinning tip mounted on the opposite side of the insulating backplane that is connected to a negative power supply. In effect it can be treated as two ES1 models (see Figure 15), one with a positive power supply and the other with a negative supply. The mass deposition rate was measured as described in Section 1.4. The initial jet diameter was measured using a digital USB microscope (Model QX5, Digital Blue Corp.); operating at 60 x

magnification and calibrated using a standard calibration slide. The diameter of the jet was then measured using the image analysis software described in Section 1.5 at a distance of 100 microns from the simulated surface of the droplet without the Taylor cone.

CHAPTER 4

EXPERIMENTAL RESULTS AND ANALYSIS

EXPERIMENTAL RESULTS AND ANALYSIS

1. STATISTICAL ANALYSIS OF THE ELECTROSPINNING PROCESS

1.1 Fibre Diameter Distributions of Electrospun PVOH

Measurement of the average fibre diameter resulted in a large data set of individual fibre diameters for each sample examined. An example of the data set obtained is shown in Figure 16. The distribution of fibre diameters has the appearance of a skewed normal distribution (see Figure 17). The skew on the distribution is probably an artefact of the measuring method (see Chapter 3, Section 1.4 and 1.5). When measuring individual fibre diameters in some cases it is impossible to identify if the fibre is a single fibre. Therefore, for the purposes of this analysis the mode of the distribution was selected as the representative statistic. This gives a fibre diameter at the centre of the highest peak in the data set that is assumed to represent the average diameter of the fibre the moment before impact with the collector.

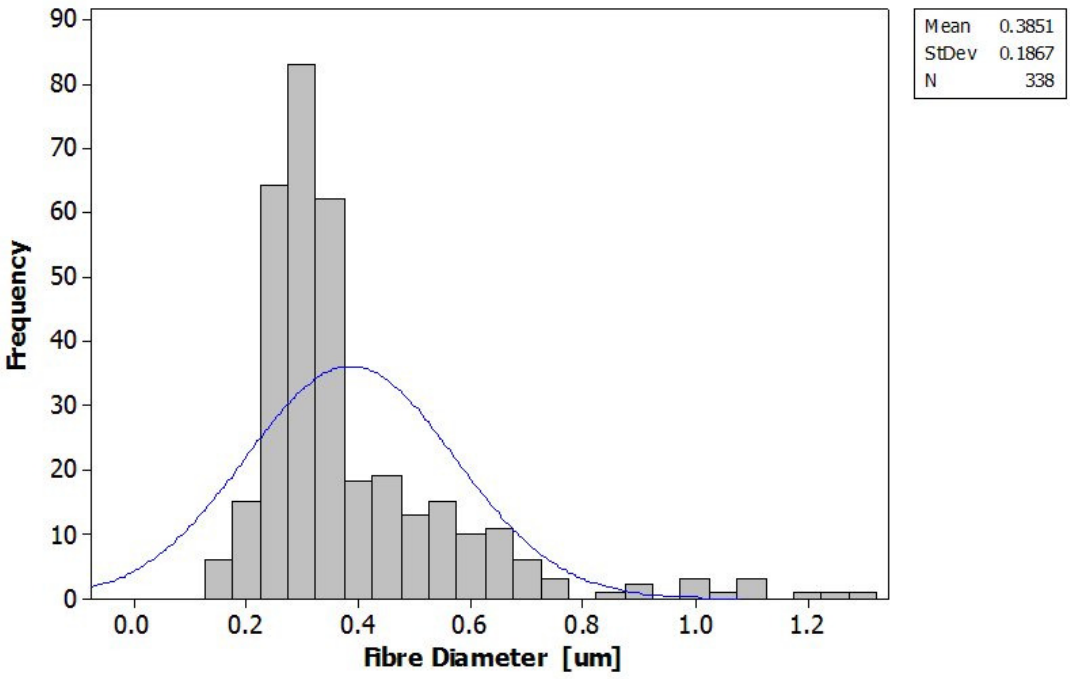

Figure 16: Distribution of fibre diameters for a typical sample of 8% PVOH.

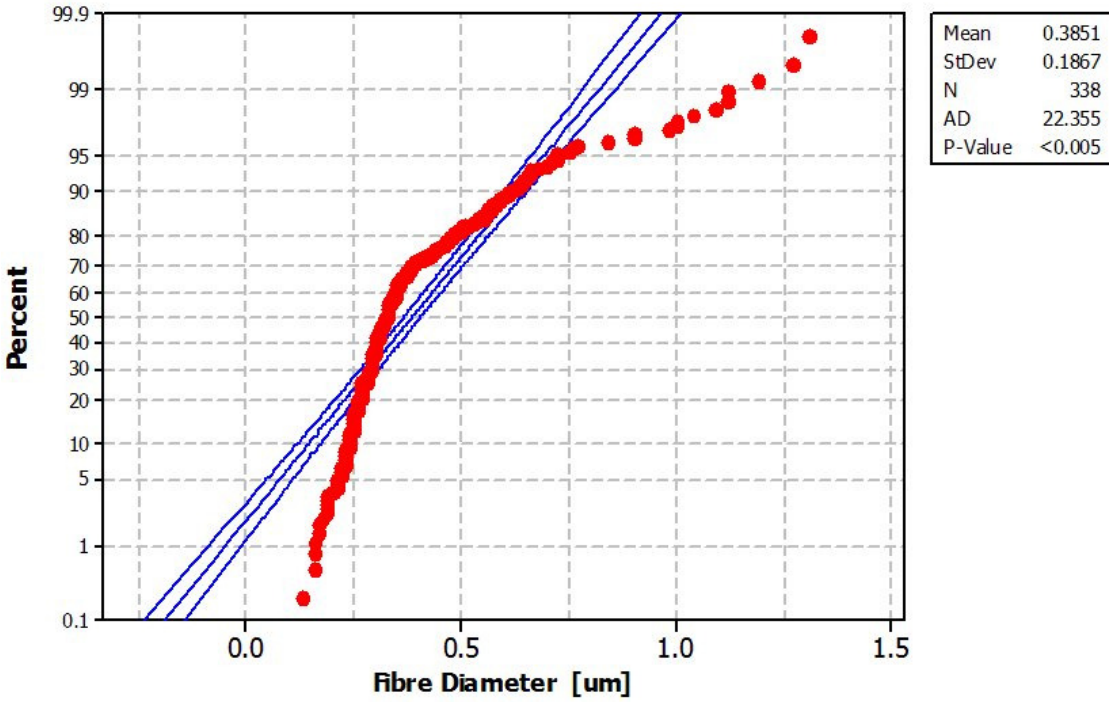

Figure 17: Normal distribution plot of the example data set showing the skewed distribution (confidence interval of 95%).

1.2 Statistical Variation of the Mass Deposition Rate and Electric Current when Electrospinning PVOH

In order to establish the expected level of variation between each experiment an analysis of variance (ANOVA) is performed for the deposition rate and electric current (see Table 3 and Table 4). Note that an ANOVA cannot be performed on the results for the average fibre diameter as there was only one sample examined per experiment. The variance between runs for deposition rate and current has been taken to be the minimum standard deviation to be expected for further observations in this experiment. This standard deviation can then be used to build an expected variation range; in this case it has been chosen to be three standard deviations meaning that there is a 95% confidence that any measured value that lies within the variation range will be from the same sample group. Taking the average of all the samples from all experiments using plain 8% PVOH gives values that can be used as levels of significance for further observations in this experiment. Table 5 shows the control values with the tolerance range.

Source of Variation	Degrees of Freedom	Mean Squares
Between Experiments	5	1.6×10^{-5}
Between Samples	12	7.6×10^{-6}
Total	17	

Table 3: Results of the ANOVA performed on the measured mass deposition rates for 8% PVOH.

Source of Variation	Degrees of Freedom	Mean Squares
Between Experiments	5	2.4×10^{-15}
Between Samples	12	5.0×10^{-17}
Total	17	

Table 4: Results of the ANOVA performed on the measured electric current for 8% PVOH.

Deposition Rate [g/h]	Current Flow [A]	Fibre Diameter [m]
$0.0117 +/- 4.8 \times 10^{-5}$	$4.0 \times 10^{-7} +/- 7.1 \times 10^{-15}$	2.60×10^{-7}

Table 5: Averaged measurements for the collected electrospun samples from 8% PVOH solution.

2. EFFECT OF IONIC SALT ADDITION ON THE ELECTROSPINNING OF PVOH SOLUTION

2.1 Raw Data Measured as a Response to the Addition of an Ionic Salt

In this series of experiments the independent variable is the concentration of ionic salt added to the 8% PVOH solution. As an initial examination of the data it was firstly determined whether there were any obvious relationships between the measured dependant variables and ionic salt concentration. The average values from the raw data collected are displayed in Table 6. It was observed that with the addition of an ionic salt there was a decrease in the mass deposition rate and fibre diameter but an increase in the electric current. Without further analysis it is unclear how the different salts behave relative to each other. It can be noted that at the lowest concentration the addition of LiF results in a higher deposition rate. Also the fibre diameter for LiCl and the deposition rate for NaCl show strong nonlinearity in their results.

Concentration of Ionic Salt	Concentration of Ionic Salt [mol/L]	Mass Deposition Rate* [g/h]	Electric Current* [μA]	Fibre Diameter* [nm]
Plain 8% PVOH				
0% wt.	0	0.0117	0.40	260
LiF (M_w = 25.9)				
0.01% wt.	0.004	0.0124	0.48	278
0.025% wt.	0.010	0.0113	0.58	379
0.1% wt.	0.039	0.0100	0.65	-
LiBr (M_w = 86.8)				
0.1% wt.	0.012	0.0097	0.58	359
0.25% wt.	0.029	0.0080	0.58	403
0.5% wt.	0.058	0.0036	0.69	453
LiCl (M_w = 42.4)				
0.1% wt.	0.024	0.0080	0.59	421
0.25% wt.	0.059	0.0067	0.63	363
0.5% wt.	0.118	0.0044	0.78	581
NaCl (M_w = 58.5)				
0.1% wt.	0.017	0.0077	0.61	384
0.25% wt.	0.043	0.0056	0.64	374
0.5% wt.	0.085	0.0043	0.74	415
KCl (M_w = 74.6)				
0.1% wt.	0.013	0.0052	0.61	468
0.25% wt.	0.034	0.0069	0.67	588
0.5% wt.	0.067	0.0054	0.75	671

Table 6: Averaged raw data collected for this experiment.

2.2 Effect of Different Ion Size

A plot of the deposition rate vs percent by weight concentration of salt (see Figure 18 taken from Table 6) shows that for each level of concentration all of the data points show little variation. On performing an ANOVA on the data for the mass deposition rate, electric current and average fibre diameter it is shown that for the variation due to the salt composition is less than that due to the salt concentration for both the mass deposition rate and electric current (see Table 7, Table 8, Table 9).

In the case of the average fibre diameter the two values are similar and the larger mean squares value due to salt composition is due to the fibre diameter measured for KCl which were taken from poor quality scanning electron microscope (SEM) images and deviated significantly from the observed trend. For the mass deposition rate the

* All values are averages of the repeats done for each ionic salt concentration

residual error in the data is larger than the variation due to salt composition. Performing a linear regression on the deposition rate data revealed that the deposition rate as a result of adding 0.1% wt. KCl is likely to be an outlier. This is demonstrated by the fact that the residual calculated for 0.1% wt. KCl was less than -2, where the residual represents the deviation from the linear trend. In Figure 19 note that the point representing 0.1% KCl is the one deviating significantly from the expected normal distribution for the unscaled residuals. As such 0.1% wt. KCl deviates significantly from the trend established by the other points and is likely to be an outlier. At the top end there is some deviation from the expected normal distribution so a linear model is not a good fit for the data, suggesting other nonlinear models should be examined.

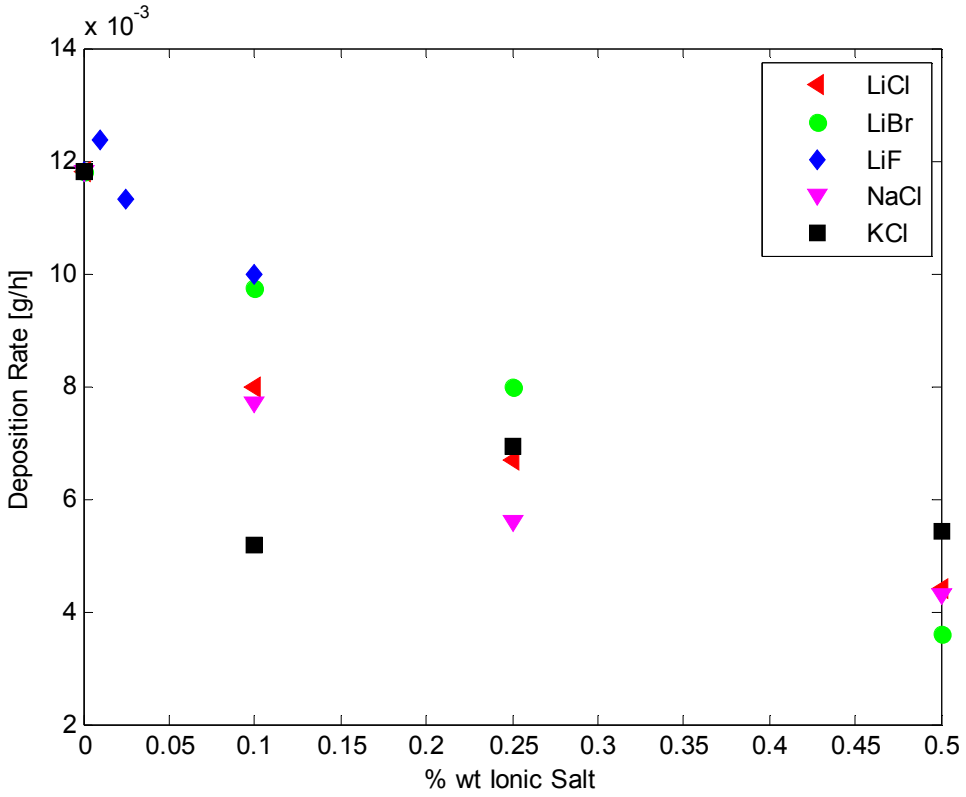

Figure 18: Average deposition rate as a function of salt concentration for all ionic salts tested.

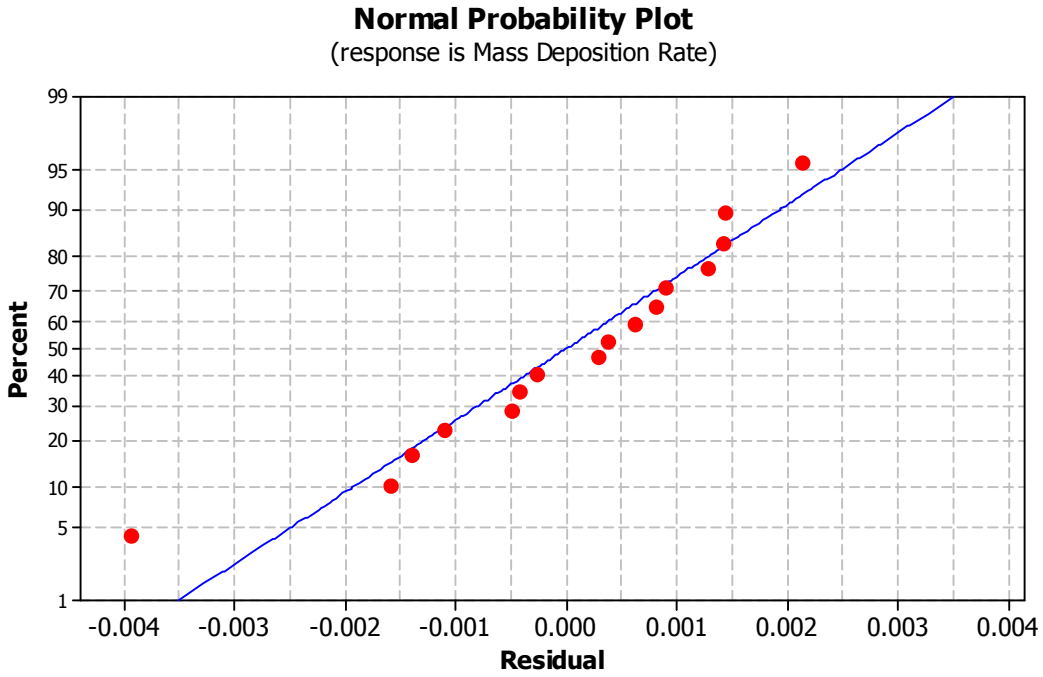

Figure 19: Normal probability plot of unscaled response for a linear regression performed on the deposition rates with percent by weight concentration as a predictor (independent variable). The point with a residual of -0.004 represents 0.1% wt. KCl.

Source of Variation	**Degrees of Freedom**	**Mean Squares**
Salt Concentration	3	3.6×10^{-5}
Salt Composition	3	1.0×10^{-6}
Residual Error in Data	9	1.4×10^{-6}
Total	15	

Table 7: Results of the two way ANOVA performed on the measured mass deposition rates for all ionic salts excluding LiF.

Source of Variation	**Degrees of Freedom**	**Mean Squares**
Salt Concentration	3	8.5×10^{-14}
Salt Composition	3	2.9×10^{-14}
Residual Error in Data	9	2.0×10^{-14}
Total	15	

Table 8: Results of the two way ANOVA performed on the measured electric current for all ionic salts excluding LiF.

Source of Variation	**Degrees of Freedom**	**Mean Squares**
Salt Concentration	3	2.5×10^{-14}
Salt Composition	3	3.5×10^{-14}
Residual Error in Data	9	5.2×10^{-15}
Total	15	

Table 9: Results of the two way ANOVA performed on the measured average fibre diameters for all ionic salts excluding LiF.

The observation that ionic concentration rather than ion size dictates a change in fibre diameter (see Figure 20 taken from Table 6) opposes the theory proposed by Mit-uppatham et al. (2004), Qin et al. (2007) and Zong et al. (2002) (see Chapter 3, Section 2.1.3). The trend proposed for the effects of different ion sizes also matches the trend for increasing conductivity in the case of Mit-uppatham et al. (2004) and Qin et al. (2007). As conductivity is directly related to ionic concentration (see Chapter 2, Section 2.2.2) it is not surprising that fibre diameter response is dependent on ionic concentration not ion size. As is shown in Figure 20 with increasing salt concentration there is an increase in the fibre diameter. The response of KCl differs significantly from the other ionic salts however as an artefact of measurement due to the lower quality of SEM pictures and consequent difficulty in measuring an accurate diameter. If ion size was the driving factor in determining the final diameter of the fibre then there should be a significant difference between the three salts of LiBr, LiCl and NaCl. If the size of the positive ions was important then NaCl should be significantly different from LiBr and LiCl. If the size of the negative ions was important then LiBr should be significantly different from LiCl and NaCl. However as shown in Figure 20 at each level of ionic salt concentration each of the three salts has a different order for the average fibre diameter.

Figure 21 (data taken from Table 6) shows a plot of fibre diameter against the conductivity of the solution. The linear trend shown in Figure 21 demonstrates that the conductivity and hence the concentration of ions is important rather than the ion size. The apparent trend for ion size is likely an artefact of using the percent by weight. measure for ionic concentration rather than one that takes into account the molecular weight of the ionic salt. As such these observations do match the trends observed by Mit-uppatham et al. (2004) and Qin et al. (2007) so long as change in conductivity is taken to be reason for the variation between each salt rather than change in ion size (see Chapter 1, Section 5.3). Unfortunately as the conductivity of the solutions (DMF not water as solvent) used by Zong et al. (2002) were not reported it not possible make the same direct comparison to this work. However Zong et al. (2002) did observe an increase in fibre diameter when potassium ions were used compared to sodium ions matching the observation here when concentration is measured in % wt. not mol/L.

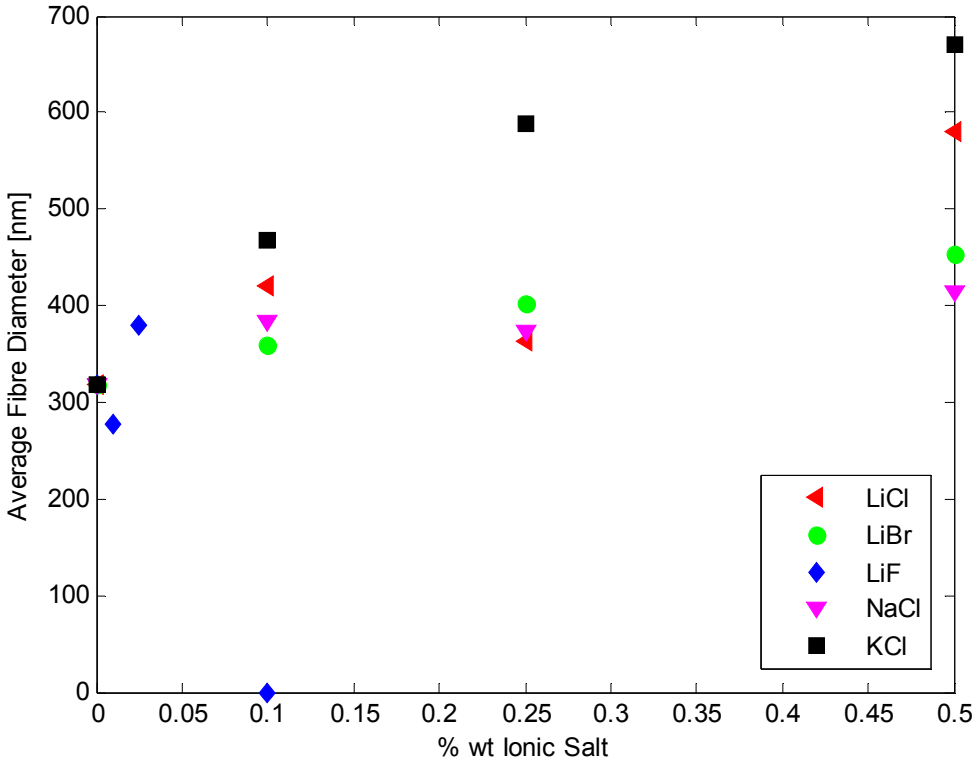

Figure 20: Average fibre diameter as a function of salt concentration for all salts tested.

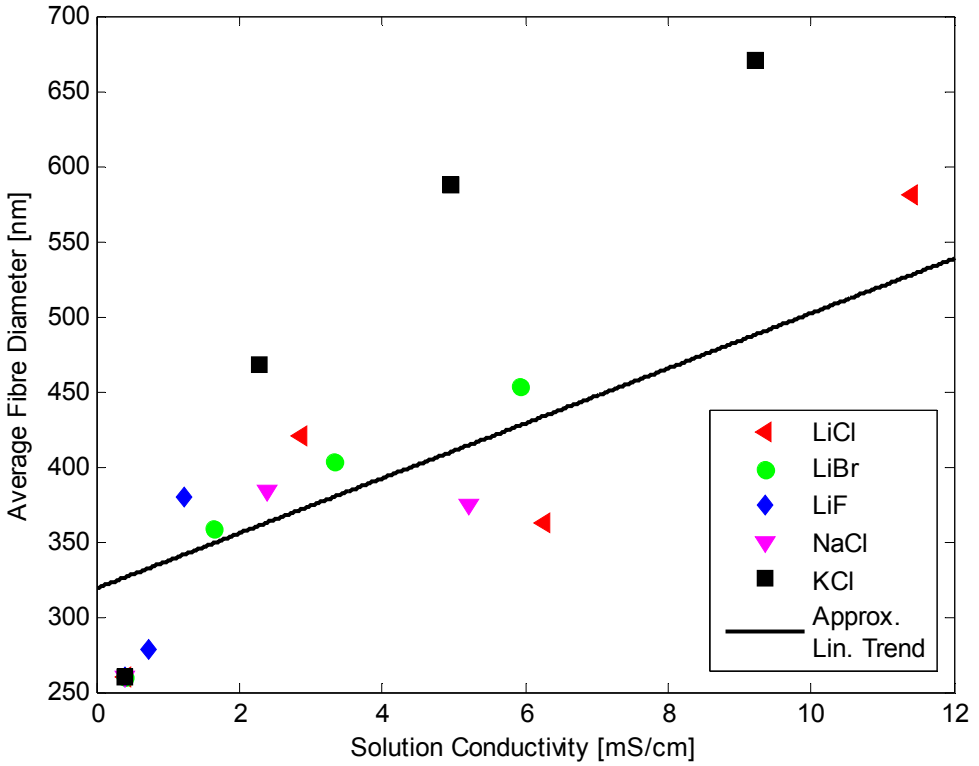

Figure 21: Average fibre diameter as a function of the solution conductivity for all salts tested showing the approximate linear trend.

Both examples above indicate that within the data collected each salt acts sufficiently like each other salt to be treated the same as long as concentration in moles per litre is used rather than percent by weight. Hence from this point onwards when fitting least squares models to the data the ion type will no longer be considered only the ionic concentration.

2.3 Trends in Observed Data

As discussed in Section 2.2 the different molecular weights of each ionic salt must be taken into account so it is more constructive to look at the salt concentration rather than the percent by weight of salt added as many other authors (such as Choi et al. 2005 or Son et al. 2004a) have in electrospinning literature. There are limits to the validity of the approach of examining the effect of a number of different ionic salts on the basis of a percent by weight concentration. As properties such as conductivity depend on the concentration of ions in solution (see Chapter 2, Section 2.2.2) then comparing 1% wt. LiCl with a molecular weight of 42.4 g/mol to 1% wt. KCl with a molecular weight of 74.6 g/mol it is clear that the number of ions in the solution in each case will be significantly different. Figure 22 shows the dependence of the mass deposition rate on the concentration of ionic salt in solution measured in moles per litre.

Performing a linear regression excluding the point at concentration 0.013 mol/L that represents 0.1% wt. KCl gives an R^2 value of 0.66, improved from 0.52 when all points are included (see Figure 22 derived from Table 6). Although it is an improvement the linear fit still does not fit the data well. A logarithmic function of the form $m_{rate} = -0.0025\ln(conc) - 0.0014$ fits the data with an R^2 value of 0.77. To fit a logarithmic function it is necessary to exclude the concentration of 0 mol/L as zero is an asymptote for a logarithmic function and hence near zero concentration the function breaks down. An exponential function of the form $m_{rate} = 0.0037 + 0.0086e^{(-26.11conc)}$ also fit the data well with an R^2 value of 0.81 (see Figure 22). The exponential form then predicts that the deposition rate will never fall below the asymptote at 0.0037 g/h regardless of the salt concentration. As it is unknown what effect adding ionic salt beyond saturation level will have on the electrospinning process neither of these relationships can be said to hold in that region. Due to the

logarithmic function breaking down as the salt concentration reaches zero it is proposed that the deposition rate is related to the ionic salt concentration by an inverse exponential function. As such at a high ionic salt concentration further addition of ionic salt should result in a reduction of the deposition rate smaller than the expected experimental error shown in Section 1.2. The trend in the mass deposition rate is the opposite of that observed by Demir et al. (2002) where it is found that the addition of the ionic surfactant triethyl benzyl ammonium chloride the mass flow rate would increase. This may be due to the decrease in the surface tension that will change the shape of the Taylor cone and resultant jet. As the ionic salts used in this work are not surfactants and surface tension (see Chapter 2, Section 2.2.3) plays an important role in electrospinning a different effect on the deposition rate is expected.

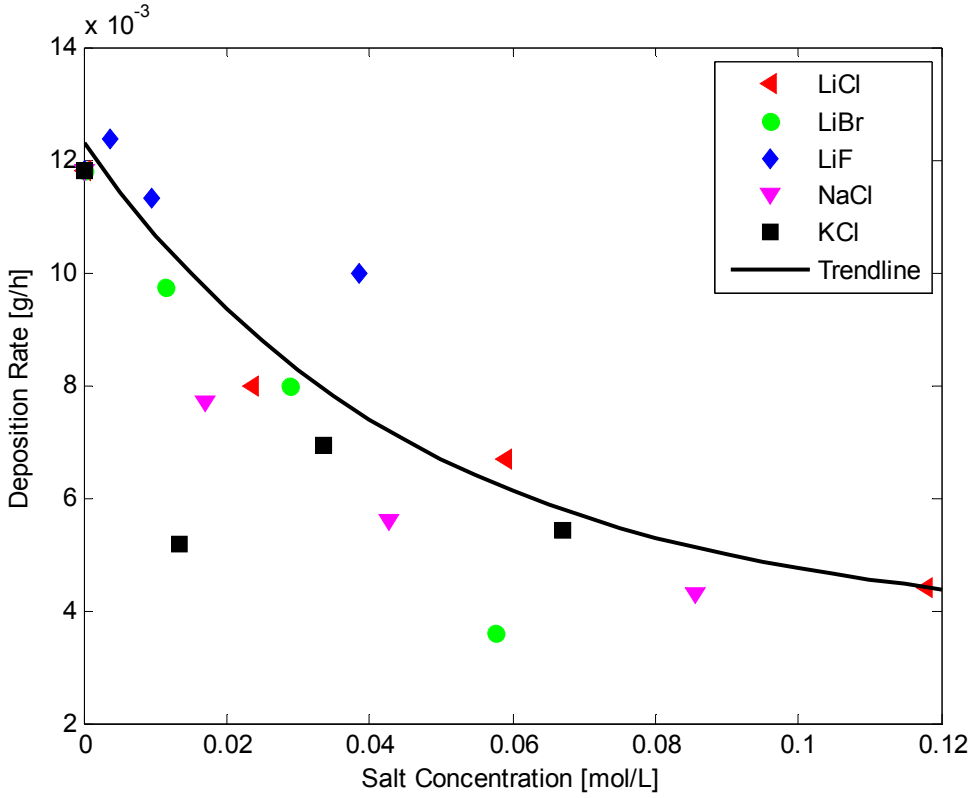

Figure 22: Average deposition rates as a function of salt concentration.

Beyond the mass deposition rate, two other factors were experimentally measured, the average fibre diameter and the measured current. As the concentration of salt increases the average fibre diameter increases as shown in Figure 23 (data derived

from Table 6). The average diameters observed for KCl show significant deviation from the trend shown by the other salts. The SEM images that were taken for KCl were done while a suitable operational procedure was still in development and resulted in poor focus making measurement of the fibre diameter difficult. As the fibre diameter is later used in the equations for the final fibre velocity and the charge per unit length the calculated values for KCl will also show a deviation from the trend shown by the other four ionic salts.

Here the trend observed for the average fibre diameter is the same as that observed by Demir et al. (2002), Mit-uppatham et al. (2004) and Qin et al. (2007). However as the trend is for the fibre diameter to increase with the addition of an ionic salt this is contrary to the trends reported by Choi et al. (2004), Zeng et al. (2003), Li et al. (2006), Son et al. (2005), Son et al. (2004b), Son et al. (2004a) and Zhang et al., (2005). In the case of Choi et al. (2004) and Zeng et al. (2003) the ionic salt added was an ionic surfactant, hence would change the surface tension which may account for the opposite trend being observed. In the case of Son et al. (2005) and Son et al. (2004b) the polymers used change their properties (polymer/solvent intermolecular interaction, protonation of side chains, degradation in acidic or basic conditions) at different pH levels which may account for the opposite trend being observed. In the case of Son et al. (2004a) and Li et al. (2006) the increase in conductivity was due to the addition of a polyelectrolyte rather than an ionic salt. A polyelectrolyte may affect the viscosity of the solution causing the opposite trend to be observed.

The measured electric current flow represents the flow of charge from a ground source to the collector electrode. In an electrostatic case this flow should be zero and so, Figure 24 (data derived from Table 6) represents an electrodynamic case. The measured electric current is assumed to be the flow of charge incoming from the PVOH fibres impacting the collector electrode. As the concentration of salt increases the electrostatic current increases; see Figure 24 where there is a rapid increase due to only a small increase in concentration with a more linear response as the concentration increases. This is likely due to the large increase in conductivity from 0.383 mS/cm to 1.63 mS/cm when only 0.1% of LiBr is added to the solution. Demir et al. (2002) also reported an increase in the measured electric current with an increase in salt concentration matching the observations in Figure 24.

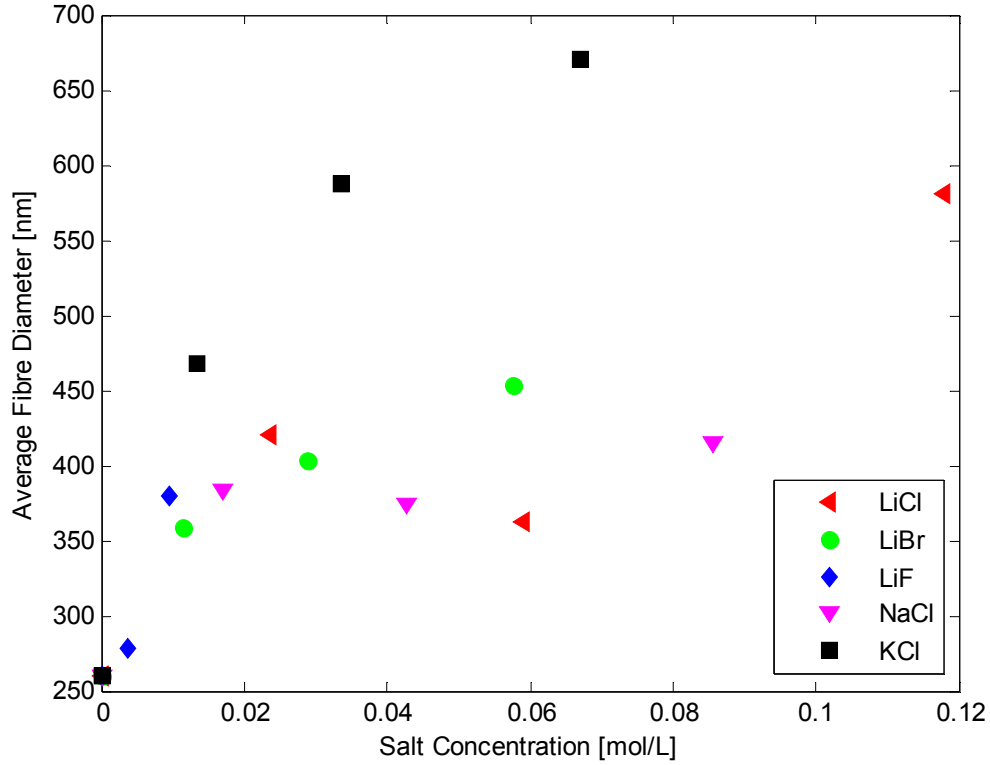

Figure 23: Observed effect of the addition of ionic salt on the average fibre diameter.

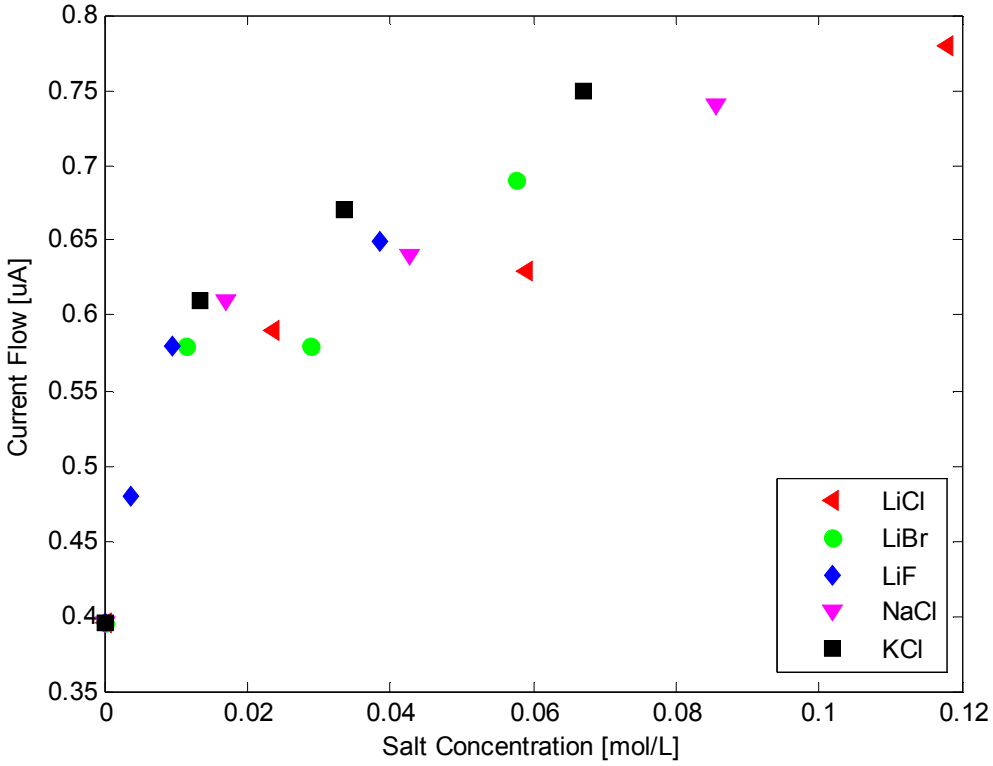

Figure 24: Observed effect of the addition of ionic salt on the electric current flowing to ground from the collector.

2.4 Trends in Derived Data

Three further variables that can be calculated from the experimental data. These variables are the final charge density, the fibre velocity at the collector electrode and the charge per unit length at the collector electrode.

Charge density is calculated using Equation 20 where I is the observed electric current [A], m_{rate} is the observed mass deposition rate [kg/s] and ρ is the density of the solid polymer [kg/m^3]. It is of the form $\sigma_{density}$ = I/(volume flow rate) where the equation is constructed using the definition of current and volume flow rate to produce a time independent ratio. The calculated quantity gives no indication of the position of the charge in the jet. As long as the assumptions of charge conservation and mass conservation hold true it is possible to use this equation to estimate the charge further up the jet. However as this equation is dependent on the observed electric current at the collector electrode and the deposition rate at the collector; this being after the transition from a liquid solution to a solid fibre, it is only true for the moment of impact at the collector. Hence the final charge density is the preferred quantity to examine. As the salt concentration increases the charge density increases as observed in Figure 25.

$$\sigma_{density} = \frac{I\rho}{m_{rate}} \qquad \text{Equation 20}$$

Fibre velocity is calculated using Equation 21 where m_{rate} is the observed mass deposition rate [kg/s], ρ is the density of the solid polymer [kg/m^3] and r is the radius of the dry fibre deposited on the collector [m]. It is constructed, similar logic to that used by Wang et al. (2006), by dividing the mass deposition rate by the weight of a unit length of fibre on the collector. This assumes that all the mass is converted into fibre and that the average fibre diameter is representative of all the collected fibre. As the values used in this equation are taken from observations at the collector electrode it represents the final velocity obtained by the fibre before it impacts with the collector. It should be noted that due to the calculation method this represents the total velocity that the fibre is laid on the collector in three dimensions, neither the velocity of an individual element of fluid travelling through space nor simply the velocity of the fibre along the z axis.

It was shown by Yarin et al. (2001) that if one tracks two points in the jet, each point will move with a much lower total velocity compared to the rate that the fibre is laid on the collector. This can be explained by considering two points on an expanding loop of jet as the loop is pulled towards the collector. The loop expands under the force from its own self repulsion, yet there is very low acceleration due to the point not moving very far in the x-y plane. This is because although the loop has increased its radius the points along the ring have only moved directly out from the centre of the loop and the jet has been thinning due to the increase in radius. The thinning of the jet results in the very high scalar velocity predicted by this formula. This point is important as incorrect interpretation of this velocity can lead to incorrect conclusions regarding the change in velocity.

As previously mentioned the fibre diameters measured for KCl are significantly different from those measured for the other ionic salts. It is clear from Equation 21 that the difficulty in accurately measuring the average fibre diameter for KCl (see Chapter 4, Section 2.3) will result in a calculated fibre velocity that will differ from the trend shown by the other ionic salts. This explains why the fibre velocities for KCl are significantly lower than those for the other ionic salts. The general trend is as the salt concentration increases the fibre velocity decreases as observed in Figure 26.

$$v = \frac{m_{rate}}{\rho \pi r^2} \qquad \text{Equation 21}$$

Charge per unit length is calculated using Equation 22 where I is the observed electric current [A] and v is the above fibre velocity calculated in Equation 21 [m/s]. The physical interpretation of this quantity is difficult as it is not immediately obvious, apart from analysis of the dimensions of the result, that it represents the charge along a length of fibre. However the velocity represents the rate at which the fibre (of undefined radius) is laid on the collector electrode and the observed electric current is the rate charge leaves this fibre as it impacts with the collector (also radius independent). As such this quantity represents the charge along a length of fibre as it is impacting with the collector. As with the charge density above the calculated value gives no indication of the position of the charge in the jet.

Again the results for KCl are significantly different from those calculated for the other ionic salts. This should be expected as Equation 22 shows that the charge per unit length is dependent on the final fibre velocity. As discussed previously, difficulty in measuring the average fibre diameter caused significant deviation, explaining the resultant deviation in the charge per unit length. With increasing concentration of salt the charge per unit length increases as observed in Figure 27.

$$\sigma_{length} = \frac{I}{v} \qquad \text{Equation 22}$$

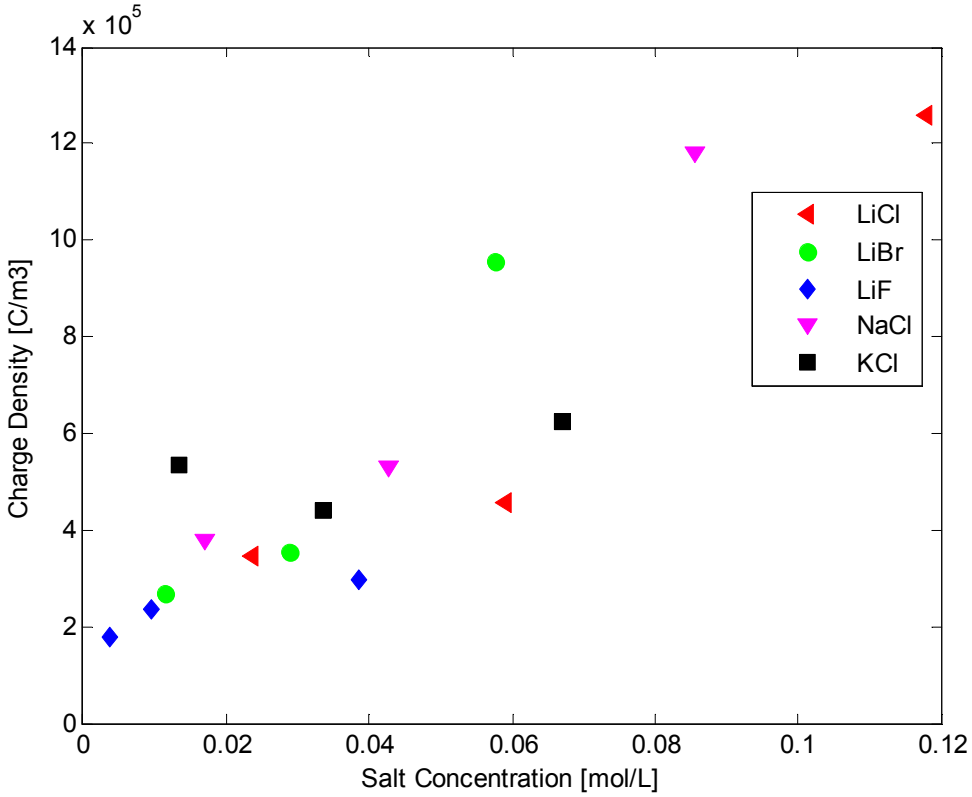

Figure 25: Observed trend between final charge density and salt concentration.

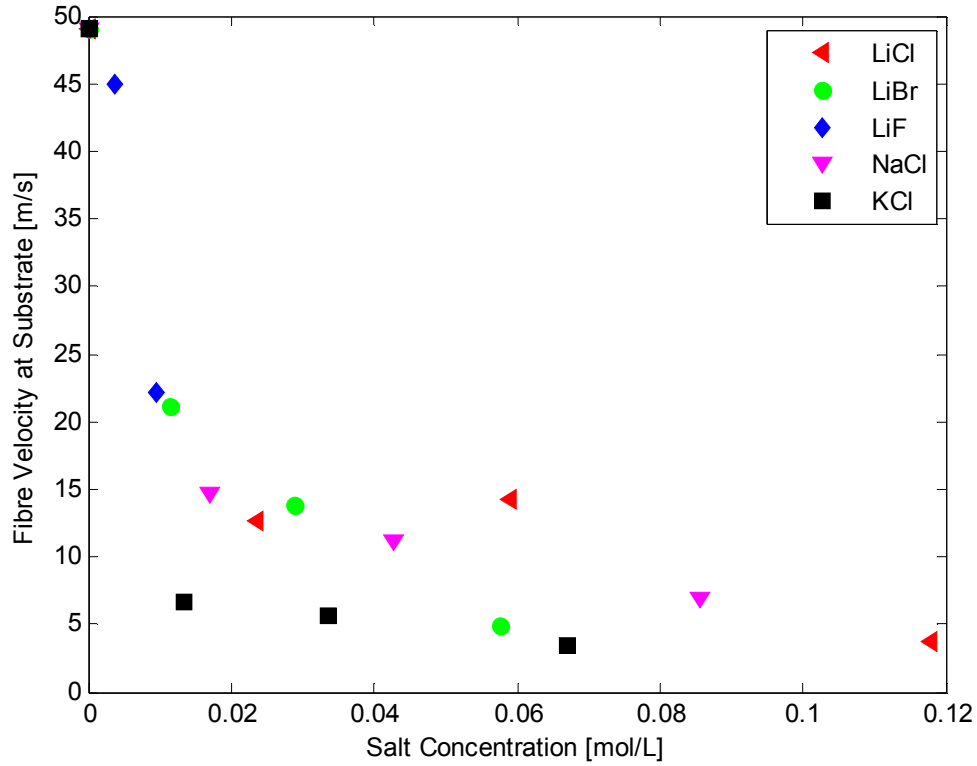

Figure 26: Observed trend between final fibre velocity and salt concentration.

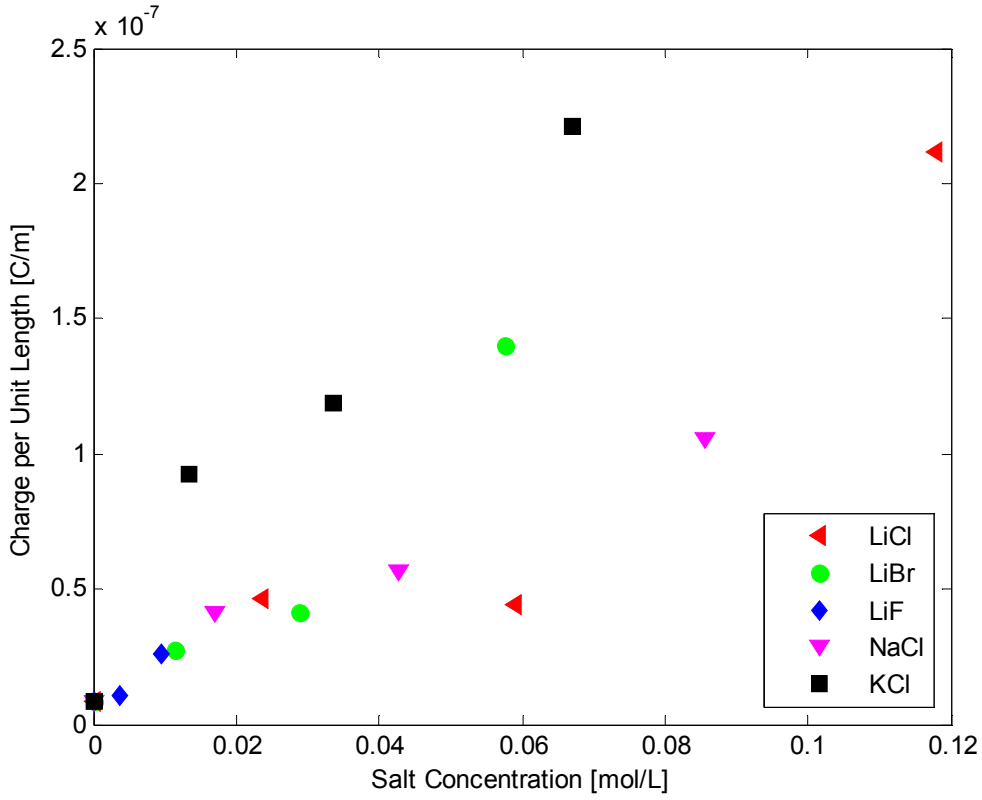

Figure 27: Observed trend between charge per unit length and salt concentration.

As a summary of all the data presented, Table 10 shows the trend observed in each measured quantity. The trend is for the quantity as the concentration of ionic salt increases but makes no statement about the form that the relationship might take.

Quantity	Trend
Deposition Rate	Decrease
Current Flow	Increase
Velocity	Decrease
Fibre Diameter	Increase
Volume Charge	Increase
Charge per unit length	Increase

Table 10: Summary of the trend for each of the measured and calculated parameters as the concentration of ionic salt increases.

2.5 Conductivity as an Independent Variable

Using the Debye-Huckel-Onsager equation (CRC-Press, 2004) (see Equation 23) and fitting it to tabulated data (CRC-Press, 2004) it is possible to calculate the approximate conductivity of these ionic solutions. Here Λ is the molar conductivity with Λ_0 being the molar conductivity at infinite dilution [S/mol], A and B are constants determined by the fitting of data to Equation 23 and c is the concentration of the salt in solution [mol/L]. The conductivity of the solution is then found from Equation 24 where κ is the conductivity [S/m] and the other variables are as above.

$$\Lambda = \Lambda_0 - (A + B\Lambda_0)c^{1/2} \qquad \text{Equation 23}$$

$$\kappa = \Lambda c \qquad \text{Equation 24}$$

Using the above fitted conductivity data and adding the conductivity of the 8% PVOH solution (using Kohlrausch's law of the independent migration of ions (Atkins, 1994)), it is then possible to plot the measured electric current against the conductivity for the known concentration (see Figure 28). When the solution conductivity is higher than 0.5 mS/cm the electric current demonstrates a linear relationship (see Figure 28). Including all the data points gives a linear fit with an R^2 value of 0.77. Exclusion of points below 0.5 mS/cm that gave residuals below -2 improves the linear fit, giving an R^2 value of 0.87. A linear relationship matches the expected relationship (see Equation 25) outlined by Reznik et al. (2004). The equation describing this fit is $I = 0.02\kappa + 0.549$. Using the form of Equation 25 it is

possible to convert the slope to SI units and, assuming the constant radius of the inner diameter of the tube forming the high voltage electrode, calculate the electric field at the point of charge carrier generation. This calculation gives an electric field of approximately 0.002 V/m which is very low corresponding to the expected behaviour of a conductor. As Equation 25 has an intercept at zero, the observed intercept at 0.549 μA may represent a second non-ohmic current that occurs during the generation of charge carriers. The linear fit does not fit the data at low values of κ and as such it is more likely that there is a more complex process of charge transport in lower conductivity solutions.

$$I_{Oh} = \kappa A E \qquad \text{Equation 25}$$

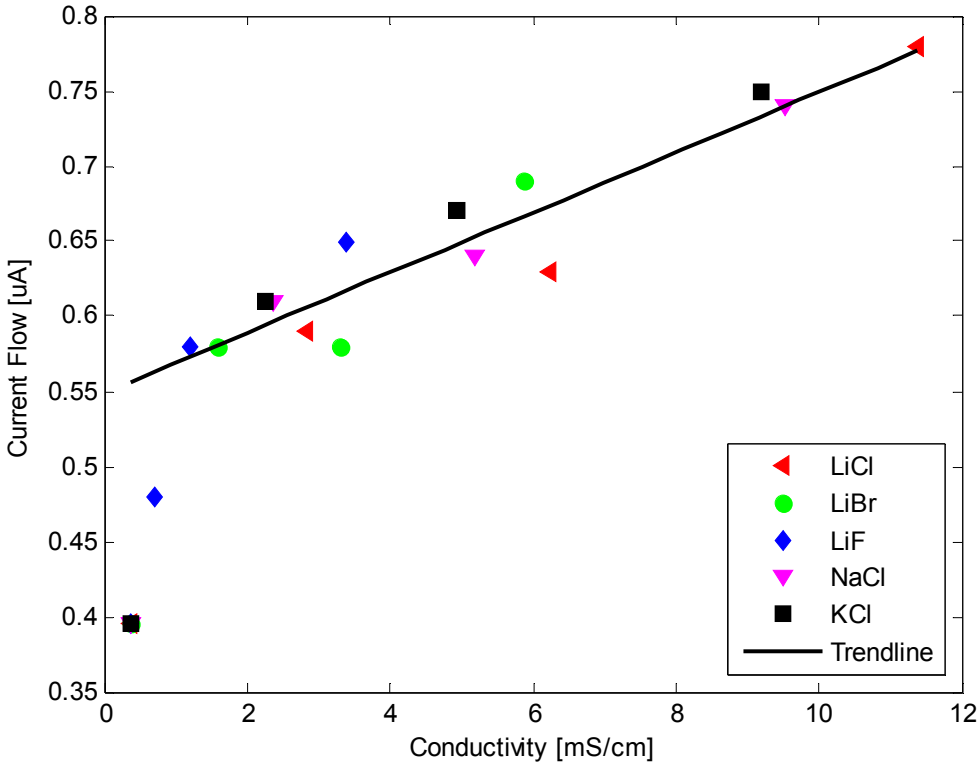

Figure 28: Linear relationship between electric current flow and calculated solution conductivity due to ionic salt addition. Linear relationship excludes the points due to no salt addition and 0.01% LiF.

Again using the calculated conductivity it is possible to examine a relationship between the charge carrier density and conductivity (see Figure 29). Shown in Figure 29 is a linear relationship between charge density and conductivity where the conductivity includes the measured conductivity for 8% PVOH (Kerr 2008 personal communication). For this relationship to fit the data elimination of the data point due

to 0.1% KCl and the data points due to 0.5% salt addition is required. As has been previously established the deposition rate measured 0.1% KCl is likely to outside the expected trend established by the other ionic salts. As charge density is dependent on the deposition rate this would result in the wrong charge density being calculated so it is excluded. Exclusion of the data points due to 0.5% salt is to the observation that in all cases when 0.5% wt. of salt is added to the solution the electrospinning process became unstable. The Taylor cone was intermittent and the measurement of the electrical current flowing in the jet was taken as the peak value during a short moment of stability. Therefore this charge density may represent the initial charge density when the jet is initiated rather than the long term average charge density established when the jet is stable and hence is excluded. A linear relationship with conductivity is expected as the solution conductivity represents the availability of charge carriers in solution.

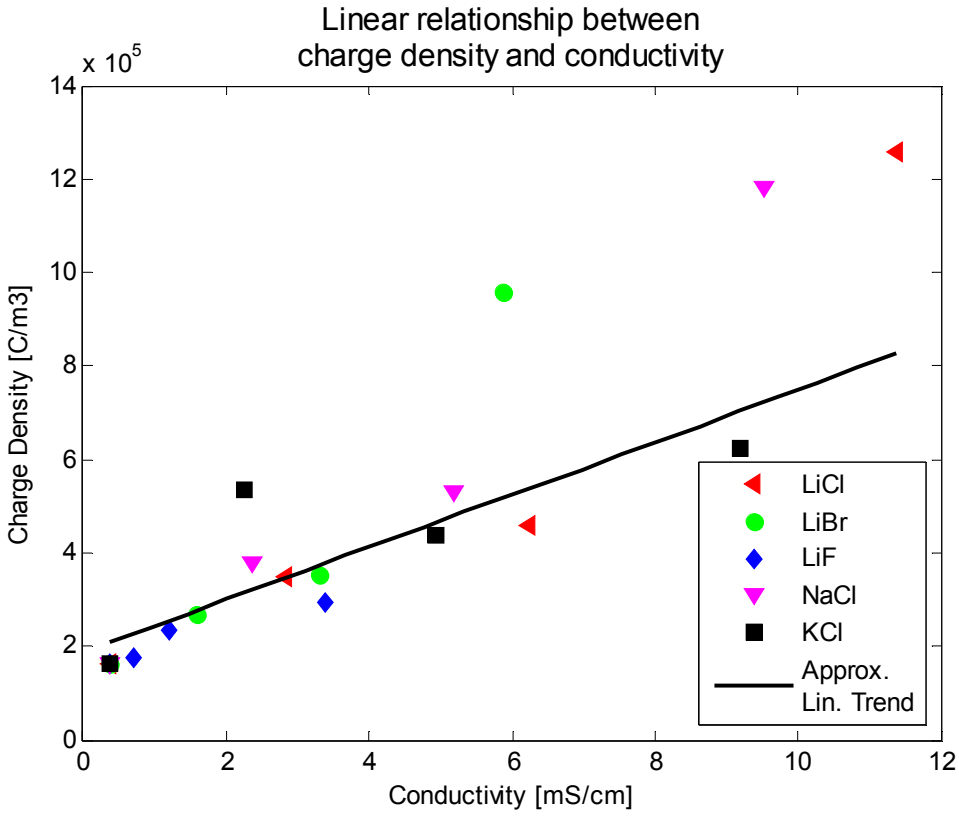

Figure 29: Linear relationship between charge density and calculated solution conductivity where the linear equation fit excludes 0.1% KCl and all salts at 0.5%.

2.6 Assumption of Total Conversion of Ions to Charge Carriers

If one assumes that all the ions in an electrospinning solution are converted to charge carriers to be transported through the jet then it should be possible given a known

concentration of ionic salt to calculate the expected electric current to be measured at the collector electrode. Hence assuming conservation of charge throughout the period the jet is in flight and assuming that there is no charge lost to the surrounding environment then Equation 26 gives the expected electric current that should be measured due to the concentration of ions in solution where F is Faradays constant, c is ion concentration, m_{rate} is the deposition rate, ρ is the density and the factor of 1000 is the conversion from litres to m^3. For each concentration of ionic salts this predicted electric current is calculated and presented in Table 11. It can be seen that the electric current measured is only a fraction of the expected electric current if total conversion of ions to charge carriers is taking place when a solution is electrospun. Taking an average of the fraction of salt that was acting as a charge carrier when the jet arrives at the collector gives approximately 18% (calculated as the average of column 4 in Table 11) of the salt is still acting as a charge carrier. This figure assumes that the quantity of ions due to the ionic salt far outweighs any other ions in the solution and hence ignores their concentration.

$$I = \frac{1000 F c m_{rate}}{\rho} \qquad \text{Equation 26}$$

Salt Concentration [mol/L]	Predicted Electric Current [μA]	Observed Electric Current [μA]	% of Prediction Observed
0.024 LiCl	4.01	0.59	15
0.059 LiCl	8.40	0.63	8
0.118 LiCl	11.04	0.78	7
0.012 LiBr	2.38	0.58	24
0.029 LiBr	4.90	0.58	12
0.058 LiBr	4.41	0.69	16
0.013 KCl	1.47	0.61	41
0.034 KCl	4.94	0.67	14
0.067 KCl	7.75	0.75	10
0.017 NaCl	2.80	0.61	22
0.043 NaCl	5.09	0.64	13
0.085 NaCl	7.82	0.74	9
0.004 LiF	1.02	0.48	47
0.010 LiF	2.33	0.58	25
0.039 LiF	8.21	0.65	8

Table 11: Electric current measured and predicted from ionic concentration for solutions with an ionic salt added.

3. FURTHER INVESTIGATION OF THE INITIAL JET DIAMETER

In this series of experiments two factors were measured for a set of four different initial conditions. Table 12 shows the results for each experiment. As this further investigation was undertaken to determine if there is any relationship between the initial jet diameter and the deposition rate this data is graphed as such (see Figure 30 taken from Table 12), assuming that the modifications to the initial conditions are summarized by the initial jet diameter formed from the tip of the Taylor cone. Fitting a linear model to the data gave a function of the form $m_{rate} = 0.0005d$ with an R^2 value of 0.87 showing a good fit. The model was forced to accept an intercept at zero as it makes no physical sense for a jet with zero initial diameter to be able to have a deposition rate.

Comparison of Table 6 and Table 12 shows that the deposition rate for 0.25% NaCl wt. in PVOH does not match those previously reported. This may be due to the different apparatus used to make these measurements, the different collector electrode size or the observation that the camera used to capture the images causes significant destabilization of the jet (camera approximately 50mm from Taylor cone), especially in the case where an ionic salt is in the solution. If there was significant destabilization of the jet then it is possible that the deposition rate has been artificially inflated by small droplets being electrosprayed onto the collector. If this were the case then it is possible that the linear model may not represent the true relationship between the initial jet diameter and nonlinear models may need to be explored in future work.

	8% PVOH without ionic salt		**8% PVOH with 0.25% NaCl wt.**	
Measured Quantity	*Initial Jet Diameter [μm]*	*Deposition Rate [g/h]*	*Initial Jet Diameter [μm]*	*Deposition Rate [g/h]*
Positive Charge on Polymer	25.6	0.0115	15.8	0.0083
Negative Charge on Polymer	16.2	0.0059	7.2	0.0040

Table 12: Observed data for the investigation of the initial jet diameter and relationship to the deposition rate. Initial jet diameter measured with a digital USB microscope (Model QX5, Digital Blue Corp.) at 60x zoom.

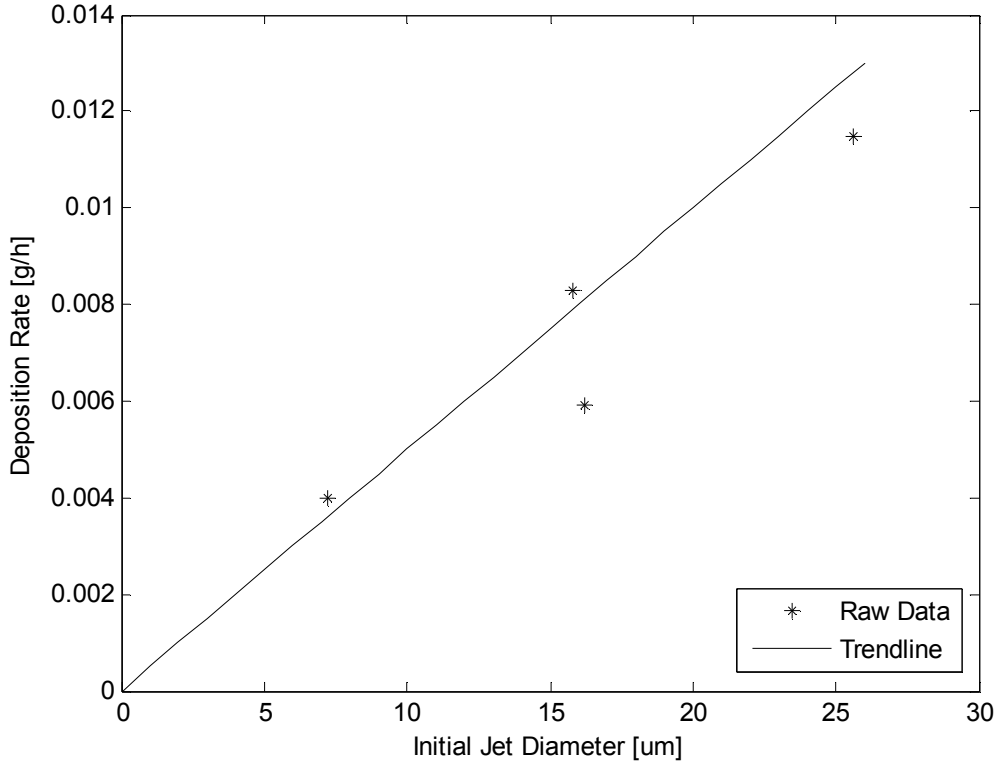

Figure 30: Graph of the deposition rates linear dependence on the initial jet diameter.

4. CALCULATION OF THEORETICAL RELAXATION TIMES

From the work by Reznik et al. (2004) it is possible to calculate the characteristic charge and hydrodynamic relaxation times in order to give an indication of the nature of charge transport mechanism at any point along the jet. In order to make these calculations many of the values used have been from the literature. Two situations will be considered, one of plain 8% PVOH and the other of 8% PVOH with 0.5% wt. of NaCl added. It should be noted that only for these calculations the CGS* unit system is used to allow direct comparison with the equations given by Reznik et al. (2004).

4.1 Characteristic Charge Relaxation Time

The characteristic charge relaxation time as defined by Reznik et al. (2004) is shown as Equation 27. Where ε is the dielectric constant of the fluid and κ is the conductivity of the fluid. The conductivity is taken to be the calculated conductivity due to the addition of an ionic salt added to the measured conductivity of an 8%

* Centimetre-Gram-Second unit system still commonly used in electrostatics

PVOH solution made up with distilled water. The dielectric constant is taken to be that of the solvent and it is assumed that the addition of PVOH or an ionic salt will not modify it significantly at the concentrations used.

$$\tau_E = \frac{\varepsilon}{4\pi\kappa} \qquad \text{Equation 27}$$

4.2 Characteristic Hydrodynamic Relaxation Time

The characteristic hydrodynamic relaxation time as defined by Reznik et al. (2004) is shown as Equation 28. Where μ is the dynamic viscosity, a_0 is the characteristic length typically taken to be the radius of a free droplet of equivalent volume to the Taylor cone and γ is the surface tension. The viscosity in both cases is taken from Briscose et al. (2000). The surface tension does not vary significantly from water (Kerr 2008 personal communication), hence the surface tension for water is used. It is assumed that the addition of ionic salt does not significantly change the surface tension at low concentrations.

$$\tau_H = \frac{\mu a_0}{\gamma} \qquad \text{Equation 28}$$

The values used for the calculation of the different relaxation times have been tabulated below (see Table 13) along with the calculated values comparing the behaviour at the insert electrode. As the charge relaxation time has decreased and the hydrodynamic relaxation time has increased with the addition of salt the fluid now behaves significantly more like a conductor than without salt.

Variable	**8% PVOH**	**8% PVOH + salt**
Dielectric Constant	80	80
Conductivity	3.28 x 10^{8} s-1	8.57 x 10^{9} s^{-1}
Viscosity	3.90 $gcm^{-1}s^{-1}$	5.10 $gcm^{-1}s^{-1}$
Characteristic Length	0.032 cm	0.032 cm
Surface Tension	40 gs^{-2}	40 gs^{-2}
Charge Relaxation Time	1.94 x 10^{-8}	7.43 x 10^{-10}
Hydrodynamic Relaxation Time	0.00312	0.00408
τ_C/τ_H	6.22 x 10^{-6}	1.82 x 10^{-7}

Table 13: Tabulated values for the fluid properties at the insert electrode and the calculated relaxation times.

5. EFFECT OF CHANGING THE SIGN OF THE CHARGE ON THE POLYMER SOLUTION

5.1 Introductory Remarks

The work presented here has been taken from the report by Jonathan Stanger (2006) entitled "Foundation Work for the Crop and Food Research Electrospinning Program" submitted for the course of PHYS480. The discussion and analysis presented in this intermediate report has been expanded and refined in relation to the other observations contained in Chapter 4. The results of this work are included here for the convenience of the reader. The experimental method for these results has been included as appendix A.

5.2 Results and Analysis

5.2.1 Deposition Rates

The average fibre deposition rate measured when electrospinning was undertaken using apparatus A at 11.5 kV is shown below in Table 14. It was observed that when the solution was connected to the positive high voltage supply a significantly larger deposition area was formed.

Electrode Configuration	Deposition Rate (mg per hour)	Deposition Radius (mm)
Collector (+ve) Solution (g)	6.5	4.5
Collector (g) Solution (+ve)	36.2	15

Table 14: Average mass deposition rates.

5.2.2 Fibre Velocity and Charge

Using the average fibre diameter presented in Table 15 it is possible to use Equation 29 to calculate the factor by which the volume changes for the deposited fibre when the electrode configuration is changed. Here V is the volume of fibre [m^3], r is the average radius of fibre [m], l is the length of fibre [m] and ρ is the density of fibre [kgm^{-3}]. Assuming a constant diameter represented by the average diameter (see Table 15) and dry fibres, hence a constant density the calculation can be simplified. Finally using a unit length allows a solution to be found. The increase in volume of fibre produced using an electrode configuration of collector (+ve) / solution (g) is a

factor of 2.7 times as much volume as produced using a configuration of collector (g) / solution (+ve). This is compared the increase in mass deposition rate by a factor of over 5 for the same electrode configurations.

Electrode Configuration	Fibre Diameter (nm)	Standard Deviation (nm)	Variance (nm)
Collector (+ve) Solution (g)	170	100	4.7
Collector (g) Solution (+ve)	280	150	8.2

Table 15: Statistical breakdown of the measurement of the fibre diameter. Approximately 400 measurements for each fibre diameter.

$$V = \pi r^2 l \rho \qquad \text{Equation 29}$$

The results from Table 14 and Table 16 allow the calculation of further parameters describing the state while electrospinning is active. Equations 30 and 31 can be solved to give the total velocity of the fibre while in flight. These equations are modified from literature (Wang et al. 2005). Here for Equation 30 v_1 is the velocity of the aqueous jet [ms^{-1}], w_1 is the weight of solution used [kg], ρ_1 is the density of the polymer solution (1013 kgm^{-3}), r_1 is the radius of the polymer jet [m], and t_1 is the time spent spinning the fibre [s]. The density of the polymer solution is based on the density of water (1000 kgm^{-3}), the density of PVOH (1260 kgm^{-3}) and that 5% of the solution mass was PVOH. Also for Equation 31, v_2 is the spinning velocity when the fibre hits the substrate [ms-1], w_2 is the weight of the fibre on the substrate [kg], ρ_2 is the density of the spun fibre (1260 kgm^{-3}), r_2 is the radius of the spun fibre [m] and t_2 is the time spent spinning the fibre [s]. Note that this velocity is the length of the vector summation of both the tangential "whipping" velocity and the parallel velocity of fibre travelling toward the collector. Additionally using the velocity from Equation 30, Equation 32 can be solved to give the charge per unit length when the fibre impacts on the substrate. Here I is the current flow in the circuit formed by the electrospinning set-up A, v_2 is the velocity when the fibre hits the substrate [ms^{-1}] and λ is the charge per unit length on the fibre as it hits the substrate [Cm^{-1}]. These values are summarized in Table 17.

Electrode Configuration	Initial Jet Diameter (μm)	Fibre Diameter (nm)	Current Flow (μA)
Collector (+ve) Solution (g)	12.2	170	0.30
Collector (g) Solution (+ve)	35.2	280	0.85

Table 16: Values of the dependant variables measured.

$$v_1 = \frac{w_1}{\rho_1 \pi r_1^2 t_1}$$ Equation 30

$$v_2 = \frac{w_2}{\rho_2 \pi r_2^2 t_2}$$ Equation 31

$$\lambda = \frac{I}{v_2}$$ Equation 32

Electrode Configuration	Initial velocity of fluid in jet v_1 (ms^{-1})	Velocity of fibre at substrate v_2 (ms^{-1})	Charge per Unit Length λ (Cm^{-1})
Collector (+ve) Solution (g)	0.30	63	4.75×10^{-9}
Collector (g) Solution (+ve)	0.20	130	6.56×10^{-9}

Table 17: Summary of the results from Equations 30, 31 and 32.

Making the assumption that the loops formed by the bending instability scale linearly with the radius of the deposition area it is possible then taking the final fibre velocity from Table 17 and dividing it by the circumference of a circle with a radius the size of the deposition area to get an approximate figure for the number of loops per second that impact with the substrate. This is only an approximation as the true loop diameter is unknown but it does allow comparison between two situations, providing the assumption holds. The results of this calculation are shown in Table 18.

Electrode Configuration	Velocity of fibre at substrate v_2 (ms^{-1})	Deposition Radius (mm)	Rate of loops impacting substrate (loops/second)
Collector (+ve) Solution (g)	63	4.5	28,648
Collector (g) Solution (+ve)	130	15	13,687

Table 18: Data used to calculate the number of loops per second impacting with the substrate.

It is possible to make an estimation of the charge per unit area along the fibre as it impacts with the substrate. Equation 33 uses the average fibre diameter and the charge per unit length to find the charge per unit volume by assuming the fibres are cylindrical. Here λ is charge per unit length [Cm^{-1}], r is the radius of the fibre [m] and σ is the charge per unit volume on the fibre as it hits the substrate [Cm^{-3}]. The results show the opposite trend that might be expected from Table 19.

$$\sigma = \frac{\lambda}{\pi r^2} \qquad \text{Equation 33}$$

Electrode Configuration	Fibre Diameter (nm)	Charge per Unit Length λ (Cm^{-1})	Charge per Unit Volume σ (Cm^{-3})
Collector (+ve) Solution (g)	170	4.75×10^{-9}	8.90×10^{-3}
Collector (g) Solution (+ve)	280	6.56×10^{-9}	7.46×10^{-3}

Table 19: Summary of the variables used and results for Equation 33.

As a summary of the trends observed here Table 20 shows the general trend in the observed and calculated variables measured in this experiment.

Quantity	Trend
Deposition Rate	Decrease
Current Flow	Increase
Velocity	Decrease
Fibre Diameter	Increase
Volume Charge	Increase
Charge per unit length	Increase

Table 20: Summary of the trend for each of the variables.

5.2.3 Confirmation that Ground can act as a True Negative Supply

One objection to the results obtained so far is that they have used the ground as the source of negative charge. As the ground is not a negative charge source, merely the absence of a positive source, the experiment was repeated using a convertible power supply so that the effects of a negative charge can be directly compared to a positive charge. It was found that a true negative supply resulted in the same trend for the deposition rate observed with the ground acting as a negative supply (see Table 21).

Electrode Configuration	Deposition Rate (mg per hour)
Collector (g) Solution (-ve)	16.4
Collector (g) Solution (+ve)	35.0

Table 21: Average mass deposition rates.

Performing the ANOVA on the raw data (see Table 22) allows further analysis. This shows that the variance due to charge polarity is significantly larger than the variance of the data and hence there is a significant effect due to the charge polarity used on the polymer solution.

Source of Variation	Degrees of Freedom	Mean Squares
Electrode configuration	1	1.00×10^{-3}
Residual	10	1.97×10^{-6}
Total	11	

Table 22: Results of the ANOVA for the raw data.

Chapter 5

Discussion

DISCUSSION

1. ELECTRIC CURRENT FLOW IN A FLUID JET

Before any in depth discussion regarding the behaviour and nature of charge in an electrospinning fluid jet one must first discuss any assumptions that have been made in literature and that will be made in this text. The assumption of the conservation of charge is the common starting point (Reznik et al. 2004, Taylor 1964 and Hohman et al. 2001) which then leads to the ability to define a generalized equation describing the flow of electric current through any virtual plane aligned with the cross section of the jet. Electric current is defined to be the number of coulombs per second that flows through a given plane.

Now consider a fluid stream containing ions in motion between two electrodes with a potential difference between them – it is possible to measure a current flow between the electrodes. There are a number of possible charge transfer mechanisms to explain this physical situation. Three identified charge transfer mechanisms are that of free electron flow, ohmic conduction and convective flow of charged fluid (see Figure 31). Assuming conservation of charge the contribution of each of the charge transfer mechanisms can be summed to give a generalized form of the electric current at any point in the jet (see Equation 34 where I is the total current, IF is the free electron current, I_{Oh} is the ohmic current and I_C is the convective current).

$$I = I_F + I_{Oh} + I_C \qquad \text{Equation 34}$$

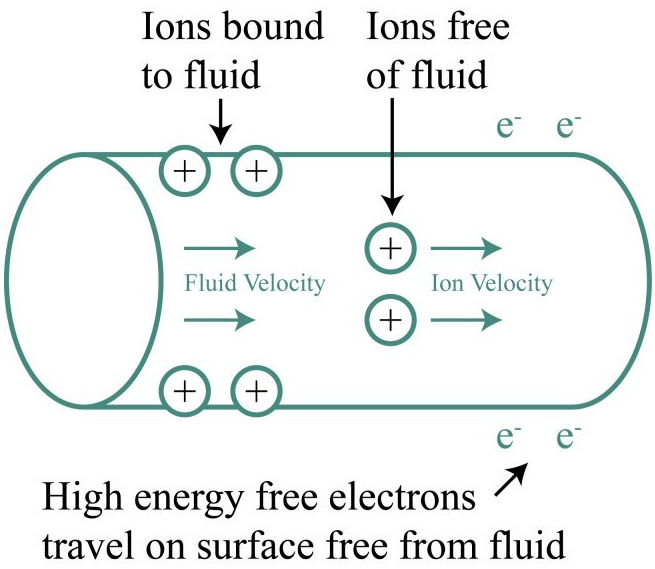

Figure 31: Charge transport mechanisms identified in the electrospinning process.

The fluid lacks free electrons such as those found within a metal matrix (Halliday et al. 2001). However due to the nature of electrons (namely having a very high degree of mobility due to a large charge to mass ratio (Halliday et al. 2001)) and the high strength electric fields in the electrospinning process it is likely that any free electrons in the local environment will participate in the electrospinning process. A significant distance downstream from the initial Taylor cone the excess free electron charge on the surface of the jet will provide an excellent target for ionized air molecules to attack. If this is the case it will result in a rapid loss of charge. The rate at which this charge is lost must be described by a function that at the least will be dependent on the distance along the jet and the time that has passed.

Due to the success by some authors (Reznik et al. 2004 and Hohman et al. 2001) in predicting an electric current with the same order of magnitude as observations using a model that excludes free electron flow, free electron flow will henceforth be excluded from further consideration. Yarin et al. (2001) also investigated the possible contributions from space charge and electrical currents in the air to the region of the Taylor cone and found that the occurrence of these phenomenon were always due to corona discharge. As in all cases examined corona discharge could be "reduced to a very low level" Yarin et al. (2001) concluded that "field evaporation and ion current effects on the half angle of the observed cones can be totally disregarded". The work by Blades et al. (1991) on electrospraying adds weight to the exclusion of free electron flow as a charge transport mechanism as it was shown that there is a strong correlation between the measured electric current and the measured ion concentration due to the dissociation of the stainless steel electrode used to charge the fluid. The contribution of free electron flow to the formation of the Taylor cone and the subsequent jet warrants further investigation.

For the case of the ohmic and convective flow of electric current first consider charge carriers in a perfect conductor. In this case the classical consideration is of liberated free electrons in a metal matrix that act as the charge carriers allowing an electric current to flow (see Figure 32). When a potential difference is applied across the metal matrix the charge carriers move in order to cancel out the externally applied

electric field so as to satisfy Gauss' law*. This motion of the charge carriers is hence dependant on the applied electric field. The metal matrix will have bulk properties that describe how the charge carriers behave. In terms of the bulk properties of the matrix the electric current is the number of charge carriers per unit volume multiplied by the charge carried by each one multiplied by the velocity that each one travels at and multiplied by the cross sectional area that the charge carriers flow through (see Equation 35 where n is the number of charge carriers, q is the charge carried on each charge carrier, A is the cross sectional area and v_{drift} is the velocity of the charge carriers). The velocity of the charge carriers can be found from the real world measurement of the molar conductivity and the applied electric field as shown in Equation 36 (where Λ is the molar conductivity, E is the electric field strength driving the motion of charge carriers and F is Faradays constant).

$$I_{Oh} = nqAv_{drift} \qquad \text{Equation 35}$$

$$v_{drift} = \frac{\Lambda E}{F} \qquad \text{Equation 36}$$

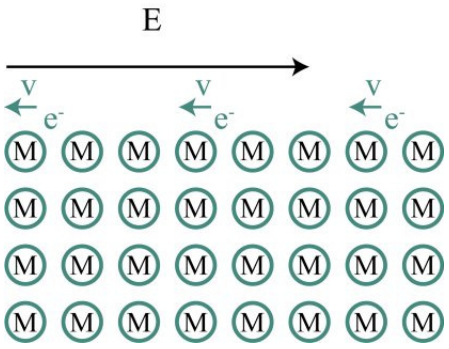

Figure 32: Free electrons in a metal matrix.

Now consider charge carriers in a perfect dielectric. With the application of a potential difference which results in an electric field the molecules in the matrix of the material will form dipoles aligned with the electric field. This results in a physical picture similar to Figure 33. In this case the extent to which the material polarizes and the strength of the electric field determines the total charge generated on either side of the bulk material. Note that unlike the previous example of the perfect conductor, the

* **Gauss' law** is the electrostatic application of the generalized Gauss's theorem giving the equivalence relation between any flux, e.g. of liquids, electric or gravitational, flowing out of any closed surface and the result of inner sources and sinks, such as electric charges or masses enclosed within the closed surface. (Halliday et al. 2001)

charge carriers here physically form the matrix. Hence if any current were to flow in a perfect dielectric the matrix must physically move with the charge. The electric current that would flow would therefore be the charge per unit volume multiplied by the unit volume per second that passes through a known cross sectional area. For the case of the perfect dielectric however, all the charge is always on the surface so the equation can therefore become the charge per unit area multiplied by the unit area per second that passes through a known cross sectional area (see Equation 37 where r is the radius of the jet, vjet is the velocity of the jet and σ_S is the surface charge density).

$$I_C = 2\pi r v_{jet} \sigma_S \qquad \text{Equation 37}$$

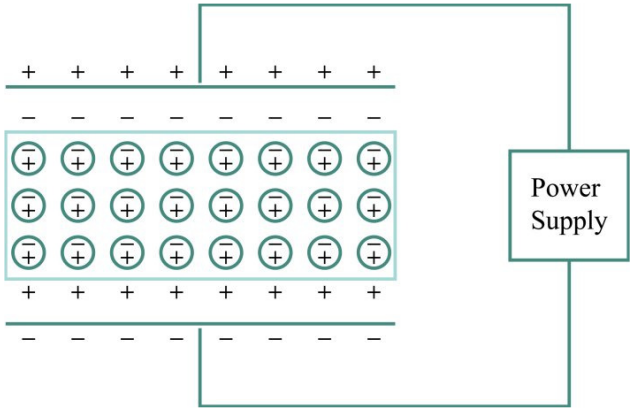

Figure 33: Alignment of dipoles in a dielectric material due to an external field.

Finally consider the motion of ions in a fluid under an applied electric field. Here the ions carry a charge and are able to move like the free electrons described for the perfect conductor. It is possible to use the molar conductivity to find the velocity that an ion will travel at using Equation 36. As a result, using the bulk conductivity of the fluid it is possible to derive Equation 38 (where κ is the solution conductivity) for the ohmic conduction of current in the fluid. However, the ions are not free to move and interact with the fluid around them. This is well known in electrophoresis and there is known as electrophoretic drag (Pombeiro and Amatore 2004). Consider the implications of electrophoretic drag on the moving ions and the fluid around them. As the ions move the fluid around them will be accelerated resulting in the bulk matrix moving as well. This is behaviour like the perfect dielectric. The dual nature of ions in a fluid was recognized by Taylor and led to the definition of a "leaky dielectric model" (Melcher and Taylor 1969). Assuming that these two behaviours are separable functions and that conservation of charge holds it is possible to define the total electric

current flowing anywhere in the jet to be of the form in Equation 39 as numerous authors have done (Hohman et al. 2001, Reznik et al. 2004 and Qin et al. 2004).

$$I_{Oh} = \kappa A E \qquad \text{Equation 38}$$

$$I = \kappa \pi r^2 E + 2\pi r v_{jet} \sigma_S \qquad \text{Equation 39}$$

However in this case the unstated assumption in Equation 39 has been that when charge flows as a result of the convection that this charge flows in a perfect dielectric mode. This is evidenced by the surface charge term in the equation. Once the fibre has lost all the solvent and become solid polymer this is likely to be a valid assumption as charge carriers will become immobile and the polymer will act as a dielectric. However for the intermediary case is such that the ionic charge carriers, although likely to be distributed symmetrically around the z-axis, may be distributed throughout the radius of the jet rather than just on the surface (see Figure 34). As such, for a generalized definition of the electric current flowing in the fluid jet the convective term should be replaced by the more general formula: convective charge density multiplied by the unit volume per second. This then describes the action of the electrophoretic drag on the fluid while the fluid is still behaving in a predominantly ohmic mode. Equation 40 (where $\sigma_{D,C}$ is the volumetric charge density moving in a convective mode) shows the modification to Equation 39 to produce a more generalized formula for the electric current flowing in the fluid jet.

$$I = \kappa \pi r^2 E + \pi r^2 v_{jet} \sigma_{D,C} \qquad \text{Equation 40}$$

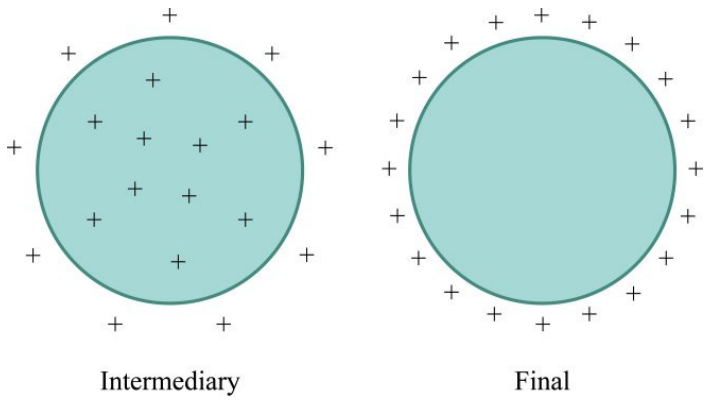

Figure 34: Potential charge distribution for the intermediary and final cases.

Beyond this generalized description of charge transport there are features of the real world physical situation that should be discussed. Firstly is that once all the solvent is lost the charge is expected to have migrated entirely to the jet surface (see Figure 34). This is due to the fact that once the solvent is lost the jet is now entirely solid polymer and hence a dielectric. This would eliminate mobile charge carriers hence reducing the ohmic mode of charge transfer to zero. The rate of migration of charge to the surface of the jet will be dependent on the dielectric constant and on how quickly the solvent is lost. The dielectric constant will represent the ability of the jet to support an internal electric field and hence drive charge to the surface faster than self repulsion. Jarusuwannapoom et al. (2005), Wannatong et al. (2004) and Lee et al. (2003) have observed effects (such as decreasing the fibre diameter and increasing the number of fibres deposited in a given area over time with increasing dielectric constant) on the electrospinning process attributed to the dielectric constant of the solvent.

A significant portion of the total mass is lost in flight due to solvent evaporation. As charge density is a volumetric density the loss of solvent results in a significant reduction of the jet volume that the charge is distributed through. Assuming conservation of charge and no charge loss the charge density must therefore increase. Unless the surface area of the jet scales with the loss of solvent then the profile of the surface charge* over the period of jet evolution will also change. As such surface charge density is dependent on the rate of solvent loss which is a function of the available surface area and the rate of charge migration to the surface. As surface charge is essential to the electrospinning process this is an important factor to address, however is beyond empirical discussion in this body of work.

As an aside, consider the flow of ions when two plates are placed in a fluid. With the application of a potential difference between the two plates there will be a flow of ions towards the respectively oppositely charged plates (see Figure 35). In this case the electrophoretic drag due to the flow of the positively and negatively charged ions will cancel each other out resulting in the apparent motion of only the charged ions. If it were the case that the flow in one direction was essentially unimpeded and the flow in

* Surface charge is the available charge divided by the surface area

the other direction was delayed by a more complex process that the fluid must undergo then the cancelling of the electrophoretic drag may fail resulting in unique behaviour.

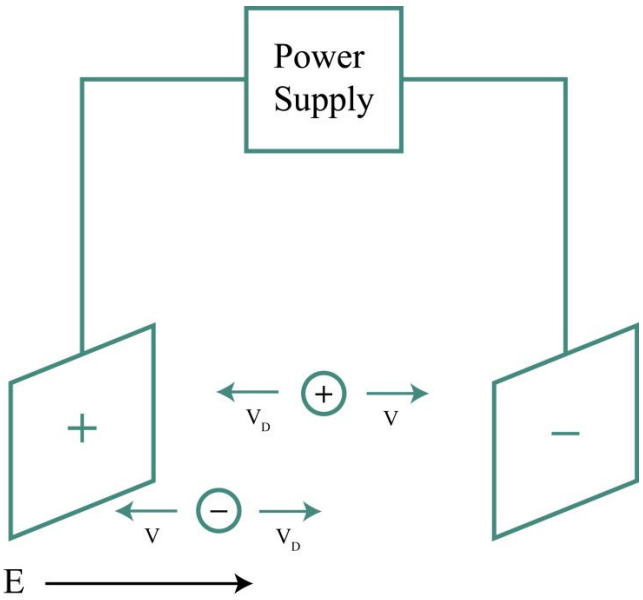

Figure 35: Motion of ions between two charged plates.

The more general form of the current flow in the jet demonstrates that the final radius of the jet is related to the electric current flowing in the jet. It has been shown by some authors (Reznik et al. 2004, Hohman et al. 2001) that a typical electrospinning fluid can be considered a perfect conductor in the initial sense. It is possible to see from Figure 28 (see Chapter 4, Section 1.2.5) that with the addition of an ionic salt to a poly(vinyl alcohol) (PVOH) solution there is a linear trend related to the conductivity. This shows that with sufficient ionic density that the fluid is indeed responding as a conductor.

2. TOTAL CONVERSION OF IONS TO CHARGE CARRIERS

There are two inherent assumptions in the typical discussion of the ohmic and convective charge transport mechanisms. First as discussed in Section 1 is the assumption that there is no charge lost during flight of the jet. Secondly is the assumption that all the ions in the solution participate in one of the two modes of charge transfer. It was shown in Section 1.2.6 of Chapter 4 that the electric current predicted when these two assumptions are made is significantly larger than the observed electric current. The calculated current ignores the dynamics of the charge transfer mechanism and simply assumes the rate of charge transfer from the mass deposition rate and hence knowing the concentration of ions in solution and assuming

that the ions are evenly distributed give a rate of charge transfer (electric current). As such this figure is independent of the mechanism of charge transport and hence should match any proposed theory.

As the observed electric current is significantly lower than the calculated electric current (see Table 11 in Section 1.2.6 of Chapter 4) then one of the two assumptions must be incorrect. If the assumption that all the ions in the solution participate in charge transfer is incorrect then only 18% on average of the ions in solution take part in the charge transfer (Section 1.2.6 of Chapter 4). For this to be true it would require the reaction kinetics of conversion of the counter ion at the electrode at the spinning head to be limited in such a way that only partial conversion could take place. This would result in only a fraction of the ions becoming unpaired and hence providing a charge that could be transported between the electrodes. However it is reasonable to assume that more ions would mean more opportunity for a reaction to occur. The increase in ion concentration (assuming reaction kinetics were responsible for the observed trend) would be expected to result in the unpaired ion fraction becoming larger. As the observed current flow becomes a smaller fraction of the predicted current as ion concentration increases, the reaction kinetics assumption seems unlikely.

If the assumption that no charge is lost during the flight of the jet is incorrect then rather than only 18% on average of the ions in the solution participating in the transfer of charge, only 18% on average of the charge in the initial jet would be retained once the jet reached the collector electrode. The other 82% of the charge would have been lost during the flight of the jet. For this to be true a significant quantity of charge would need to be leaked from the jet in flight. As the electrospun jet has a very small radius of curvature due to its small diameter it may behave similarly to a sharp point, with concentrated field lines near the surface that would draw in the free ions in the air. These ions could then capture the charge on the surface of the jet leading to a slow loss of a significant quantity of charge. Additionally as described by Yarin et al. (2001), during flight the jet loses solvent. As the solvent is lost from the surface of the jet it may also carry some of the charge from the jet providing another pathway for charge to be lost from the jet in flight. An estimation of the expected rate of charge lost from a jet of thinning fluid in electrospinning is beyond the scope of this work it is

unclear as to how well charge loss would fit to the observed trend. Further work examining the electric current drawn from the high voltage power supply could help determine which assumption is incorrect of if both are incorrect the relative contribution to the difference between the calculated and observed electric current.

3. EFFECT OF INCREASING THE CHARGE DENSITY IN AN ELECTROSPINNING FLUID

3.1 Mass Transport when Charge Density is Increased

The application of a suitable electrostatic field to a fluid drop causing it to adopt the shape of the Taylor cone was originally mathematically described by Taylor (1964) and subsequently improved by Reznik et al. (2004). Cone formation is due to the accumulation of charge in the fluid and the resultant competition between surface tension and surface charge repulsion. Therefore it might be expected that an increase in the charge density in an electrospinning fluid should influence the resultant behaviour of the fluid droplet.

The droplet evolution (see Figure 36) moves towards a cone shape with a sharp radius of curvature at the tip. This figure represents a supercritical state as defined by Reznik et al. (2004) where the final time step represents the moment just before jet evolution. The jet evolution is likely to be driven by the concentration of electric stresses at the tip due to the small radius of curvature. Investigation of how the shape of the Taylor cone changes due to different values of charge density has not been published, and it is likely that mathematical modelling would be fruitful. However experimental observations of the decrease in the initial jet diameter when conditions for increased charge density are used (see Chapter 4, Section 2.3 and Section 2.4) suggest that as the charge density increases the cone will adopt a steeper angle with a much smaller radius of curvature at the tip by virtue of a narrower jet being formed at the cone tip.

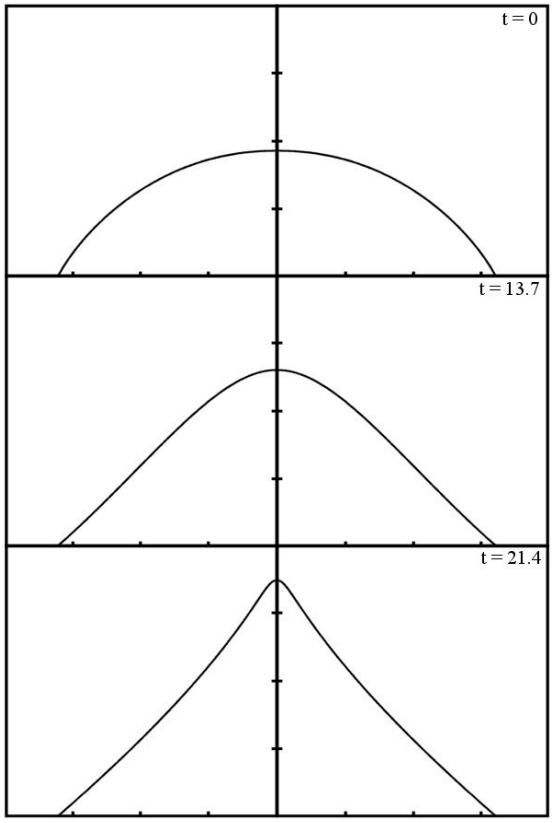

Figure 36: Time evolution of a droplet in an electrostatic field as calculated by Reznik et al. (2004).

With a smaller radius of curvature at the tip of the cone there will be a smaller cross section with a high charge density that the electrostatic field will act on to form a fluid jet. This could be visualized as a "virtual orifice" through which the jet is formed (see Figure 37). If this is true the result will be that a smaller jet will be evolved when the radius of curvature is decreased. Observations in Table 14, Table 19 and Figure 25 show that when there is a higher charge density the initial jet diameter decreases. This supports the theory that increasing the charge density results in a smaller radius of curvature which in turn results in a thinner initial jet.

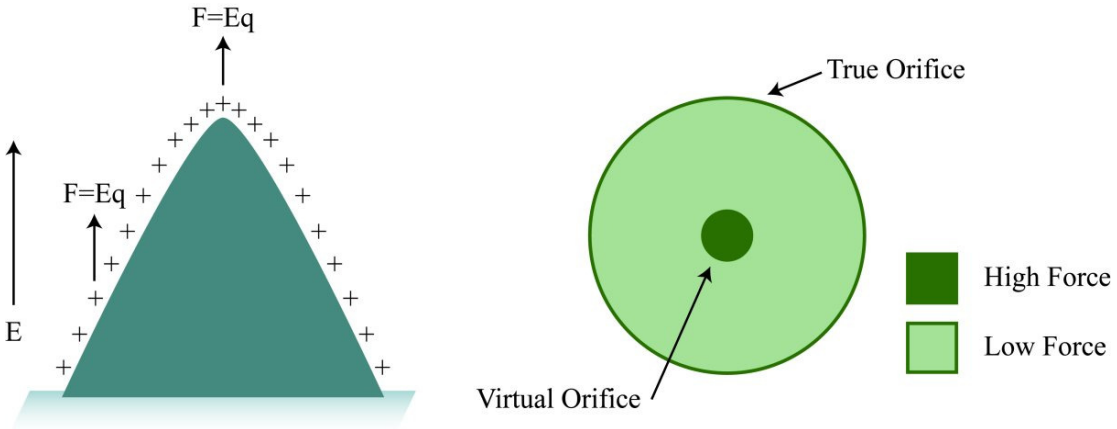

Figure 37: Charge concentration at the tip produces a virtual orifice.

As a direct consequence of reducing the initial jet diameter it would be expected that there will be a decrease in the quantity of mass being transported between the two electrodes. It is established in Figure 25 that with increasing ionic salt concentration there is a corresponding increase in the charge density. Pairing this with the trend for the mass deposition rate (see Figure 22) decreasing with increasing ionic salt concentration shows clearly that as the charge density increases there is a corresponding decrease in the mass deposition rate. This matches with the observed trend in Section 4 of Chapter 4, where the increase in the charge density is not due to the addition of ionic salt. This shows that the decrease in the deposition rate is due to an increase in the charge density.

3.2 Bending Instability when Charge Density is Increased

The bending instability as defined by Yarin et al. (2001) is driven by the self repulsion of a curved fluid jet. The force driving this instability is of the form shown in Equation 41 (Yarin et al. 2001). The onset of this force only occurs once the jet has already been in flight for a length of time as the surface perturbations take time to build up and cause sufficient deflection from the central axis for the jet to become unstable. As such the evolution of the bending instability is highly time dependant. As there is a fixed length of time for the fibre to be in flight, any change in the flight time will affect the extent to which the bending instability occurs. This is important in the typical case of electrospinning because as Reneker et al. (2001) states that the bending instability is vital to the thinning of the jet.

$$F = -\sigma_S^2 \ln\left(\frac{L}{r}\right)|k|d\xi$$

Equation 41

By the definition of charge density there will be more charge per unit volume on the fibre when charge density increases. Consider the case where the volume is constant, an increase in charge density will result in an increase in the force due to the electrostatic field (see Figure 38). An increase in the force along the z-axis will result in a corresponding increase in the acceleration of the fibre along the z-axis. This obviously then corresponds to a decrease in the total flight time and hence the extent to which the bending instability will occur. It will modify the slope of the bending

instability envelope as shown in Figure 39. It is therefore expected that with an increase in charge density there should be a corresponding decrease in the deposition area assuming the surface charge stays constant.

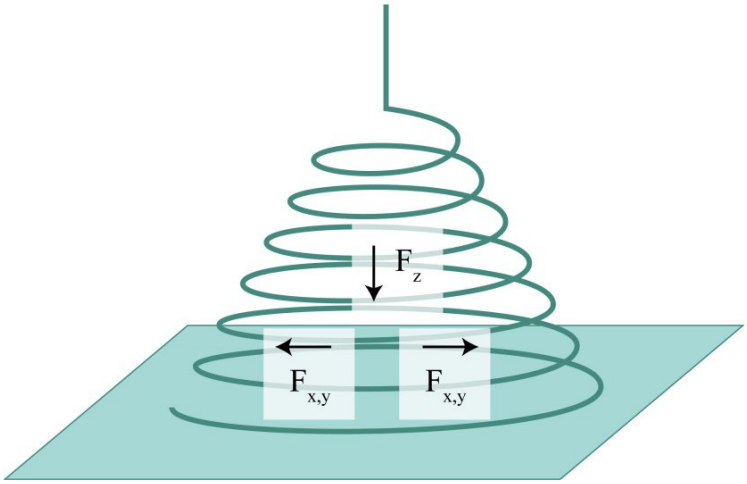

Figure 38: Forces acting on the fibre jet in flight.

Figure 39: Modification of the envelope cone due to increased attraction to the collector assuming equal bending instability force.

4. DOMINANCE OF DIFFERENT CHARGE TRANSFER MECHANISMS

Both Hohman et al. (2001) and Reznik et al. (2004) demonstrate by calculating the ratio of the characteristic charge relaxation time to the characteristic hydrodynamic relaxation time that the region near the electrode an electrospinning fluid behaves as a very good conductor. As discussed in Section 3 of Chapter 4 this shows the relative freedom of charge to move independent to the motion of the fluid. This being the case the ohmic mode of charge transfer will dominate in this region.

Reznik et al. (2004) extended this examination to points further down the jet and found that the ratio quickly approaches unity and then continues to move into a dielectric like behaviour. Near unity the fluid behaves as a "leaky dielectric" where the dielectric and conductive behaviour is approximately equal. This transition of behaviour was found to occur at approximately 5cm from the Taylor cone for a polyethylene oxide solution (see Figure 40). The transition is attributed to the increasing velocity of the jet causing the hydrodynamic relaxation time to decrease. It should be noted that solvent loss was not included in the equations hence failing to take into account the change in the jet properties due to solvent loss. So his model is only valid while the jet retains properties close to the initial solution.

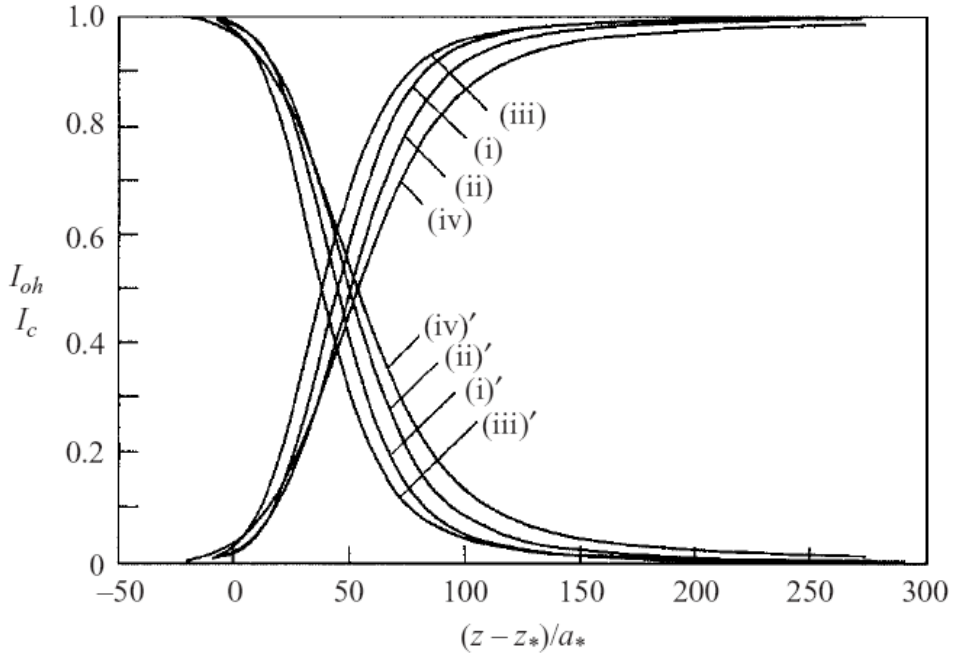

Figure 40: The convective and conductive parts of the electric current versus the coordinate z for the case αs =π/3. Curves (i) and (i) correspond to BoE =5.29, (ii) and (ii) BoE =9, (iii) and (iii) BoE =16, (iv) and (iv) BoE =25. Curves without the prime represent the convective part, those with the prime the conductive one. (Reznik et al. 2004).

It was found that with the introduction of ionic salt to the solution that at the same points along the jet there is an increase in the conductive behaviour. This in turn will increase the dominance of the ohmic mode of charge transfer. This suggests the delaying of the transition into the convective mode of charge transfer. Given the previous discussion on the electric current in the jet (see Section 1), even though charge carried in a convective mode may be partially distributed throughout the jet, unlike the ohmic mode of charge transfer it is possible for charge to accumulate on the

surface. Hence forcing the jet to stay with the ohmic charge transfer mode dominating will delay the transfer of charge to the surface. As shown by Equation 41 in Section 3.2 this will result in a significant decrease in the force that drives the bending instability.

This should then correspond to a drop in the final fibre velocity and the fibre diameter should increase as more ionic salt is added confirmed in Figure 26 (see Chapter 4, Section 1.2.4). Further with the increase in ionic salt concentration there is a corresponding increase in the fibre diameter. One might expect the fibre diameter to decrease as the total charge density has increased, hence once the transition is made there will be a much larger surface charge density and as the force is dependent on the square of surface charge density this will significantly increase the force. However consider the effects of solvent loss. When the increased force is applied the jet will have lost more solvent and hence the jet will change from being a viscous liquid jet to a viscoelastic polymer gel or solid polymer with a modulus. This means that once the jet has lost sufficient solvent to have gained significant elastic properties the force must first overcome the elastic portion of the viscoelastic response before further permanent deformation can occur.

5. TRENDS OBSERVED DUE TO THE ADDITION OF AN IONIC SALT

The proposed mechanisms that results in the trends seen in Table 10 (see Chapter 4, Section 1.2.4) will be consecutively discussed here. Electric current flow increases because of the increase in conductivity of the PVOH solution. There is an increase in the charge density and charge per unit length due to the increase in the conductivity of the PVOH solution. The mass deposition rate decreases due to the increase in charge density causing a steeper Taylor cone to develop with a smaller zone for the electric force to act on. This causes a thinner jet to be evolved from the tip of the Taylor cone (see Chapter 5, Section 3.1). The final fibre velocity deceases due to two likely reasons. Firstly, a reduction in the time available for the bending instability will occur due to the increase in charge density and hence a higher force along the z-axis. Secondly, slower migration of charge from the centre of the jet to the surface will result in a decrease in the force driving the instability. The radius of the final fibre increases due to the decrease in the final fibre velocity.

As shown in Equation 38 (see Section 1) the electric current for an ohmic charge transfer mechanism is dependent on the solution conductivity. At the high voltage electrode the diameter of the jet is fixed by the inner diameter of the insert. Making the reasonable assumption that the addition of an ionic salt will not significantly affect the z-axis component of the electric field present near the high voltage electrode, an increase in conductivity should directly relate to an increase in the electric current flow. This is found to be the case at salt concentrations above 0.005 molL-1 which correspond to a conductivity of above 0.5 mScm-1 where the electric current shows a linear response to conductivity hence following Ohm's law.

An increase in conductivity represents an increase in one or two factors. The ionic drift velocity or the number of ions in the solution. As the concentration of ionic salt increases the drift velocity decreases slightly but the number of available ions to carry charge increases significantly. As such it would be expected that an increase in the charge density should result from an increase in the ionic salt concentration. It is also expected that unless the jet radius is directly dependant on the charge density that the charge per unit length should also increase with increasing charge density. As previously discussed less mass is transported between the two electrodes when the charge density increases due to a smaller radius of curvature at the Taylor cone tip resulting in a narrower jet.

The velocity will decrease due to three possible changes to the electrospinning mechanism. First as previously discussed; the increase in charge density will result in a decrease in the available time for the bending instability to develop resulting in a narrowing of the envelope cone. If all other effects are constant this will result in a lower velocity. Secondly also as previously discussed; the increase in the solution conductivity will modify the charge relaxation time, delaying the migration of charge from within the jet to the surface. If all other effects are constant this will reduce the force from the bending instability causing less stretching resulting in less fibre per second deposited. This delay of charge migration will also result in more solvent being lost before the charge does migrate to the surface and hence the jet will have a viscoelastic behaviour moving closer being a solid polymer with a modulus and hence resist acceleration and stretching. Finally if the initial development of the bending

instability has been modified then the final result once the fibre reaches the collector would have been modified significantly. Specifically if there was a lower initial whipping frequency then that would result in a significantly lower final velocity.

The final fibre diameter will have increased due to the decreased extent of the bending instability when more ionic salt is added. Due to the decrease in time available for the bending instability to evolve and the delay in the migration of charge to the surface there must be a decrease in the final fibre velocity. The extent to which the bending instability can accelerate the fibre must be limited by charge conservation (assuming no charge is lost from the system) demonstrated by the form the convective charge transport term takes in Equation 40. Here, if the quantity of charge transported is a constant, then the square of the radius is proportional to the inverse of the velocity of the jet. Hence the fibre diameter must follow the trend set by the final fibre velocity.

6. TRENDS DUE TO CHANGING THE SIGN OF THE CHARGE ON THE POLYMER SOLUTION

The results shown in Table 14 and Table 15 (see Chapter 4, Section 4.2.1 and Section 4.2.2) clearly contradict those found by Mit-Uppatham et al. (2004) and Supaphol et al. (2005). In this case the authors claim that the dissolution of polyamide-6 (PA-6) in formic acid results in the formation of ammonium cationic tails on the polymer and formic acid anions and attribute the change in behaviour to the difference in ion size. As shown by Son et al. (2004) the dissolution of PVOH in water will result in the protonation of some alcohol side chains at an acidic pH. A fresh solution of PVOH made up in distilled water typically has a pH of around 6.5 and hence must have some cationic side chains.

However Mit-Uppatham et al. (2004) and Supaphol et al. (2005) found that a negative charge on the polymer resulted in more mass being transported and larger fibres being formed; this being the opposite of the observations in Section 4 from Chapter 4. Further the authors claim that the increase in mass transport is due to an increase in charge density due to the smaller size of the formic acid anion. Yet observations in Table 19, Table 14 (see Chapter 4, Section 4.2.1 and Section 4.2.2) and Section 2.3 of Chapter 4, clearly show that an increase in charge density corresponds to a decrease in

the mass transported. As the charge density was not measured by either Mit-Uppatham et al. (2004) or Supaphol et al. (2005) it cannot be confirmed that an increase in charge density resulted in an increase in mass being transported in their case.

Further to this, in the work by Sustasinpromprae et al. (2006) where polyarcylonitrile (PAN) is spun from dimethylformamide (DMF) there is no difference found due to changing the sign of the charge on the polymer solution. This clearly shows that if PVOH dissolved in water shows opposite effects to PA-6 dissolved in formic acid and PAN dissolved in DMF shows no effect at all that the cause of this effect must be due to the polymer/solvent system. It is difficult to discern why there is an increase in the charge density of the PVOH solution when it is charged with a positive sign and is beyond the scope of this document. It does however warrant further in depth investigation as the number of observations available is obviously too small to allow the mechanism to be clear.

As a mirror to Section 4 the proposed mechanisms that results in the trends seen in Table 20 (see Chapter 4, Section 4.2.2) will be consecutively discussed here. There is an increase in the charge density due to an unknown mechanism. The charge per unit length stays approximately constant between the two signs of charge suggesting the possibility that this is a constant unaffected by the change in the charge sign however without more observations it is premature to make such an assumption. Electric current flow decreases because of the decrease in the deposition rate and as such with less mass transported and without a corresponding increase in conductivity that would allow more ohmic charge transport there is less total charge transported. The deposition rate decreases due to the increase in charge density resulting in a smaller zone for the electric force to act on causing a thinner jet to be evolved from the tip of the Taylor cone as correlated with observations due to the addition of an ionic salt.

The decrease in velocity and final fibre diameter is likely due to a complex relationship between the initial conditions of the jet and the development of the bending instability. As is can be seen from Table 18 (see Chapter 4, Section 4.2.2) taking the final fibre velocity and assuming that the bending instability loop diameters are linearly proportional to the final deposition area diameter it is possible to calculate

the number of loops impacting with the collector per second. Although this isn't the true number of loops per second due to the more complex behaviour of the bending instability than shown in Figure 11 (see Chapter 2, Section 3.2.4), it can still be used for comparison purposes if the assumption holds that the loop sizes are linearly related to the maximum diameter of the bending instability envelope cone. All this being the case the results show that there is an increase in the number of loops per second for the higher charge density situation which will correspond to the frequency of the initiation of the bending instability. As such, without the increase in the ohmic charge transfer mechanism shown by the addition of an ionic salt, the increase in the charge density results in an increase in the bending instability shown by the increased number of loops per second impacting with the collector and the larger ratio of initial radius to final radius. To fully explore the mechanism by which the increased number of smaller loops is formed a detailed analysis similar to the work done by Hohman et al. (2001) combined with the work by Yarin et al. (2001) would need to be undertaken which is beyond the scope of this work.

Chapter 6

Conclusions

CONCLUSIONS

It was found that current models for charge transfer in electrospinning models neglect free electron effects and make the assumption that all charge transported by a convective transport mode resides on the surface of the jet. A generalized equation describing the different charge transport modes has been presented as Equation 40.

An expected electric current was calculated for a number of electrospinning solutions, making the assumptions that the ions in an electrospinning solution were evenly distributed, that all ions participate in the transfer of charge and that no charge is lost during flight. It was found that the observed electric current was typically only approximately 18% of the predicted electric current, demonstrating that at least one of the assumptions was incorrect.

In two different experiments it was found that an increase in charge density corresponded to a decrease in the mass deposition rate. It is proposed that an increase in charge density results in a smaller radius of curvature at the tip of the Taylor cone creating a smaller virtual orifice and that hence a smaller electrospun jet is formed due to the concentration of electric stresses on a smaller area. Further theoretical modelling has been proposed to test this theory.

Further, it was proposed that the strength and behaviour of the bending instability would depend on the relative strengths of the two charge transfer mechanisms (ohmic and convective). If the electrospinning solution was initially more like a conductor then it is expected that there will be a delay of the migration of charge to the surface of the jet resulting in a delay on the full strength of the bending instability (see Equation 19). This explains the observation that a thicker fibre is produced when the conductivity of an electrospinning solution increases.

It was also observed that the addition of an ionic salt to an electrospinning solution resulted in the increase in the charge density and electric current. This was attributed to the increase in conductivity and hence, an increase in the initial ohmic charge transfer. As mentioned previously, the increased charge density resulted in a smaller virtual orifice and a consequent decrease in mass deposition rate. The increase in conductivity caused a delay in the transition between predominantly ohmic charge

transfer to predominantly convective charge transfer that resulted in a decrease in the amount of stretching when the jet was still liquid resulting in thicker fibres with a lower final velocity.

Using these insights, the observations from changing the sign of the charge on the polymer were re-examined. When changing from a positive charge to a negative charge it was found that there was an increase in the charge density. The increase in charge density resulted in a decrease in the mass deposition rate due to a smaller virtual orifice. Further, it was demonstrated that although a lower final fibre velocity was observed when a negative charge was used; the bending instability was actually stronger showing that the calculation of the final fibre velocity using Equation 21 can lead to incorrect interpretation. The increase in the bending instability accounts for the decrease in the final fibre diameter. It was found that currently proposed theories to explain this difference in behaviour between positive and negative charge were insufficient in the matter of predicting the observed behaviour, however another theory was not proposed.

REFERENCES

ANTON, H. (1999) *Calculus: A new horizon*, Wiley Press.

ATKINS, P. W. (1994) *Physical Chemistry,* Oxford, Oxford University Press.

BATCHELOR, G. K. (2000) *An Introduction to Fluid Dynamics*, Cambridge University Press.

BAUMGARTEN, P. K. (1971) Electrtostatic Spinning of Acrylic Microfibres. *Journal of Colloid Interface Science,* 36**,** 75-79.

BLADES, A. T., IKONOMOU, M. G. & KEBARLE, P. (1991) Mechanism of Electrospray Mass Spectrometry. Electrospray as an Electrolysis Cell. *Analytical Chemistry,* 63**,** 2109-2114.

BRISCOE, B., LUCKHAM, P. & ZHU, S. (2000) The effects of hydrogen bonding upon the viscosity of aqueous poly(vinyl alcohol) solutions. *Polymer,* 41**,** 3851-3860.

BUCHKO, C. J., CHEN, L. C., SHEN, Y. & MARTIN, D. C. (1999) Processing and microstructural characterization of porous biocompatible protein polymer thin films. *Polymer,* 40**,** 7397–7407.

CASPER, C. L., STEPHENS, J. S., TASSI, N. G., CHASE, D. B. & RABOLT, J. F. (2004) Controlling Surface Morphology of Electrospun Polystyrene Fibers: Effect of Humidity and Molecular Weight in the Electrospinning Process. *Macromolecules,* 37**,** 573-578.

CHANG, R. (1998) *Chemistry*, McGraw Hill.

CHOI, J. S., LEE, S. W., JEONG, L., BAE, S.-H., MIN, B. C., YOUK, J. H. & PARK, W. H. (2004) Effect of organosoluble salts on the nanofibrous structure of electrospun poly(3-hydroxybutyrate-co-3-hydroxyvalerate). *International Journal of Biological Macromolecules,* 34**,** 249-256.

CHUANGCHOTE, S. & SUPAPHOL, P. (2006) Fabrication of aligned poly(vinyl alcohol) nanofibers by electrospinning. *Journal of Nanoscience and Nanotechnology,* 6**,** 125-129.

CRC-PRESS (2004) *CRC Handbook of Chemistry and Physics,* Cleveland, Ohio, CRC Press.

DABIRIAN, F., HOSSEINI, Y. & RAVANDI, S. A. H. (2007) Manipulation of the electric field of electrospinning system to produce polyacrylonitrile nanofiber yarn. *Journal of the Textile Institute,* 98**,** 237-241.

DEITZEL, J. M., KLEINMEYER, J., HARRIS, D. & TAN, N. C. B. (2001) Effect of processing variables on the morphology of electrospun nanofibers and textiles. *Polymer,* 42**,** 261-272.

DEMIR, M. M., YILGOR, I., YILGOR, E. & ERMAN, B. (2002) Electrospinning of polyurethane fibers. *Polymer,* 43**,** 3303-3309.

DOSHI, J. & RENEKER, D. H. (1995) Electrospinning Process and Applications of Electrospun Fibers. *Journal of Electrostatics,* 35**,** 151-160.

EDA, G., LIU, J. & SHIVKUMAR, S. (2007) Flight path of electrospun polystyrene solutions: Effects of molecular weight and concentration. *Materials Letters,* 61**,** 1451-1455.

FANG, D., HSIAO, B. S. & CHU, B. (2003) Multiple-jet Electrospinning of Non-woven Nanofiber Articles. *Polymer Preprints,* 44**,** 59-60.

FENG, J. J. (2002) The stretching of an electrified non-Newtonian jet: A model for electrospinning. *Physics of Fluids,* 14**,** 3912-3926.

FONG, H., CHUN, I. & RENEKER, D. H. (1999) Beaded nanofibers formed during electrospinning. *Polymer,* 40**,** 4585-4592.

FONG, H. & RENEKER, D. H. (1999) Elastomeric nanofibers of styrene-butadiene-styrene triblock copolymer. *Journal of Polymer Science, Part B: Polymer Physics,* 37**,** 3488-3493.
FORMHALS, A. (1934) Process and Apparatus for Preparing Artificial Threads. United States of America.
FORMHALS, A. (1943) Production of Artificial Fibers from Fiber forming Liquids. United States of America.
FORMHALS, A. (1944) Method and Apparatus for Spinning. United States of America.
GILBERT, W. (1628) *De Magnete, Magneticisque Corporibus, et de Magno Magnete Tellure (On the Magnet and Magnetic Bodies, and on That Great Magnet the Earth),* London, Peter Short.
GU, B. K., SHIN, M. K., SOHN, K. W., KIM, S. I., KIM, S. J., KIM, S. K., LEE, H. & PARK, J. S. (2007) Direct fabrication of twisted nanofibers by electrospinning. *Applied Physics Letters,* 90.
GUPTA, P. & WILKES, G. L. (2003) Some investigations on the fiber formation by utilizing a side-by-side bicomponent electrospinning approach. *Polymer,* 44**,** 6353-6359.
HALLIDAY, D., RESNICK, R. & WALKER, J. (2001) *Fundamentals of physics,* New York, John Wiley & Sons.
HEADLEY, L. C., PIERCE, C. I. & SAWYER, W. K. (1970) Fluid flow in channels, capillaries and porous media under the influence of an electric field. Washington, United States Department of the Interior, Bureau of Mines.
HOHMAN, M. M., SHIN, M., RUTLEDGE, G. & BRENNER, M. P. (2001) Electrospinning and electrically forced jets. I. Stability theory. *Physics of Fluids,* 13**,** 2201-2220.
HUANG, Z.-M., ZHANG, Y. Z., KOTAKI, M. & RAMAKRISHNA, S. (2003) A review on polymer nanofibers by electrospinning and their applications in nanocomposites. *Composites Science and Technology,* 63**,** 2223-2253.
JARUSUWANNAPOOM, T., HONGROJJANAWIWAT, W., JITJAICHAM, S., WANNATONG, L., NITHITANAKUL, M., PATTAMAPROM, C., KOOMBHONGSE, P., RANGKUPAN, R. & SUPAPHOL, P. (2005) Effect of solvents on electro-spinnability of polystyrene solutions and morphological appearance of resulting electrospun polystyrene fibers. *European Polymer Journal,* 41**,** 409-421.
JIRSAK, O., MARTINOVA, L., SANETRNIK, F., CHALOUPEK, J., LUKAS, D. & KOTEK, V. (2006) A method of nanofibres production from a polymer solution using electrostatic spinning and a device for carrying out the method. IN ORGANIZATION, W. I. P. (Ed.) Czech Republic, Technicka Univerzita Liberci.
KERR, J. (2008) Conductivity of Poly(vinyl alcohol) solutions in distilled water. IN STANGER, J. (Ed.) Christchurch.
KIM, C.-W., FREY, M. W., MARQUEZ, M. & JOO, Y. L. (2005) Preparation of Submicron-Scale, Electrospun Cellulose Fibres via Direct Dissolution. *Journal of Polymer Science,* 43**,** 1673-1685.
KOSKI, A., YIM, K. & SHIVKUMAR, S. (2004) Effect of molecular weight on fibrous PVA produced by electrospinning. *Materials Letters,* 58**,** 493-497.
LARSEN, G., SPRETZ, R. & VELARDE-ORTIZ, R. (2004) Use of coaxial gas jackets to stabilize Taylor cones of volitile solutions and to induce particle-to-fibre transitions. *Advanced Materials,* 16**,** 166-169.

LEE, J. S., CHOI, K. H., GHIM, H. D., KIM, S. S., CHUN, D. H., KIM, H. Y. & LYOO, W. S. (2004) Role of Molecular Weight of Atactic Poly(vinyl alcohol) (PVA) in the Structure and Properties of PVA Nanofabric Prepared by Electrospinning. *Journal of Applied Polymer Science,* 93**,** 1638-1646.
LEE, K. H., KIM, H. Y., KHIL, M. S., RA, Y. M. & LEE, D. R. (2003) Characterization of nano-structured poly(1-caprolactone) nonwoven mats via electrospinning. *Polymer,* 44**,** 1287-1294.
LI, D., OUYANG, G., MCCANN, J. T. & XIA, Y. (2005) Collecting Electrospun Nanofibers with Patterned Electrodes. *Nano Letters,* 5**,** 913-916.
LI, D., WANG, Y. & XIA, Y. (2004) Electrospinning Nanofibers as Uniaxially Aligned Arrays and Layer-by-Layer Stacked Films. *Advanced Materials,* 16**,** 361-366.
LI, D. & XIA, Y. (2004) Direct Fabrication of Composite and Ceramic Hollow Nanofibers by Electrospinning. *Nano Letters,* 4**,** 933-938.
LI, M., GUO, Y., WEI, Y., MACDIARMID, A. G. & LELKES, P. I. (2006) Electrospinning polyaniline-contained gelatin nanofibers for tissue engineering applications. *Biomaterials,* 27**,** 2705-2715.
LIN, Y., YAO, Y. Y., YANG, X. Z., WEI, N., LI, X. Q., GONG, P., LI, R. X. & WU, D. C. (2008) Preparation of poly(ether sulfone) nanofibers by gas-jet/electrospinning. *Journal of Applied Polymer Science,* 107**,** 909-917.
MEGELSKI, S., STEPHENS, J. S., CHASE, D. B. & RABOLT, J. F. (2002) Micro- and Nanostructured Surface Morphology on Electrospun Polymer Fibers. *Macromolecules,* 35**,** 8456-8466.
MELCHER, J. R. & TAYLOR, G. (1969) Electrohydrodynamics: A Review of the Role of Interfacial Shear Stresses. *Annual Review of Fluid Mechanics,* 1**,** 111-146.
MIT-UPPATHAM, C., NITHITANAKUL, M. & SUPAPHOL, P. (2004a) Effects of Solution Concentration, Emitting Electrode Polarity, Solvent Type, and Salt Addition on Electrospun Polyamide-6 Fibres: A Preliminary Report. *Macromolecular Symposium,* 216**,** 293-299.
MIT-UPPATHAM, C., NITHITANAKUL, M. & SUPAPHOL, P. (2004b) Ultrafine Electrospun Polyamide-6 Fibers: Effect of Solution Conditions on Morphology and Average Fiber Diameter. *Macromolecular Chemistry and Physics,* 205**,** 2327-2338.
MO, X. M., XU, C. Y., KOTAKI, M. & RAMAKRISHNA, S. (2004) Electrospun P(LLA-CL) nanofiber: a biomimetic extracellular matrix for smooth muscle cell and endothelial cell proliferation. *Biomaterials,* 25**,** 1883-1890.
MORTON, W. J. (1902) Method of dispersing fluids. IN OFFICE, U. S. P. (Ed.) United States of America.
POMBEIRO, A. J. L. & AMATORE, C. (2004) *Trends in Molecular Electrochemistry*, CRC Press.
QIN, X.-H., WAN, Y.-Q., HE, J.-H., ZHANG, J., YU, J.-Y. & WANG, S.-Y. (2004) Effect of LiCl on electrospinning of PAN polymer solution: theoretical analysis and experimental verification. *Polymer,* 45**,** 6409-6413.
QIN, X.-H., YANG, E.-L., LI, N. & WANG, S.-Y. (2007) Effect of Different Salts on Electrospinning of Polyacrylonitrile (PAN) Polymer Solution. *Journal of Applied Polymer Science,* 103**,** 3865-3870.
RAM, A. (1997) *Fundamentals of Polymer Engineering*, Springer Publishing.
RAMAKRISHNA, S., FUJIHARA, K., TEO, W., LIM, T. & MA, Z. (2006) *An Introduction to Electrospinning and Nanofibers*, World Scientific.

RENEKER, D. H., YARIN, A. L., FONG, H. & KOOMBHONGSE, S. (2000) Bending instability of electrically charged liquid jets of polymer solutions in electrospinning. *Journal of Applied Physics,* 87**,** 4531-4547.
REZNIK, S. N., YARIN, A. L., THERON, A. & ZUSSMAN, E. (2004) Transient and steady shapes of droplets attached to a surface in a strong electric field. *Journal of Fluid Mechanics,* 516**,** 349-377.
RUTLEDGE, G. C., SHIN, M. Y., WARNER, S. B., BUER, A., GRIMLER, M. & UGBOLUE, S. C. (2001) A Fundamental Investigation of the Formation and Properties of Electrospun Fibers. *National Textile Center Annual Report: November 2001*.
SASLOW, W. M. (2002) *Electricity, Magnetism and Light*, Academic Press.
SHIN, Y. M., HOHMAN, M. M., BRENNER, M. P. & RUTLEDGE, G. C. (2001a) Electrospinning: A whipping fluid jet generates submicron polymer fibers. *Applied Physics Letters,* 78**,** 1149-1151.
SHIN, Y. M., HOHMAN, M. M., BRENNER, M. P. & RUTLEDGE, G. C. (2001b) Experimental characterization of electrospinning: the electrically forced jet and instabilities. *Polymer,* 42**,** 9955-9967.
SIMONET, M., SCHNEIDER, O. D., NEUENSCHWANDER, P. & STARK, W. J. (2007) Ultraporous 3D polymer meshes by low-temperature electrospinning: Use of ice crystals as a removable void template. *Polymer Engineering and Science,* 47**,** 2020-2026.
SON, W. K., HO YOUK, J., SEUNG LEE, T. & PARK, W. H. (2005) Effect of pH on electrospinning of poly(vinyl alcohol). *Materials Letters,* 59**,** 1571-1575.
SON, W. K., YOUK, J. H., LEE, T. S. & PARK, W. H. (2004a) The effects of solution properties and polyelectrolyte on electrospinning of ultrafine poly(ethylene oxide) fibers. *Polymer,* 45**,** 2959-2966.
SON, W. K., YOUK, J. H., LEE, T. S. & PARK, W. H. (2004b) Electrospinning of Ultrafine Cellulose Acetate Fibers: Studies of a New Solvent System and Deacetylation of Ultrafine Cellulose Acetate Fibers. *Journal of Polymer Science: Part B: Polymer Physics,* 42**,** 5-11.
SUPAPHOL, P., MIT-UPPATHAM, C. & NITHITANAKUL, M. (2005a) Ultrafine Electrospun Polyamide-6 Fibers: Effect of Emitting Electrode Polarity on Morphology and Average Fibre Diameter. *Journal of Polymer Science: Part B: Polymer Physics,* 43**,** 3699-3712.
SUPAPHOL, P., MIT-UPPATHAM, C. & NITHITANAKUL, M. (2005b) Ultrafine Electrospun Polyamide-6 Fibers: Effects of Solvent System and Emitting Electrode Polarity on Morphology and Average Fiber Diameter. *Macromolecular Materials and Engineering,* 290**,** 933-942.
SUTASINPROMPRAE, J., JITJAICHAM, S., NITHITANAKUL, M., MEECHAISUE, C. & SUPAPHOL, P. (2006) Preparation and characterization of ultrafine electrospun polyacrylonitrile fibers and their subsequent pyrolysis to carbon fibers. *Polymer International,* 55**,** 825-833.
TABELING, P. (2005) *Introduction to Microfluidics*, Oxford University Press.
TAYLOR, G. (1964) Disintegration of Water Drops in an Electric Field. *Proceedings of the Royal Society of London A: Mathematical, Physical & Engineering Sciences,* 280**,** 383-397.
TAYLOR, G. (1965) The force exerted by an electric field on a long cylindrical conductor. *Proceedings of the Royal Society of London A: Mathematical, Physical & Engineering Sciences,* 291**,** 145-158.

TAYLOR, G. (1969) Electrically Driven Jets. *Proceedings of the Royal Society of London A: Mathematical, Physical & Engineering Sciences,* 313**,** 453-475.
TEO, W. E., KOTAKI, M., MO, X. M. & RAMAKRISHNA, S. (2005) Porous tubular structures with controlled fibre orientation using a modified electrospinning method. *Nanotechnology,* 16**,** 918-924.
TEO, W. E. & RAMAKRISHNA, S. (2005) Electrospun fibre bundle made of aligned nanofibres over two fixed points. *Nanotechnology,* 16**,** 1878-1884.
THOMPSON, C. J., CHASE, G. G., YARIN, A. L. & RENEKER, D. H. (2007) Effects of parameters on nanofiber diameter determined from electrospinning model. *Polymer,* 48**,** 6913-6922.
WANG, H., SHAO, H. & HU, X. (2006) Structure of Silk Fibroin Fibres Made by an Electrospinning Process from a Silk Fibroin Aqueous Solution. *Journal of Applied Polymer Science,* 101**,** 961-968.
WANNATONG, L., SIRIVAT, A. & SUPAPHOL, P. (2004) Effects of solvents on electrospun polymeric fibers: preliminary study on polystyrene. *Polymer International,* 53**,** 1851-1859.
YANG, Y., JIA, Z. D., HOU, L., LI, Q. A., WANG, L. M. & GUAN, Z. C. (2008) Controlled deposition of electrospinning jet by electric field distribution from an insulating material surrounding the barrel of the polymer solution. *Ieee Transactions on Dielectrics and Electrical Insulation,* 15**,** 269-276.
YARIN, A. L. (1993) *Free Liquid Jets and Films: Hydrodynamics and Rheology,* New York, Longman, Harlow and Wiley.
YARIN, A. L., KOOMBHONGSE, S. & RENEKER, D. H. (2001) Bending instability in electrospinning of nanofibers. *Journal of Applied Physics,* 89**,** 3018-3026.
YARIN, A. L. & ZUSSMAN, E. (2004) Upward needleless electrospinning of multiple nanofibers. *Polymer,* 45**,** 2977-2980.
YUAN, X., ZHANG, Y., DONG, C. & SHENG, J. (2004) Morphology of ultrafine polysulfone fibers prepared by electrospinning. *Polymer International,* 53**,** 1704-1710.
ZELENY, J. (1914) The Electrical Discharge from Liquid Points, and A Hydrostatic Method of Measuring the Electric Intensity at thier Surfaces. *Physical Review,* 3**,** 69-91.
ZENG, J., XU, X., CHEN, X., LIANG, Q., BIAN, X., YANG, L. & JING, X. (2003) Biodegradable electrospun fibers for drug delivery. *Journal of Controlled Release,* 92**,** 227-231.
ZHANG, C., YUAN, X., WU, L., HAN, Y. & SHENG, J. (2005) Study on morphology of electrospun poly(vinyl alcohol) mats. *European Polymer Journal,* 41**,** 423-432.
ZHAO, S., WU, X., WANG, L. & HUANG, Y. (2004) Electrospinning of Ethyl–Cyanoethyl Cellulose/Tetrahydrofuran Solutions. *Journal of Applied Polymer Science,* 91**,** 242-246.
ZONG, X., KIM, K., FANG, D., RAN, S., HSIAO, B. S. & CHU, B. (2002) Structure and process relationship of electrospun bioabsorbable nanofiber membranes. *Polymer,* 43**,** 4403-4412.

APPENDIX A
ELECTRON MICROSCOPE IMAGES

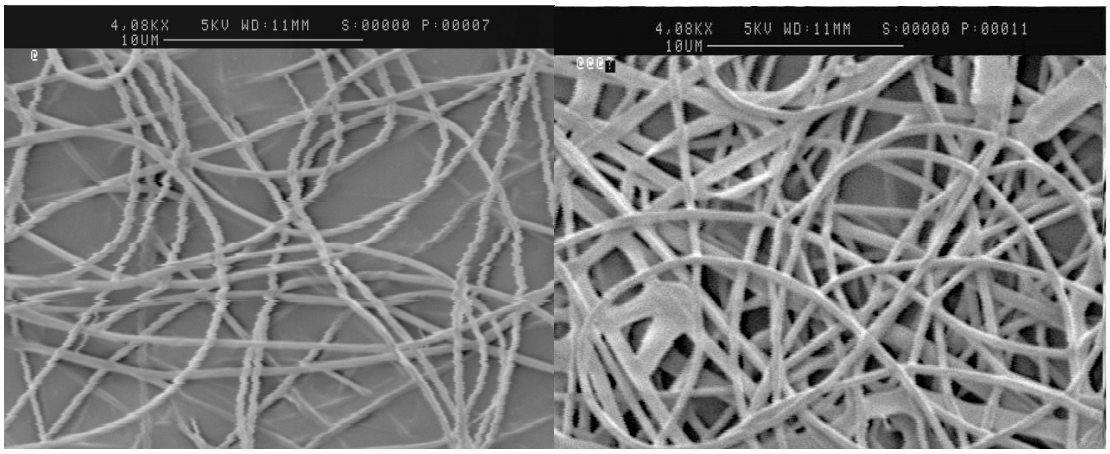

Figure 1: SEM images of electrospun PVOH fibres with no ionic salt added (left) and 0.1% KCl (right)

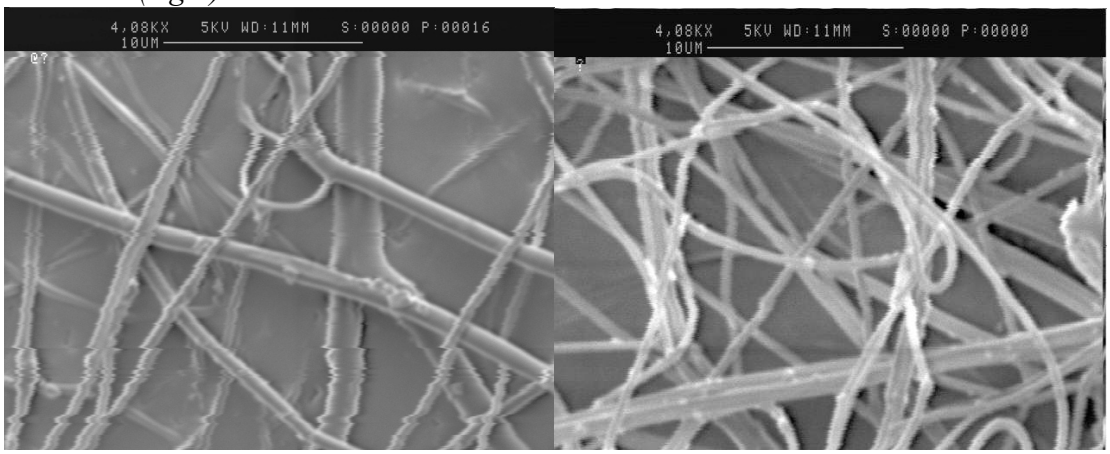

Figure 2: SEM images of electrospun PVOH fibres with 0.25% KCl (left) and 0.5% KCl (right)

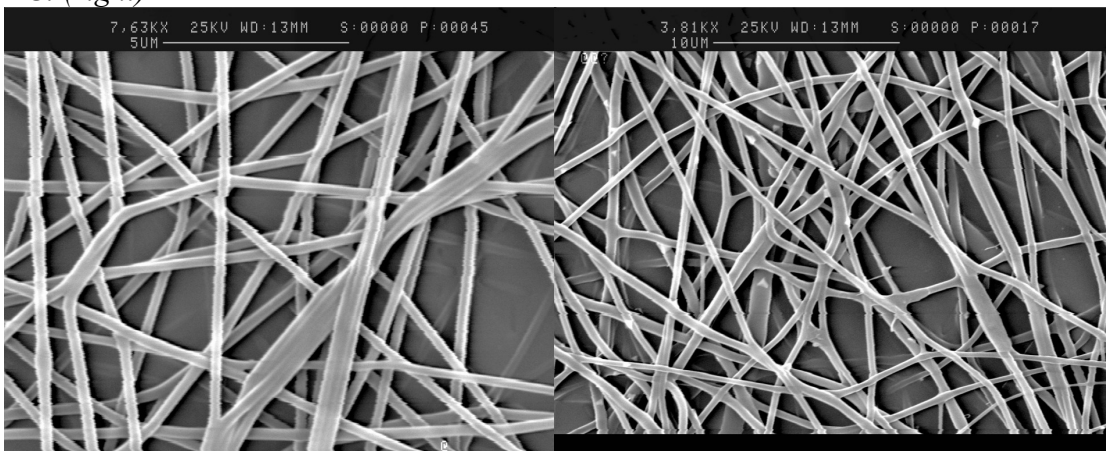

Figure 3: SEM images of electrospun PVOH fibres with 0.1% LiCl (left) and 0.25% LiCl (right)

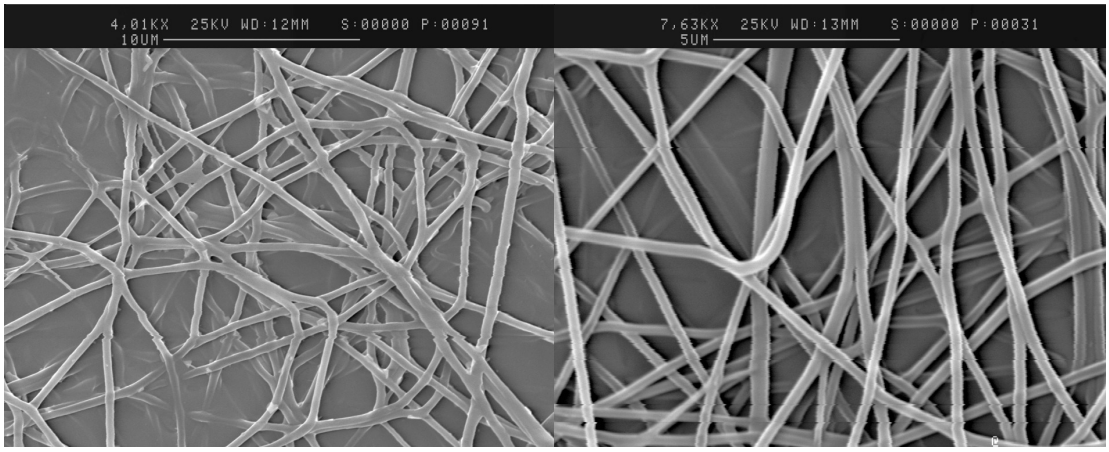

Figure 4: SEM images of electrospun PVOH fibres with 0.5% LiCl (left) and 0.01% LiF (right)

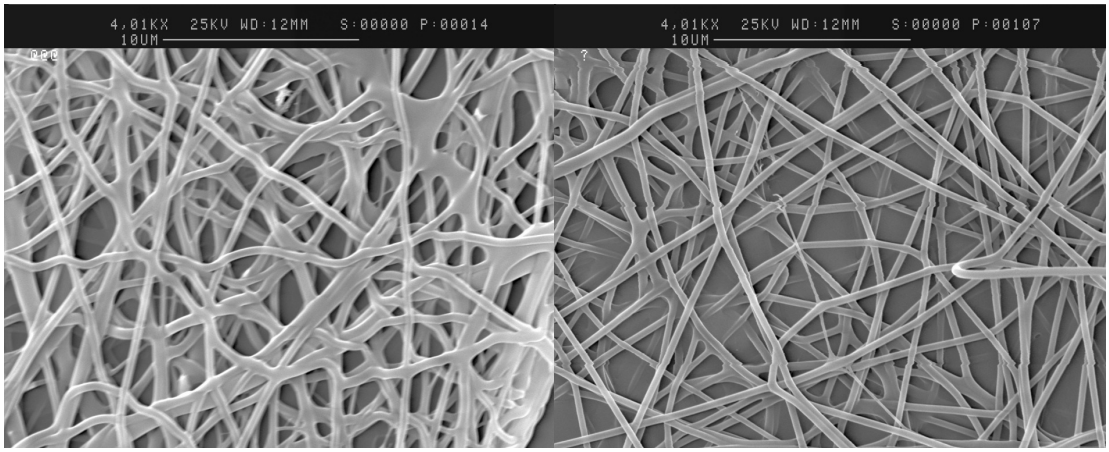

Figure 5: SEM images of electrospun PVOH fibres with 0.025% LiF (left) and 0.1% LiBr (right)

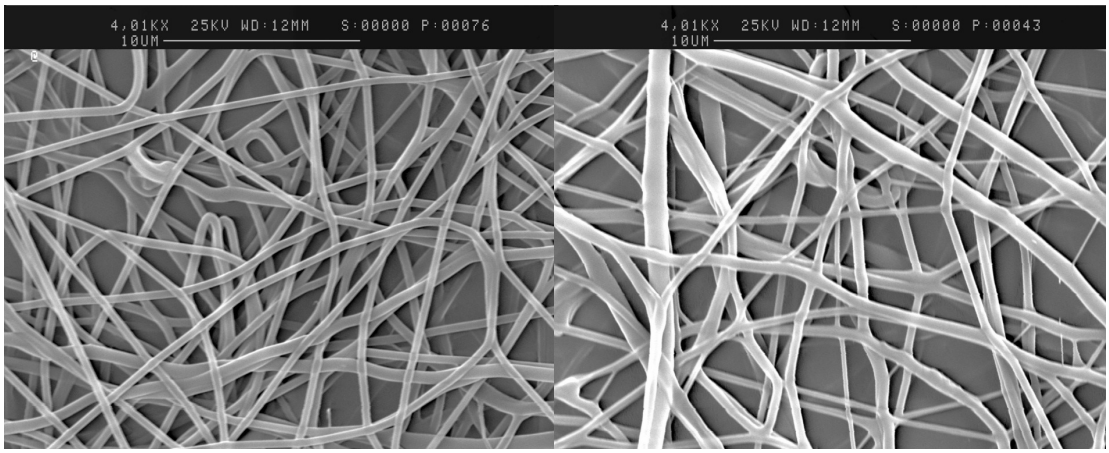

Figure 6: SEM images of electrospun PVOH fibres with 0.25% LiBr (left) and 0.5% LiBr (right)

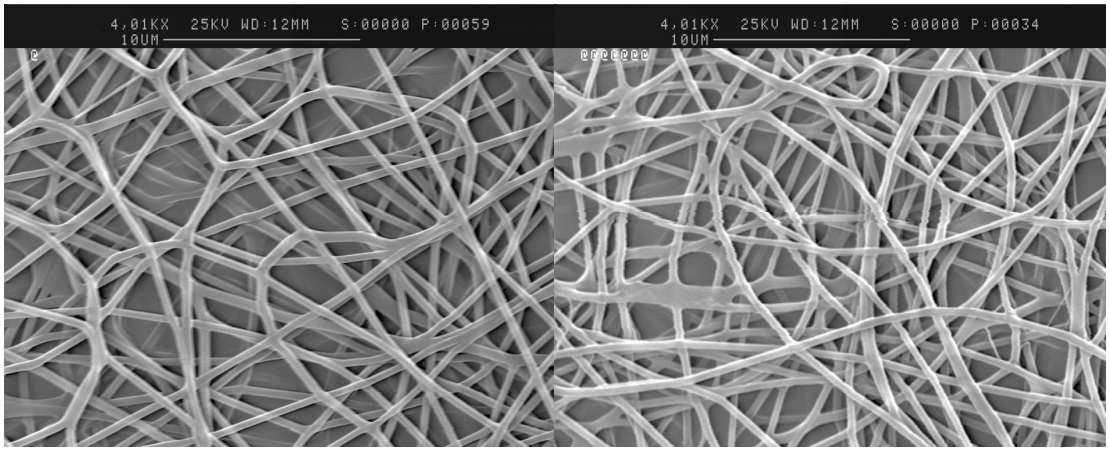

Figure 7: SEM images of electrospun PVOH fibres with 0.1% NaCl (left) and 0.25% NaCl (right)

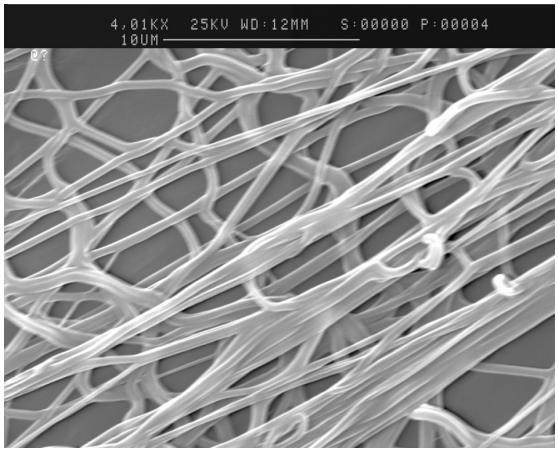

Figure 8: SEM image of electrospun PVOH fibres with 0.5% NaCl

APPENDIX B
PREVIOUS EXPERIMENTAL WORK

1. EXPERIMENTAL METHODS

1.1 Electrospinning Solution

Electrospinning was carried out using poly(vinyl alcohol) (PVOH) (ID#297914D, BDH Chemicals, VWR International) with an average molecular weight of 115,000 $gmol^{-1}$ and a minimum degree of hydrolysis (DH) of 87%. The polymer solution was prepared by dissolving PVOH in distilled water at a concentration of 10% by weight, for 2 hrs at 80°C with constant stirring. A dilution of 5% by weight was used in the following experiments.

1.2 Electrospinning Apparatus

Two different electrospinning set-ups were used in this study. The first set-up (A) consisted of two electrodes, (needle and collector mounted horizontally on a linear rail with their centers aligned. The collector electrode was a 25 × 25 mm copper plate upon which different material substrates were placed. The needle was a plastic Axygen T-200-Y 200 µL pipette tip with an orifice diameter of 0.8 mm and a copper tube 30 mm long and 3 mm diameter placed in line with the pipette tip to charge the polymer solution. The polymer was charged with an EMCO high voltage power supply. (EMCO High Voltage Corp, Model 4330). A digital universal serial bus (USB) microscope (Model QX5, Digital Blue Corporation) was used to observe the Taylor cone during electrospinning to assist with maintaining a stable spinning jet.

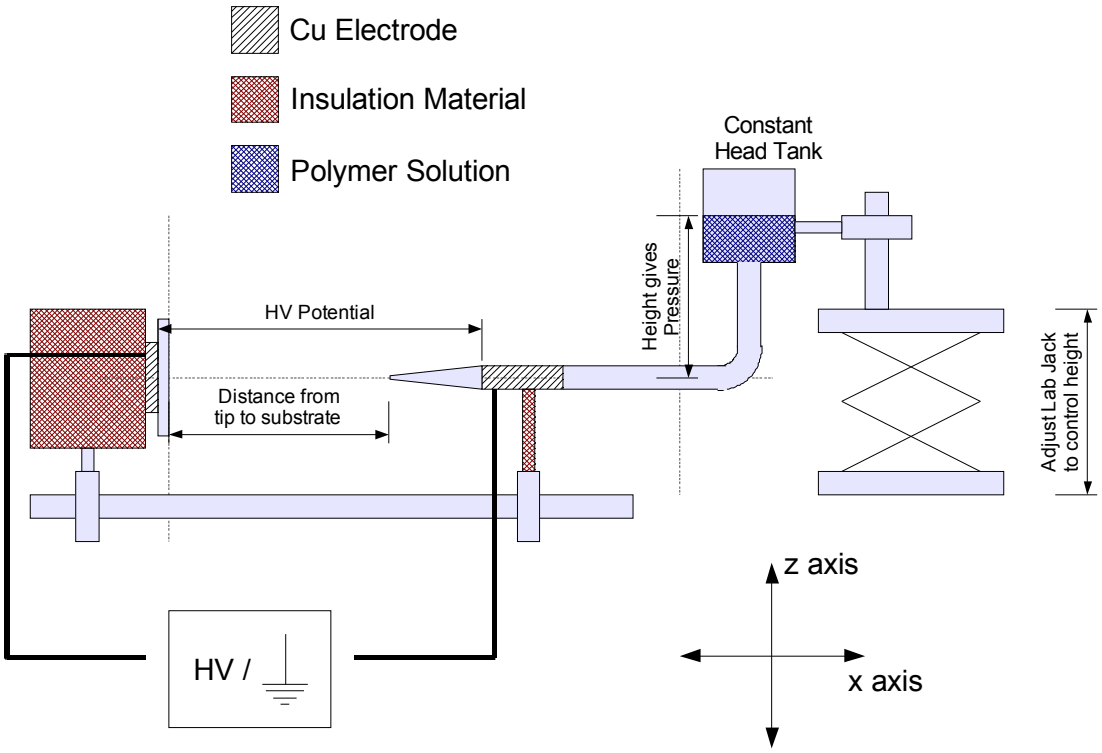

Figure 1: Schematic of the electrospinning set-up A.

In a second electrospinning set-up (B), a parallel plate arrangement was used with one plate acting as the collector while the other charged the polymer solution as it flowed through a metal syringe needle in a vertical arrangement. The parallel plate electrodes were circular disks of aluminium with a diameter of 100 mm and thickness of 8mm. The electrode plates were aligned and separated by mounting the electrodes on three acetyl posts equidistant around the edge of the plates. In addition, a 21 gauge syringe needle was used for the electrospinning. The polymer solution was charged using a Glassman High Voltage supply (EW series). The polymer solution flow rate was controlled with a syringe pump (KD Scientific 100).

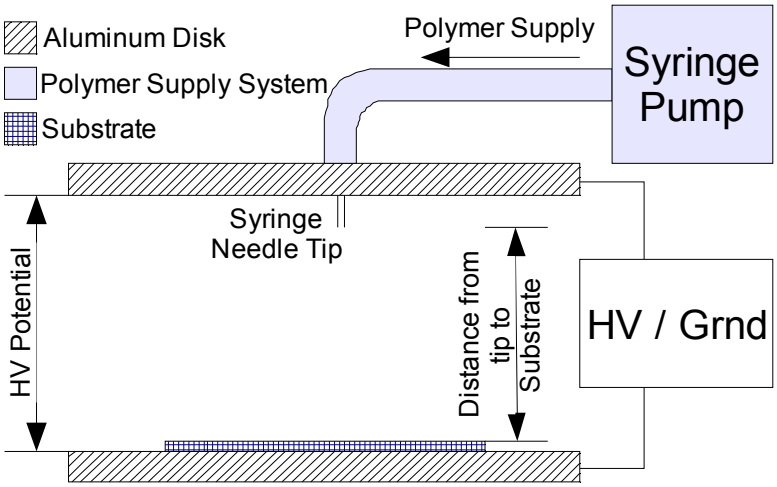

Figure 2: Schematic of the electrospinning set-up B.

1.3 Electrode Configuration

The primary independent variable being examined in all experiments was the electrode configuration. This refers to changing the method of inducing charge on the electrodes used in the electrospinning process. The different electrode configurations are summarized in
Table 1.

	Collector electrode	Polymer solution
Electrode pair I	Positive High Voltage (+ve)	Ground (g)
	Ground (g)	Positive High Voltage (+ve)
Electrode pair II	Ground (g)	Negative High Voltage (-ve)
	Ground (g)	Positive High Voltage (+ve)

Table 1: Summary of the different electrode configurations

1.4 Measurement of Fibre Deposition Rate

The mass deposition rate was measured as the primary dependant variable, and taken as the raw mass of fibre deposited on the collector per hour. The mass deposition rate was determined from the weight change of the collector substrate with a Mettler Toledo AG204 balance (accuracy 0.0001 g).

1.5 Fibre Velocity and Charge

The fibre diameter, initial jet diameter and current were measured as a function of the electrode configuration. The production of fibre was performed with set-up A (Table 2). Fibre samples were produced by depositing for 10 seconds onto an aluminium substrate as described above using Electrode pair I. After these samples were obtained the deposition was continued and the initial jet diameter and current flow was measured.

Field-emission scanning electron microscopy (FESEM) (JEOL JSM-7000F) was used to image the electrospun fibres with an accelerating voltage of 2 kV. Samples were taken after 10 seconds of deposition and gold sputtered. The fibre diameter was measured using FESEM micrographs and image analysis software[*].
The initial jet diameter was measured using a digital USB microscope (Model QX5, Digital Blue Corp.); operating at 60 x magnification and calibrated using a standard calibration slide. The charge on the depositing fibre during electrospinning was determined by measuring the current between ground and the electrode connected to ground using a Keithley Instruments 610B Electrometer (Cleveland, OH, USA). The electrometer was placed in series with the grounded electrode when measuring the current flow to protect it from high voltages.

[*] UTHSCSA ImageTool program (developed at the University of Texas Health Science Center at San Antonio, Texas and available from the Internet by anonymous FTP from ftp://maxrad6.uthscsa.edu).

Set-up	A
Needle-to-collector distance	50 mm
Electrostatic potential	11.5 kV
Deposition time	10 s

Table 2: Summary of process parameters

1.6 Specific Experimental Outline

The mass deposition rate was measured as a function of the electrode configuration using electrode configuration I and set-up A. At least 5 samples were collected for each of the two different electrode configurations.

Fibre was deposited for 10 min for each sample using a constant voltage of 11.5 kV. Stable spinning could be obtained for both electrode configurations with this voltage. The substrate material was a 25 mm x 75 mm sheet of aluminium (0.3mm thick). The constant head pressure was varied to ensure that a stable Taylor cone is formed (Table 4).

Set-up	A
Needle to collector distance	50 mm
Electrostatic potential	11.5 kV
Deposition time	10 min

Table 3: Summary of process parameters

The mass deposition rate was measured as a function of the electrode configuration using electrode configuration II and set-up B. At least 5-7 samples were collected for each of the two different electrode configurations.

Fibre was deposited for 10 min for each sample using a constant voltage of 33 kV. Stable spinning could be obtained for both electrode configurations with this voltage. The substrate material was a 60 mm x 60 mm sheet of aluminium foil. The flow rate was 0.32 mL/h when the polymer solution electrode was charged to a negative potential and increased to 0.62 mL/h when the electrode was charged to a positive potential (Table 4).

Set-up	B
Needle to collector distance	100 mm
Electrostatic potential	33 kV
Feed rate (negative)	0.32 mL/h
Feed rate (positive)	0.62 mL/h
Deposition time	10 min

Table 4: Summary of process parameters

APPENDIX C
SUPPORTING INFORMATION

1. PUBLICATION LIST

1. **"Effect of ionic salts on the electrospinning of poly(vinyl alcohol)"** J Stanger, M P Staiger, K Kirwan, S Coles, D Jacobs, N Lason, 4th Advanced Materials and Nanotechnology Conference, University of Otago, Duneden, New Zealand, 8th February 2009
2. **"Effect of charge density on the Taylor cone in electrospinning"** J Stanger, M P Staiger, K Kirwan, S Coles, D Jacobs, N Lason, Nanotechnology, Submitted 26th September 2008
3. **"Effect of charge carrier modes on the bending instability in the electrospinning process"** J Stanger, N Tucker, M Staiger, K Kirwan, S Coles, D Jacobs, N Larson, 30th Australasian Polymer Symposium, Melbourne, Australia, November 2008
4. **"Effect of charge density on the Taylor cone in electrospinning"** J Stanger, M Staiger, N Tucker, K Kirwan, E-MRS Fall Meeting, Warsaw University of Technology, Warsaw, Poland, 15th September 2008
5. **"In flight charge loss from electrospinning jets"** N Tucker, J Stanger, N Larsen, M Staiger, R Revees, K Kirwan, Poster, E-MRS Fall Meeting, Warsaw University of Technology, Warsaw, Poland, 15th September 2008
6. **"Cellulose acetate butyrate long fibre poly(vinyl alcohol) nanofibre composites"** N Tucker, L Hansen, J Stanger, K Hofman, N Larsen, M Staiger, Poster, E-MRS Fall Meeting, Warsaw University of Technology, Warsaw, Poland, 15th September 2008
7. **"The effect of electrode configuration and substrate material on the mass deposition rate of electrospinning"** J Stanger, N Tucker, M Staiger, A. Wallace, N Larsen, R Reeves, Journal of Materials Processing Technology, submitted 14th March 2008
8. **"Electrospinning"** J Stanger, N Tucker, M Staiger, Rapra Review Reports, vol. 16, 2008 – in preparation
9. **"A laboratory scale electrospinning machine"** N. Tucker, N. Larsen, J. Stanger, Mark P. Staiger, N. Buunk, A. Lucas, A. Clark, T. Hornblow, A. Z. Chen, B. Kearns, Poster, Gordon research conference – composites, Crowne Plaza, Ventura Ca. 13th January 2008
10. **"Polarity and deposition substrate as control parameters for the electrospinning process"** JJ Stanger, N Tucker, N Larsen, M Staiger, R Reeves, paper – International sustainable materials, polymers & composites conference and exploratory workshop, University of Warwick, Coventry, UK. 11-12th September 2007
11. **"The effect of polarity and deposition substrate on the electrospinning process**" JJ Stanger, N Tucker, N Larsen, M Staiger, R Reeves, paper, Materials Asia 2007, Beijing, September 2007
12. **"Aspects of electrospinning process control from fundamental mechanisms"** J Stanger, N Tucker, N Larsen, R Reeves, M Staiger, Paper, ANTEC 2007, Cincinnati, Ohio, May 6-10th, 2007

13. **"Fundamental Mechanisms applied to Electrospinning Process Control"** J Stanger, N Tucker, N Larsen, R Reeves, M Staiger, Paper 29th Australasian Polymer Symposium (29th APS) Hobart, Australia, 11-15th February 2007

2. MATERIALS WORLD ARTICLE

The following article written by Dr. Nick Tucker will appear in a future issue of Materials World published by IOM Communications Ltd. It has been included here as a demonstration of the publication and media interest in the electrospinning project this thesis was part of. The development of the mentioned electrospinning apparatus was a direct result of the work done and submitted for the PHYS480 project at the Physics Department, University of Canterbury, Christchurch.

Bottom-up materials from down under

Nick Tucker, Research Leader in biomaterials at the New Zealand Institute for Crop and Food Research says New Zealand industry has maximised its advantage of being small but well connected, particularly in the field of biopolymers and biocomposite materials.

The connection between world war one fighter aircraft and nanofibre production is nowhere more obvious than in Blenheim, New Zealand. The remote position of New Zealand necessarily breeds a certain independence of spirit when comes to realising bright ideas. In the informal Blenheim engineering cluster on New Zealand's South Island projects currently on the go include automated openers for green lip mussels, robotic replenishment of crop dusting aeroplanes, precision steam weeding, waterproof potato starch packaging materials and at the Omaka aerodrome, the remanufacture of world war one fighter aeroplanes.

Electrospinning in the laboratory

It is against this background that one more equally unusual initiative is taking place. Electrospinz Ltd has started to make laboratory scale electrospinning machines for research organisations. Electrospinning is a lively area of nano materials research with as yet few small and versatile spinning machines on the market. The machines are used to make ultra-fine and nano-scale fibres.

Reflecting current manufacturing best practice Electrospinz Ltd subcontract the specialist metal working skills needed to produce their machines, retaining in-house only the design capability and power and control electronics. Working with sheet metal workers at Omaka meant that the other half of the stainless steel used for the first electrospinning machine went on to become the firewall in a Steerman biplane.

The data used in the design of the machine comes from a crown research institute, the New Zealand Institute for Crop and Food Research (CFR). In the early 1990s, the government created nine crown research institutes as New Zealand's largest providers of science research. They are also science businesses, taking ideas from basic research through to market or near market. Founder of Electrospinz Ltd, Neil Buunk was working on an unrelated project with CFR when he noticed the prototype

electrospinning machine, and realised the commercial potential of small scale lab spinning machines. It took six weeks to translate the prototype into a production machine.

Bottom-up polymers and composites

Crop and Food Research scientists are testing the potential of electrospun proteins and polysaccharides as industrial raw materials. They are interested in how the materials perform either as filters or structural elements. These spun materials have exceptional mechanical properties and high specific surface areas that can be exploited to make low-pressure-drop selective active filtration elements.

The electrospinning method does not use high temperatures or invasive coagulating chemicals to produce fibres and hence scientists are able to exploit the methods of self-organisation used in nature to directly manufacture articles on an industrial scale using such materials as marine collagen. This method steps around the traditional industrial way of working with natural materials, which is to dismantle the original structure, for example a tree, and reconstruct it into something that usually has poorer properties, for example a kitchen unit. The new method is dubbed bottom-up manufacture by those involved.

CFR collaborates extensively with local and overseas universities as well as commercial development partners. New Zealand's Massey University provides large scale processing laboratories as well as characterisation techniques such as atomic force microscopy, the University of Canterbury is also working on electrospinning of nanofibres and the production of protein based fibrillar structures with potential as reinforcement and as sites for chemical functionality. Warwick University is CFR's European development partner in this field.

Drivers for change

There are a number of national initiatives under way aimed at exploiting crop origin industrial materials, these initiatives are a mixture of technical and supply-chain establishing ventures. In the past two decades, New Zealand has evolved from an agrarian economy exporting mainly to the UK into a more industrialized economy. In terms of the polymer industry about 400 plastic companies contribute a turnover of NZ$1.8 billion per year to the economy. Products are mainly for the packaging (58%), agricultural (15%), construction (13%) sectors.

In terms of the drivers for the adoption of bio-origin polymers, external regulations such as European end-of-life regulations are important to an exporting nation like New Zealand, as the perception of the size of the ecological footprint of materials imported from distant shores may well be allowed to act as a de-facto tariff barrier. The adoption of biopolymers – especially made from local crops, will offer significant advantages to the food exporter. It makes little sense to be importing expensive fossil origin polymers only to ship them back out again as low added value food wrap.

Aside from limited production of **Polyhydroxyalkanoate**, acid, and the import of significant quantities of Cargill-Dow Natureworks, the main producer of biopolymer materials in NZ is Blenheim based Potatopak (NZ) Ltd. This company has developed a viable production route for food packaging trays made from potato starch: the starch is sourced from potato processing waste.

Research and industry in joint ventures

The national effort on crop origin polymers and composites is organised through the New Zealand wide Biopolymer Network (BPN). The Biopolymer Network is a company uniting three CRIs (Crop & Food Research, Scion, and AgResearch) and a group of industrial partners and universities, bringing together expertise in producing materials from a range of renewable resources, including animal by-products, arable products (cereals and vegetables), and forestry. The company aims to manage the involvement of the partner organisations with overlapping research expertise in a growing biomaterials industry, and to establish the supply chain for such materials.

BPN is targeting agricultural and forestry raw materials as potential replacements for petroleum-based products. Potential products include a wide range of biopolymer-based formulating agents for cosmetics, personal care products, adhesives, and other specialty chemicals. Replacements for fossil origin plastics will be derived from wood cellulose, grain polysaccharides and proteins, and other locally renewable resources. BPN is particularly keen to encourage the use of New Zealand grown and native materials, and establish a supply chain for crop origin biodegradable polymers and composites. The native fibre crop is NZ flax or Harakeke (*Phormium tenax*), formerly used to make matting and cordage, and also a minor source of a naturally astringent jelly, and seed oil. The BPN has been working with growers, processors, designers and end-users to revive the plant as a fibre crop. The largest scale introduced fibre crop is hemp (*Cannabis sativa*), although legal constraints restrict the free exploitation of this material. The BPN has examined fibre processing techniques with a view to establishing the crop in New Zealand as a fibre source. The licensed hemp crop in New Zealand is established for the production of high grade culinary oil.

Collaborative research and development strategies such as this one allow the world's most southerly developed nation to produce more scientific papers per research dollar than any other country in the world. Researchers take advantage of the unique situation of New Zealand as a small and remote nation of only 4.2 million and lead the evolution of New Zealand as a significant R&D player. In per capita terms, New Zealand's ranking for published research is 11th in the world. The small scale of the country and the resulting short and simple lines of communication gives the local manufacturing industry a competitive edge with an ability to mix and match materials and research results.

Electrospinning development

1628 - Electrostatic attraction of liquids was first observed by William Gilbert

1902 W.J Morton - Method of dispersing fluids. US Patent 705,691 a process that is recognisably electrospinning and spraying

1914 – J. Zelany – empirically observed the formation of a fluid jet at the end of a capillary under electrostatic force

1930s Anton Formhals: a sequence of patents on industrial scale electrospinning

1964 G.I. Taylor defined the idea of the "leaky dielectric model" and mathematically modelled the formation of the eponymous Taylor cone and the formation of a thread.

1995 J. Doshi and D.H Reneker – started the electrospinning research nanofibre "gold rush"

Electrospinning is emerging as a ready way to produce nanoscale polymer fibres. Potential applications for these materials include biocomposites, bioprocessing media, electronic technologies, bioprosthetics, medicine, packaging and bioremediation.

3. DATASHEET FOR ES1 AND ES4 MODEL OF ELECTROSPINNING APPARATUS FROM ELECTROSPINZ

Electrospinz
nanofibre engineering

www.electrospinz.co.nz sales@electrospinz.co.nz

Specifications for Model ES1 Laboratory Electrospinning platform.

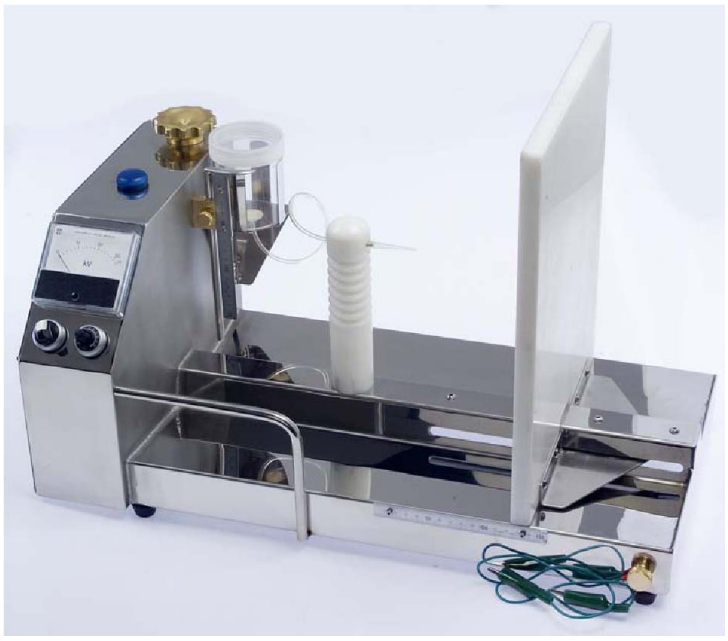

Description:

The ES1 is designed to be used by competent operators in a laboratory environment, using an aqueous solution. Other solutions may be spun but the materials of the header tank, hose and spinning tip may need to be changed.
The ES1 is a self contained bench top machine with a solid, easy to clean base. The constant head system is calibrated for head and simple to adjust. The moveable target plane can be set from 0 to 150mm; this can be adjusted during operation. The power to the spinning head is adjustable from 0 to 33,000 VDC.

Materials:

Base and control box are constructed from 316 stainless steel.
Insulating materials are acetal.
Electrical connection fittings are brass.
Header tank is high impact polystyrene.
Hose is polyurethane.
Spinning tip is polypropylene.

Power Supply:

Single phase 100 to 230 VAC, 1 amps maximum.

Pricing:

The base price is $NZ10,000.00 (+ GST if applicable)
Plus freight, insurance, and any other charges necessary for delivery from Blenheim NZ.

Electrospinz
nanofibre engineering

www.electrospinz.co.nz sales@electrospinz.co.nz

Specifications for Model ES4 Laboratory Electrospinning platform.

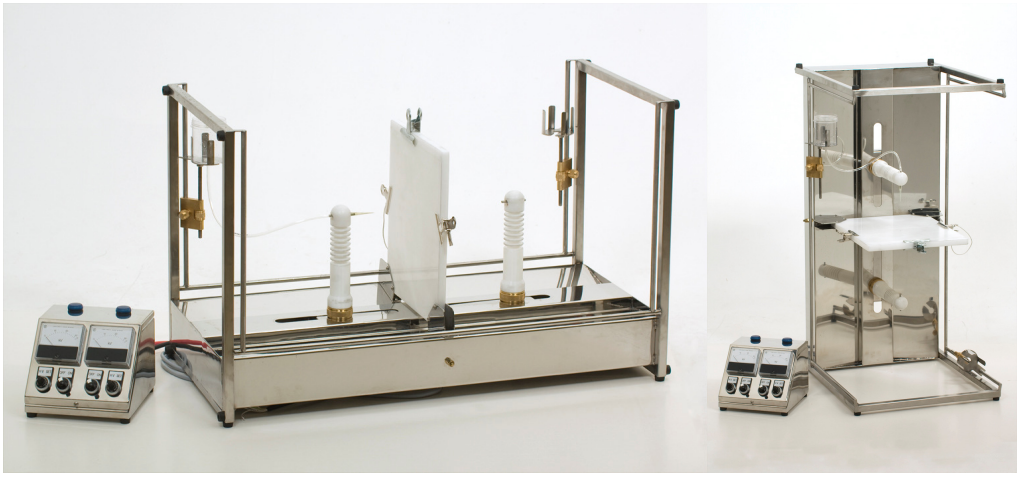

Description:

The ES4 is designed to be used by competent operators in a laboratory environment, using an aqueous solution. Other solutions may be spun but the materials of the header tank, hose and spinning tip may need to be changed.

The ES4 has a solid, easy to clean base and is designed to be operated in any one of three orientations; the constant head system is capable of being set for any of these. The controls are contained in a separate box connected to the spinning platform; this allows the platform to be separately enclosed.

Two moveable spinning heads are mounted either side of a fixed target plane. The heads have 200mm of travel and the spinning axis is 200mm above the base. Each head has a built in high voltage (33KV DC) power supply; the heads (1 Positive and 1 Negative) may be used independently or at the same time allowing 66KV potential if required.

Materials:

Base and control box are constructed from 316 stainless steel.
Insulating materials are acetal.
Electrical connection fittings are brass.
Header tank is polystyrene.
Hose is polyurethane.

Power Supply:

Single phase 100 to 230 VAC, 2 amps maximum.

Pricing:

The base price is $NZ19,000.00 (+ GST if applicable)
Plus freight, insurance, and any other charges necessary for delivery from Blenheim NZ